**Title**
CRTC2 Regulates Plasma Cell Metabolism and Survival to Maintain Humoral Immune Responses



**Author**
Hong, Jason S

**Publication Date**
2020

UNIVERSITY OF CALIFORNIA

Los Angeles

# CRTC2 Regulates Plasma Cell Metabolism and Survival to Maintain Humoral Immune Responses

A dissertation submitted in partial satisfaction of the

Requirements for the degree of Doctor of Philosophy in

Cellular and Molecular Pathology

by

Jason S. Hong

2020

ABSTRACT OF THE DISSERTATION

CRTC2 Regulates Plasma Cell Metabolism and Survival

to Maintain Humoral Immune Responses

by

Jason S. Hong

Doctor of Philosophy in Cellular and Molecular Pathology

University of California, Los Angeles, 2020

Professor Michael A. Teitell, Chair

The humoral immune response is mediated by antigen activated B cells that have terminally differentiated into antibody secreting cells (ASCs). The ASC pool is composed of short-lived plasma cells (SLPCs) and long-lived plasma cells (LLPCs) that secrete antigen-specific antibodies to clear an infection and maintain long-term protective antibody titers to prevent subsequent reinfections. SLPCs have generally been viewed to be formed from T cell-independent immune responses and localized in the spleen. LLPCs have been viewed to be formed from T cell-dependent immune responses and localized in the bone marrow. However, regardless of the type of stimulating antigen, ASCs of varying lifespans, both SLPCs and LLPCs are found in the spleen and bone marrow. Currently, it remains unclear as to what factors and pathways regulate PC longevity.

Our laboratory previously identified the CREB coactivator CRTC2 as a regulator of ASC differentiation. DNA double strand breaks associated with class switch

recombination activates a signaling pathway in human germinal center (GC) B cells that results in the phosphorylation and inactivation of CRTC2. Phosphorylated CRTC2 is re-localized to the cytoplasm and CRTC2 target genes are down-regulated. Dysregulation of CRTC2 activity through over-expression of a nucleus-localized and constitutively active form of CRTC2 (CRTC2-AA) in human tonsillar B cells, prevented GC B cells from exiting the GC reaction and inhibited ASC differentiation. However, it remained unclear whether the function of CRTC2 in this *in vitro* differentiation system would be recapitulated *in vivo* and whether CRTC2 played any other roles in an *in vivo* humoral immune response.

To evaluate these questions, we generated a transgenic (TG) mouse model which expresses CRTC2-AA at all stages of B cell development. Using these TG mice, we demonstrate that *Crtc2* repression in PCs is an intrinsic requirement for PC metabolic fitness. Sustained CRTC2 activity shortened the survival of splenic and bone marrow PCs which resulted in the reduction of long-lived PCs and antibody deficits in response to immunizations and acute viral infection. We further demonstrated that TG PCs adopt characteristics associated with SLPCs which include reduced antibody secretion, glycolysis, oxidative metabolism, and spare respiratory capacity. Mechanistically, *Crtc2* repression is necessary for the fidelity of PC gene expression and mRNA alternative-splicing programs, with both programs altered in TG PCs. Combined, our results show that *Crtc2* repression in PCs must occur to support PC metabolism and extend PC survival and lifespan during a humoral immune response. We hypothesize that the level of *Crtc2* repression in differentiated ASCs determines metabolic fitness and ultimately PC survival and longevity in the bone marrow.

The dissertation of Jason S. Hong is approved.

Linda Baum

Kenneth Dorshkind

Stephen Smale

Michael A. Teitell, Committee Chair

University of California, Los Angeles

2020

# DEDICATION

This dissertation is dedicated to my parents for their endless love and support.

And to my wife Tammy, for everything.

TABLE OF CONTENTS

LIST OF TABLES AND FIGURES

Chapter 2

# ACKNOWLEDGEMENTS

I first have to thank my PhD advisor, Dr. Michael Teitell, for taking me into his lab over 15 years ago. Over the years, Mike has made a significant impact on my life and has had a part in shaping who I am today. He is one of the hardest working people I know and his drive and passion for what he does is truly inspirational. Mike's enthusiasm for science and his ability to continuously impart that excitement to his students is one of his greatest strengths. Regardless of how long this journey has taken, the freedom and independence to drive my project has made me into a stronger scientist and a more resilient person. I cannot thank Mike enough for this opportunity and for all his positivity, support, and advice over the years.

My committee has also been instrumental in guiding my graduate career and getting me to the finish line. I truly wish I had utilized them earlier and more often. I would like to thank Dr. Baum, Dr. Dorshkind, and Dr. Smale for their ideas, encouragement, and support throughout this process.

I would also like to thank all the past and present members of the Teitell laboratory who have given me technical, scientific, and emotional support throughout my graduate career. I'd especially like to thank Drs. Sam French, Dave Dawson, Larry Wong, Matt Frank, Hsiao-Wen Chen, Ali Kuraishy, Mara Sherman, Jin Zhang, Jessica Fowler, Nicole Walsh, Rani Najdi, Tom Zangle, Tara TeSlaa, Eriko Shimada, Lynnea Waters, Dian Huang, Laura Jimenez, and Alex Patananan along with Mai Nguyen, Alex Sercel, Vivian Lu, Diane Kim, Thang Nguyen, Amy Yu, Robert Nguyen, Alejandro Torres, Amy Carver, and Fasih Ahsan for their friendship and support.

Thank you to my parents and my brother for always being supportive and always willing to buy me meals whenever they are nearby. Finally, I want to thank my lovely wife, Tammy, who has supported and believed in me throughout this long and difficult journey. Your kindness, warmth, and unwavering positivity has sustained me over these years. I can never thank you enough for all that you have done.

My work has been supported by NIH awards R01CA90571, R01CA156674, R01GM073981, R21CA227480, and P30CA016042, and the Air Force Office of Scientific Research FA9550-15-1-0406.

Chapter 2 is a version of a manuscript currently in submission and under review at *Nature Immunology* "Hong JS, Ahsan FM, Pioli PD, Lee M-S, Nguyen TL, Brooks DG, Golovato J, Niazi KR, & Teitell MA. CRTC2 regulates plasma cell metabolism and survival."

Appendix I is a version of a published manuscript, "Sherman MH, Kuraishy AI, Deshpande C, Hong JS, Cacalano NA, Gatti RA, Manis JP, Damore MA, Pellegrini M, & Teitell MA. AID-induced genotoxic stress promotes B cell differentiation in the germinal center via ATM and LKB1 signaling. *Molecular Cell* 39.6 (2010): 873-885" reproduced here with permission from Elsevier Inc.

Appendix II is a version of a published manuscript, "Waters LR, Ahsan FM, ten Hoeve J, Hong JS, Kim NHD, Minasyan A, Braas D, Graeber TG, Zangle TA, & Teitell, MA. Ampk regulates IgD expression but not energy stress with B cell activation. *Scientific Reports* 9.1 (2019): 8176" reproduced here in accordance with the Creative Commons Attribution 4.0 International License.

VITA

| | |
|---|---|
| 2004 | B.S. Molecular Cell Developmental Biology<br>University of California, Los Angeles |
| 2004-2011 | Staff Research Associate,<br>University of California, Los Angeles |
| 2011-2020 | Graduate Student Researcher<br>University of California, Los Angeles |

SELECTED PUBLICATIONS

Man, T., Zhu, X., Chow, Y.T., Dawson, E.R., Wen, X., Patananan, A.N., Liu, T.L., Zhao, C., Wu, C., **Hong, J.S.**, Chung, P-S., Clemens, D.L., Lee, B.-Y., Weiss, P.S., Teitell, M.A., and Chiou, P.-Y. **Intracellular Photothermal Delivery for Suspension Cells Using Sharp Nanoscale Tips in Microwells.** *ACS Nano*, 2019 In press.

Waters, L.R., Ahsan, F.M., ten Hoeve, J., **Hong, J.S.**, Kim, D.N.H., Minasyan, A., Braas, D., Graeber, T.G., Zangle, T.A., and Teitell, M.A. **Ampk Regulates IgD Expression but not Energy Stress with B Cell Activation.** *Scientific Reports*, 2019 June 3; 5:99-109

Wu, T.-W., Sagullo, E., Case, D., **Hong, J.S.**, Graeber, T.G., Chiou, P.-Y., and Teitell, M.A. **Mitochondrial Transfer by Photothermal Nanoblade Restores Metabolite Profile in Mammalian Cells.** *Cell Metabolism*, 2016 May 10; 23: 921-929

Zhang, J., Nuebel, E., Wisidagama, D.R.R., Setoguchi, K., **Hong, J.S.**, Van Horn, C. M., Imam, S.S., Vergnes, L., Malone, C.S., Koehler, C.M., and Teitell, M.A. **Measuring Energy Metabolism in Human Pluripotent Stem Cells and Differentiated Cells.** *Nature Protocols*, 2012 May 10; 7(6): 1068-85

Wang, G., Shimada, E., Zhang, J., **Hong, J.S.**, Smith, G., Teitell, M.A., and Koehler, C.M. **Correcting Human Mitochondrial Mutations with Targeted RNA Import.** *Proceedings of the National Academy of Sciences,* 2012 March 27; 109(13): 4840-5

Zhang, J., Khvorostov, I., **Hong, J.S.**, Oktay, Y., Vergnes, L., Nuebel, E., Wahjudi, P.N., Setoguchi, K., Wang, G., Do, A., Jung, H.J., McCaffery, J.M., Kurland, I.J., Reue, K., Lee, W.N.P., Koehler, C.M., and Teitell, M.A. **UCP2 Regulates Energy Metabolism and Differentiation Potential of Human Pluripotent Stem Cells.** *EMBO Journal*, 2011 November 15; 30: 4860-4873

Sherman, M.H., Kuraishy, A.I., Desphpande, C., **Hong, J.S.**, Cacalano, N.A., Gatti, R.A., Manis, J.P., Damore, M.A., Pellegrini, M., and Teitell, M.A. **AID-Induced**

**Genotoxic Stress Promotes B Cell Differentiation in the Germinal Center via ATM and LKB1 Signaling.** *Molecular Cell*, 2010 September 24; 39(6): 873-885

Wang, G., Chen, H.-W., Oktay, Y., Zhang, J., Allen, E.L., Smith, G.M., Fan, K.C., **Hong, J.S.**, French, S.W., McCaffery, J.M., Lightowlers, R.N., Morse, H.C. 3rd., Koehler, C.M., and Teitell, M.A. **PNPASE Regulates RNA Import into Mitochondria.** *Cell*, 2010 August 6; 142(3): 456-467

Balatoni, C.E., Dawson, D.W., Suh, J., Sherman, M., Sanders, G., **Hong, J.S.**, Frank, M.J., Malone, C.S., Said, J.W., and Teitell, M.A. **Epigenetic Silencing of STK39 in B-Cell Lymphoma Inhibits Apoptosis from Genotoxic Stress**. *American Journal of Pathology*, 2009 October; 175(4): 1653-61

Frank, M.J., Dawson, D.W., Bensinger, S.J., **Hong, J.S.**, Knosp, W.M., Xu, L., Balatoni, C.E., Allen, E.L., Shen, R.R., Bar-Sagi, D., Martin, G.R., and Teitell, M.A. **Expression of sprouty2 Inhibits B-Cell Proliferation and is Epigenetically Silenced in Mouse and Human B-Cell Lymphomas**. *Blood*, 2009 March 12; 113(11): 2478-87

Dawson, D.W., **Hong, J.S.**, Shen, R., French, S.W., Troke, J.J., Wu, Y.Z., Chen, S., Gui, D., Regelson, M., Marahrens, Y., Morse, H.C., Said, J., Plass, C., and Teitell, M.A. **Global Assessment of DNA Methylation in a Mouse Model of B Cell Lymphoma Identifies Epigenetic Silencing of a Variant Transcript of Epha7 in Lymphocytes.** *Oncogene*, 2007 June 21; 26(29): 4243-52

Chen, H.-W., Rainey, R.N., Balatoni, C.E., Dawson, D.W., Troke, J.J., Wasiak, S., **Hong, J.**, McBride, H., Koehler, C.M., Teitell, M.A., and French, S.W. **Mammalian PNPase is an Intermembrane Space Ribonuclease that Maintains Mitochondrial Homeostasis.** *Molecular and Cellular Biology*, 2006 November; 26(22): 8475-87

## POSTERS and PRESENTATIONS

**Hong, J.S.**, Ahsan, F.M., and Teitell, M.A. (2018). Poster: CRTC2 Inactivation is Required for Antibody Secreting Cell Survival During a Humoral Response. La Jolla Immunology Conference, San Diego, CA.

**Hong, J.S.** (2016). Presentation: CRTC2 inactivation is required for plasma cell differentiation and effective humoral immunity. I3T Research in Progress Seminar, Los Angeles, CA.

**Hong, J.S.**, Walsh, N.C., Elsaesser, H., Brooks, D.G., and Teitell, M.A. (2015). Poster: CRTC2 inactivation in activated B cells is required for plasma cell differentiation and humoral immunity. Keystone Symposia: The Golden Anniversary of B cell Discovery, Banff, Canada

# CHAPTER 1:

# Introduction

The humoral immune response represents one arm of the adaptive immune system. B cells that are antigen activated, rapidly proliferate and differentiate into transient plasmablasts (PBs) or plasma cells (PCs). These antibody secreting cells (ASCs) represent a small, but critical effector population of the B cell lineage responsible for neutralizing pathogens and maintaining long-term humoral immunity[1, 2]. Since the discovery of antibody mediated immunity well over 100 years ago, much has been learned about this critically important cell population[3].

## B CELL DEVLOPMENT

In humans and mice, B cells are continuously generated from hematopoietic stem cells in the bone marrow. Developing B cells pass through several developmental checkpoints that ensure immunoglobulin genes are completely assembled from a diverse pool of gene segments in a process known as V(D)J recombination. This process results in the expression of a diverse repertoire of membrane bound antigen receptors, or B cell receptors (BCRs), which allow for the recognition of a near limitless number of unique antigens[4]. Both the BCR and the secreted form of the BCR, known as an antibody, are unique to each B cell and binds antigens with varying levels of affinity. A single BCR or antibody molecule is composed of four polypeptide chains (2 heavy and 2 light) that are held together by disulfide bonds to form a Y-shaped molecule. The N-terminus regions, or the tips of the Y, represent the variable regions which recognize and bind antigen. The C-terminus, or the base of the Y, forms the constant region which determines the isotype of the molecule. Antibodies of different isotypes (IgM, IgD, IgG,

IgE, and IgA) differ in their effector functions and localizations to ensure proper immune response to a given pathogen or infection[5].

The developmental stages in the bone marrow progress sequentially from pro-B, pre-B, to immature B cells. Immature B cells that retain low-level BCR signaling are positively selected and retained, whereas those incapable of signaling through the BCR are eliminated. Many B cell clones with strong reactivity to self-antigens are eliminated through negative selection. Importantly, much of the BCR diversity that was generated earlier in the bone marrow is eliminated at this stage in development[6]. Immature B cells will leave the bone marrow and home to the spleen where they differentiate into transitional B cells and mature further into follicular (FO) or marginal-zone (MZ) B cells. These mature B cells are retained in the spleen while FO B cells recirculate through the bone marrow and other secondary lymphoid organs (SLOs)[5, 7].

## B CELL ACTIVATION AND TERMINAL DIFFERENTIATION

Mature B cells remain quiescent until they are activated via BCR engagement to their cognate antigens. B cell activation results in cell proliferation and differentiation and can be elicited by either a T cell-independent (TI) or T cell-dependent (TD) antigen. B cells activated by TI antigens, which include large carbohydrates or phospholipids with repeating epitopes, do not require T cell help as these antigens are capable of cross-linking multiple BCRs and/or activating toll-like receptors (TLRs). A TI immune response rapidly generates PBs that secrete non-mutated low-affinity antibodies[8]. B cells activated by a protein or TD antigen, rapidly proliferate and differentiate into PBs in an extrafollicular response which produce the first wave of unmutated low affinity

antibodies. Concurrent with the extrafollicular response, activated B cells that have acquired T cell help, can form histological structures called germinal centers (GCs). Within GCs, rapidly proliferating B cells undergo somatic hypermutation (SHM) and class switch recombination (CSR). SHM introduces single base-pair mutations in the variable region of the immunoglobulin gene. The resulting BCR mutants that have acquired increased antigen affinity, can successfully out-compete other B cells for access to limited antigen on follicular dendritic cells (FDCs) and signals mediated by T follicular helper ($T_{FH}$) cells that sustain GC B cell responses. This process of affinity maturation continually selects for B cells with higher affinity BCRs. B cells that survive the GC reaction can terminally differentiate into either memory B cells capable of quickly responding to repeat antigen exposure or differentiate into PCs that secrete higher affinity antibodies of various isotypes through CSR[9].

The signals that initiate the differentiation of activated B cells into ASCs remain to be fully characterized. However, studies have shown that BCR affinity and intracellular signals delivered through the BCR and/or other ligands associated with FDCs may initiate differentiation[10]. In addition, metabolic reprogramming and mitochondrial remodeling have been shown to affect ASC differentiation and thus may contribute signals that initiate differentiation[11, 12].

## ANTIBODY SECRETING CELLS

The primary role of an ASC is to synthesize and secrete large amounts of antibodies. To perform this task, differentiating B cells expand their cytoplasm, endoplasmic reticulum (ER), and Golgi apparatus while also altering their metabolic,

cellular, and molecular programs. These adaptations require the coordinated change in the expression of hundreds of genes in a division dependent manner[1, 13].

At the transcriptional level, differentiation of activated B cells into ASCs requires reorganization of transcriptional networks and expression of distinct gene programs. B cell specifying transcription factors such as paired box gene 5 (PAX5) and B-cell lymphoma 6 (BCL6) are extinguished while ASC transcription factors such as PR-domain containing protein 1 (BLIMP1), X box-binding protein 1 (XBP1), and interferon regulatory factor 4 (IRF4) are induced. These mutually exclusive factors maintain the clear distinctions between B cell and ASC identities[14]. BLIMP1 is the master regulator of ASC differentiation and is required for the establishment of the ASC gene expression program. Once established, however, the maintenance of the program is primarily BLIMP1 independent[15]. To support the synthesis and secretion of antibodies, BLIMP1 and XBP1 regulate the unfolded protein response (UPR), a stress response pathway that ASCs and other secretory cells activate to respond to and alleviate ER stress generated by misfolded proteins[15, 16]. IRF4, facilitates ASC differentiation by repressing BCL6 and activating BLIMP1. It is also critical for PC survival, partly through the regulation of myeloid cell leukemia sequence 1 (MCL1), a key PC survival molecule[15, 17, 18]. RNA binding proteins (RBPs), which post-transcriptionally regulate mRNAs are also involved in regulating B cell programs. As an example, knock-out of the RBP HuR, which regulates alternative splicing in activated B cells, inhibits mitochondrial metabolism and cell proliferation, thereby negatively affecting ASC differentiation[19].

ASCs must alter their metabolism to synthesize and secrete large quantities of antibodies. Quiescent B cells undergo low levels of glycolysis and moderate levels of

oxidative metabolism. Upon antigen stimulation through the BCR, glycolysis and oxidative metabolism are increased along with an increase in mitochondrial mass which helps the cell keep up with metabolic demands[20, 21]. Further, B cells stimulated with the TI antigen lipopolysaccharide (LPS), revealed that genes critical for oxidative metabolism were upregulated and required for PB differentiation[22]. Recent studies show terminally differentiated PCs actively import glucose and amino acids and rely on both glycolysis and oxidative metabolism for their bioenergetic needs. Additionally, the supply of amino acids appear to be partly regulated through BLIMP1 activation of several amino acid carriers such as CD98[15]. Further, ASCs must induce autophagy to generate metabolic substrates and to regulate sustainable antibody production to prevent cell death[23].

ASCs are broadly divided into short-lived and long-lived populations. PBs generated in the spleen from TI or TD extrafollicular responses are generally short-lived and do not survive past the contraction of the primary antibody response. These PBs are also referred to as short-lived PCs (SLPCs). PCs formed from GC reactions that migrate to the bone marrow are generally believed to be long-lived and are referred to as long-lived PCs (LLPCs)[1]. The bone marrow niche is made up of multiple cell types including mesenchymal stromal cells and eosinophils. Evidence shows that the bone marrow niche supports PC survival through cell-cell contacts and/or soluble signals from these cells[24]. LLPCs, however, localize to the spleen and other tissue types in the body following TI and TD immune responses and therefore are not confined to the bone marrow niche[25, 26]. Further, PCs of varying lifespans, are present in the bone marrow-one study suggesting that as many as 50% of bone marrow PCs are newly formed and

short-lived[27]. These studies reveal that access to survival niches and cell extrinsic factors are not the sole determining factors regulating ASC longevity[25, 28].

The simplest method to determine intrinsic factors and pathways that regulate longevity is to directly compare SLPCs with LLPCs. In mice, ASCs in the spleen and bone marrow are currently identified based on the surface expression of B220 and CD138. SLPCs have been identified as $B220^{+}CD138^{+}$ while LLPCs have been identified as $B220^{-}CD138^{+}$[29]. Human bone marrow ASCs are identified by the expression of CD19, CD27, CD38, and CD138 with SLPCs identified as $CD19^{+}CD38^{+}$ and LLPCs identified as $CD19^{-}CD38^{+}$[30]. Recently, Lam *et al.* used the fluorescently-labeled glucose analog 2NBDG to sort mouse $CD138^{+}$ splenic and bone marrow PCs into subsets based on B220 expression and 2NBDG import. They found 2NBDG import could discriminate PCs of differing lifespans. RNA-sequencing of splenic PC subsets representing SLPCs and a bone marrow PC subset representing LLPCs failed to identify significant transcriptional changes that could account for lifespan differences. Major factors involved in ASC differentiation and survival, as well as UPR regulators and related transcripts, were not differentially expressed. Additionally, RNA-seq analysis of human bone marrow $CD19^{-}$ LLPCs and $CD19^{+}$ SLPCs also found relatively little difference between the two subsets[31].

Although transcriptionally similar, mouse LLPCs from the bone marrow were found to be metabolically distinct from SLPCs from the spleen. LLPCs import more glucose compared to SLPCs, which is used primarily for antibody glycosylation and to sustain increased antibody secretion. Under bioenergetic stress, LLPCs are capable of diverting glucose away from glycosylation and shift it to glycolysis, using the resultant

pyruvate to increase oxidative metabolism and generate higher spare respiratory capacity (SRC). Mitochondrial SRC is the difference between the maximal and basal respiratory capacities. SRC has been correlated with enhanced cell survival and a reduction in SRC has been associated with cell death[32]. When pyruvate import was inhibited in LLPCs, oxidative metabolism was reduced to levels observed in SLPC levels and SRC was ablated. Further, deletion of the *mitochondrial pyruvate carrier 2* (*Mpc2*) gene in mouse B cells, resulted in the progressive loss of bone marrow PCs[33].

The lack of significant transcriptional differences may suggest that lifespan and longevity are not transcriptionally regulated. However, due to the heterogeneity of the ASC population in the spleen and bone marrow and an inability to purely sort PC subsets with differing half-lives, relevant but subtle transcriptional differences may be muted and masked[34].

## CREB AND CRTCs

The cyclic-AMP response element binding protein (CREB) is a ubiquitously expressed member of the basic leucine zipper (bZIP) transcription factor superfamily. Regulated through phosphorylation, cellular signals such as cAMP and $Ca^{2+}$ flux promotes the phosphorylation of serine-133 (S133) in the kinase inducible domain of CREB. Phosphorylation at this residue, leads to CREB interaction with the histone acetyltransferase CREB binding protein (CBP) and the CBP paralog p300. Interaction with CBP/p300 activates transcription of CREB responsive genes by acetylating local histones and recruiting the transcriptional machinery. CREB binds to DNA through

recognition of an 8-base pair palindromic DNA binding motif known as a full cAMP response element (CRE) or a less active half CRE site in the promoter of genes[35].

In the canonical CREB activation pathway, phosphorylation of CREB at serine-133 (S133) is sufficient for its interaction with CBP/p300 and gene activation. However, CREB can also activate genes independently of S133 phosphorylation. A cDNA over-expression screen identified the transducers of regulated CREB (TORC) as potent activators of CREB[36, 37]. TORC proteins were later renamed the CREB-regulated transcriptional coactivators (CRTCs) to not be confused with the mTOR signaling complexes. The CRTC family consists of three members (CRTC1-3) in mammals and a single functional homolog in *D. melanogaster* and *C. elegans*. CRTCs contain a conserved N-terminal CREB binding domain, a central regulatory domain, a splicing domain, and a C-terminal transactivation domain. CRTC2 and CRTC3 are ubiquitously expressed while CRTC1 is mainly expressed in the brain.

CRTCs are negatively regulated through phosphorylation by AMP-activated protein kinase (AMPK) and AMPK family member proteins, which lead to their interaction with 14-3-3 proteins and cytoplasmic sequestration. Dephosphorylation of CRTCs by the serine/threonine phosphatase calcineurin leads to CRTC activation by triggering its nuclear re-localization and binding to CREB[35]. The list of CREB-dependent CRTC targets reveal that the CREB-CRTC signaling axis is important for regulating global energy homeostasis[38]. Beyond transcriptional regulation, CRTCs have been implicated to have a role in alternative splicing. Although CRTCs lack recognizable RNA binding domains, *in-vitro* splicing assays revealed that CRTCs could regulate alternative exon usage and 3’ splice-site selection independently or coupled with their gene

activation function. In addition, the CRTC1/MAML2 (mastermind-like protein 2) fusion oncogene which induces mucoepidermoid carcinomas, results in the deletion of the splicing domain of CRTC1. When tested for splicing activity *in vitro*, CRTC1/MAML2 negatively affected splicing when compared to full-length CRTC1[39]. However, CRTCs have yet to be shown to regulate mRNA alternative splicing in a physiologically relevant system.

CRTC2

CRTC2 is abundantly expressed in the liver, spleen, and lymph nodes and has been extensively studied for its role in glucose homeostasis. In hepatocytes, the release of glucagon induces CRTC2 activation and CREB regulated transcription of gluconeogenic enzymes that promote glucose output[40]. *In vitro* kinase assays showed that the AMPK family member proteins salt inducible kinase 2 (SIK2) and microtubule affinity regulating kinase 2 (MARK2) phosphorylate CRTC2 at serine-171 (S171) and serine-275 (S275), respectively. Inhibition of phosphorylation at each of these residues through serine to alanine mutations retain CRTC2 in the nucleus while a double mutant containing S171A and S275A (CRTC2-AA) results in the complete nuclear localization and constitutive activation of CRTC2[41, 42].

Work on the role of CRTC2 in lymphocyte biology is limited. In T cells, the CREB-CRTC2 pathway was shown to regulate IL-17 expression. In a CRTC2 knock-out mice, CRTC2 mutant T cells expressed lower levels of IL-17 and exhibited impaired Th17 cell differentiation[43]. Also in T cells, CRTC2 functions to preserve genome integrity as the

loss of CREB and CRTC2 was found to reduce the expression of mismatch repair genes, which resulted in increased mutation frequencies in various T cell lymphomas[44].

Our laboratory previously described a signaling pathway that linked DNA double strand breaks associated with CSR to the inactivation and cytoplasmic localization of CRTC2 in human GC B cells. DNA damage triggers the activation of the DNA damage sensor ataxia-telangiectasia mutated (ATM), which signals through liver kinase B1 (LKB1) and to an AMPK family member protein which phosphorylates CRTC2. Activation of this signaling pathway promotes GC exit and ASC differentiation of human B cells by down-regulating CRTC2 target genes[45]. In addition, we have shown that BCR signaling can also inactivate CRTC2 and down-regulate its target genes in GC B cells[45, 46]. When CRTC2 inactivation was dysregulated through the expression of the constitutively active CRTC2-AA mutant, stimulated B cells maintained expression of CRTC2 target genes which resulted in maintenance of GC markers and increased proliferation. Consequently, the expression of the ASC marker *Prdm1* (BLIMP1) along with antibody secretion was inhibited compared to control B cells[45]. Therefore, we speculated that CRTC2 inactivation initiated by CSR in the GC may potentially function as a physiologic trigger that initiates ASC differentiation. However, it remains unknown when CRTC2 inactivation is critical for ASC formation because activation, proliferation, and PC differentiation are plausible regulatory nodes. Additionally, whether CRTC2 plays a critical role in ASC formation *in vivo* has not been investigated.

This dissertation aims to address the gaps in our understanding of the *in vivo* role of CRTC2 in B cell differentiation and to determine its effects on the generation and

maintenance of long-term humoral immunity. Additionally, this work may provide insights into augmenting antibody responses and providing potential therapeutic targets to inhibit ASCs that generate pathogenic antibodies.

## References


1. Nutt, S.L., Hodgkin, P.D., Tarlinton, D.M. & Corcoran, L.M. The generation of antibody-secreting plasma cells. *Nat Rev Immunol* **15**, 160-171 (2015).

2. Amanna, I.J. & Slifka, M.K. Mechanisms that determine plasma cell lifespan and the duration of humoral immunity. *Immunol Rev* **236**, 125-138 (2010).

3. Cooper, M.D. The early history of B cells. *Nat Rev Immunol* **15**, 191-197 (2015).

4. Bassing, C.H., Swat, W. & Alt, F.W. The mechanism and regulation of chromosomal V(D)J recombination. *Cell* **109 Suppl**, S45-55 (2002).

5. Hoffman, W., Lakkis, F.G. & Chalasani, G. B Cells, Antibodies, and More. *Clin J Am Soc Nephrol* **11**, 137-154 (2016).

6. Melchers, F. Checkpoints that control B cell development. *J Clin Invest* **125**, 2203-2210 (2015).

7. Hardy, R.R. & Hayakawa, K. B cell development pathways. *Annu Rev Immunol* **19**, 595-621 (2001).

8. Cerutti, A., Cols, M. & Puga, I. Marginal zone B cells: virtues of innate-like antibody-producing lymphocytes. *Nat Rev Immunol* **13**, 118-132 (2013).

9. Victora, G.D. & Nussenzweig, M.C. Germinal centers. *Annu Rev Immunol* **30**, 429-457 (2012).

10. Krautler, N.J. *et al.* Differentiation of germinal center B cells into plasma cells is initiated by high-affinity antigen and completed by Tfh cells. *J Exp Med* **214**, 1259-1267 (2017).

11. Tsui, C. *et al.* Protein Kinase C-beta Dictates B Cell Fate by Regulating Mitochondrial Remodeling, Metabolic Reprogramming, and Heme Biosynthesis. *Immunity* **48**, 1144-1159 e1145 (2018).

12. Jang, K.J. *et al.* Mitochondrial function provides instructive signals for activation-induced B-cell fates. *Nat Commun* **6**, 6750 (2015).

13. Hasbold, J., Corcoran, L.M., Tarlinton, D.M., Tangye, S.G. & Hodgkin, P.D. Evidence from the generation of immunoglobulin G-secreting cells that stochastic mechanisms regulate lymphocyte differentiation. *Nat Immunol* **5**, 55-63 (2004).

14. Shi, W. *et al.* Transcriptional profiling of mouse B cell terminal differentiation defines a signature for antibody-secreting plasma cells. *Nat Immunol* **16**, 663-673 (2015).

15. Tellier, J. *et al.* Blimp-1 controls plasma cell function through the regulation of immunoglobulin secretion and the unfolded protein response. *Nat Immunol* **17**, 323-330 (2016).

16. Hetz, C. The unfolded protein response: controlling cell fate decisions under ER stress and beyond. *Nat Rev Mol Cell Biol* **13**, 89-102 (2012).

17. Peperzak, V. *et al.* Mcl-1 is essential for the survival of plasma cells. *Nat Immunol* **14**, 290-297 (2013).

18. Sciammas, R. *et al.* Graded expression of interferon regulatory factor-4 coordinates isotype switching with plasma cell differentiation. *Immunity* **25**, 225-236 (2006).

19. Diaz-Munoz, M.D. *et al.* The RNA-binding protein HuR is essential for the B cell antibody response. *Nat Immunol* **16**, 415-425 (2015).

20. Akkaya, M. & Pierce, S.K. From zero to sixty and back to zero again: the metabolic life of B cells. *Curr Opin Immunol* **57**, 1-7 (2019).

21. Waters, L.R., Ahsan, F.M., Wolf, D.M., Shirihai, O. & Teitell, M.A. Initial B Cell Activation Induces Metabolic Reprogramming and Mitochondrial Remodeling. *iScience* **5**, 99-109 (2018).

22. Price, M.J., Patterson, D.G., Scharer, C.D. & Boss, J.M. Progressive Upregulation of Oxidative Metabolism Facilitates Plasmablast Differentiation to a T-Independent Antigen. *Cell Rep* **23**, 3152-3159 (2018).

23. Pengo, N. *et al.* Plasma cells require autophagy for sustainable immunoglobulin production. *Nat Immunol* **14**, 298-305 (2013).

24. Cassese, G. *et al.* Plasma cell survival is mediated by synergistic effects of cytokines and adhesion-dependent signals. *J Immunol* **171**, 1684-1690 (2003).

25. Bortnick, A. *et al.* Long-lived bone marrow plasma cells are induced early in response to T cell-independent or T cell-dependent antigens. *J Immunol* **188**, 5389-5396 (2012).

26. Mahevas, M. *et al.* B cell depletion in immune thrombocytopenia reveals splenic long-lived plasma cells. *J Clin Invest* **123**, 432-442 (2013).

27. Chernova, I. *et al.* Lasting antibody responses are mediated by a combination of newly formed and established bone marrow plasma cells drawn from clonally distinct precursors. *J Immunol* **193**, 4971-4979 (2014).

28. Bortnick, A. & Allman, D. What is and what should always have been: long-lived plasma cells induced by T cell-independent antigens. *J Immunol* **190**, 5913-5918 (2013).

29. Wilmore, J.R., Jones, D.D. & Allman, D. Protocol for improved resolution of plasma cell subpopulations by flow cytometry. *Eur J Immunol* **47**, 1386-1388 (2017).

30. Halliley, J.L. *et al.* Long-Lived Plasma Cells Are Contained within the CD19(-)CD38(hi)CD138(+) Subset in Human Bone Marrow. *Immunity* **43**, 132-145 (2015).

31. Lam, W.Y. & Bhattacharya, D. Metabolic Links between Plasma Cell Survival, Secretion, and Stress. *Trends Immunol* **39**, 19-27 (2018).

32. Nickens, K.P., Wikstrom, J.D., Shirihai, O.S., Patierno, S.R. & Ceryak, S. A bioenergetic profile of non-transformed fibroblasts uncovers a link between death-resistance and enhanced spare respiratory capacity. *Mitochondrion* **13**, 662-667 (2013).

33. Lam, W.Y. *et al.* Mitochondrial Pyruvate Import Promotes Long-Term Survival of Antibody-Secreting Plasma Cells. *Immunity* **45**, 60-73 (2016).

34. Lam, W.Y. *et al.* Metabolic and Transcriptional Modules Independently Diversify Plasma Cell Lifespan and Function. *Cell Rep* **24**, 2479-2492 e2476 (2018).

35. Altarejos, J.Y. & Montminy, M. CREB and the CRTC co-activators: sensors for hormonal and metabolic signals. *Nat Rev Mol Cell Biol* **12**, 141-151 (2011).

36. Conkright, M.D. *et al.* TORCs: transducers of regulated CREB activity. *Mol Cell* **12**, 413-423 (2003).

37. Iourgenko, V. *et al.* Identification of a family of cAMP response element-binding protein coactivators by genome-scale functional analysis in mammalian cells. *Proc Natl Acad Sci U S A* **100**, 12147-12152 (2003).

38. Tasoulas, J., Rodon, L., Kaye, F.J., Montminy, M. & Amelio, A.L. Adaptive Transcriptional Responses by CRTC Coactivators in Cancer. *Trends Cancer* **5**, 111-127 (2019).

39. Amelio, A.L., Caputi, M. & Conkright, M.D. Bipartite functions of the CREB co-activators selectively direct alternative splicing or transcriptional activation. *EMBO J* **28**, 2733-2747 (2009).

40. Koo, S.H. *et al.* The CREB coactivator TORC2 is a key regulator of fasting glucose metabolism. *Nature* **437**, 1109-1111 (2005).

41. Jansson, D. *et al.* Glucose controls CREB activity in islet cells via regulated phosphorylation of TORC2. *Proc Natl Acad Sci U S A* **105**, 10161-10166 (2008).

42. Screaton, R.A. *et al.* The CREB coactivator TORC2 functions as a calcium- and cAMP-sensitive coincidence detector. *Cell* **119**, 61-74 (2004).

43. Hernandez, J.B. *et al.* The CREB/CRTC2 pathway modulates autoimmune disease by promoting Th17 differentiation. *Nat Commun* **6**, 7216 (2015).

44. Fang, M. *et al.* The CREB Coactivator CRTC2 Is a Lymphoma Tumor Suppressor that Preserves Genome Integrity through Transcription of DNA Mismatch Repair Genes. *Cell Rep* **11**, 1350-1357 (2015).

45. Sherman, M.H. *et al.* AID-induced genotoxic stress promotes B cell differentiation in the germinal center via ATM and LKB1 signaling. *Mol Cell* **39**, 873-885 (2010).

46. Kuraishy, A.I. *et al.* TORC2 regulates germinal center repression of the TCL1 oncoprotein to promote B cell development and inhibit transformation. *Proc Natl Acad Sci U S A* **104**, 10175-10180 (2007).

# CHAPTER 2:

# CRTC2 regulates plasma cell metabolism and survival

# CRTC2 regulates plasma cell metabolism and survival

Jason S. Hong[1], Fasih M. Ahsan[1,8], Peter D. Pioli[1,9], Min-sub Lee[2], Thang L. Nguyen[3], David G. Brooks[4,10], Justin Golovato[5], Kayvan R. Niazi[6], and Michael A. Teitell*[1,3,7]

[1]Department of Pathology and Laboratory Medicine, David Geffen School of Medicine, University of California, Los Angeles, CA, USA

[2]Department of Molecular and Medical Pharmacology, David Geffen School of Medicine, University of California, Los Angeles, CA, USA

[3]Department of Bioengineering, University of California, Los Angeles, CA, USA

[4]Department of Microbiology, Immunology, and Molecular Genetics, David Geffen School of Medicine, University of California, Los Angeles, CA, USA

[5]NantOmics, LLC, Culver City, CA, USA

[6]ImmunityBio, Culver City, CA, USA

[7]Jonsson Comprehensive Cancer Center, Molecular Biology Interdepartmental Program, California NanoSystems Institute, Department of Pediatrics, and Broad Center for Regenerative Medicine and Stem Cell Research, University of California, Los Angeles, CA, USA

[8]Current address: Program in Biological and Biomedical Sciences, Harvard Medical School, Boston, MA, 02215, USA

[9]Current address: Department of Biomedical Sciences, Center for Immunobiology, Homer Stryker M.D. School of Medicine, Kalamazoo, MI 49007, USA

[10]Current address: Princess Margaret Cancer Center, University Health Network, Toronto, ON, M5G 2M9 Canada

*Corresponding author: e-mail: mteitell@mednet.ucla.edu; tele: 310-206-6754; fax: 310-267-0392

**Abstract**

Antibody secreting cell (ASC) function and longevity determines the strength and durability of a humoral immune response. Using transgenic (TG) mice that express a constitutively active form of the CREB coactivator CRTC2 (*Crtc2-AA*), we demonstrate that *Crtc2* repression in plasma cells (PCs) is an intrinsic requirement for ASC metabolic fitness. Sustained CRTC2 activity shortens the survival of splenic and bone marrow PCs, resulting in reduced numbers of long-lived PCs and antibody deficits against T-dependent and T-independent antigens, and an acute viral infection. TG PCs adopt a short-lived PC phenotype as shown by reduced antibody secretion, glycolysis, oxidative metabolism, and spare respiratory capacity. Mechanistically, *Crtc2* repression is necessary for the fidelity of PC gene expression and mRNA alternative-splicing programs, with both programs altered in TG PCs. Combined, *Crtc2* repression in PCs must occur to support PC metabolism and extend ASC survival and lifespan during a humoral immune response.

## Introduction

In secondary lymphoid tissues, B cell activation in response to certain antigens can result in the rapid differentiation of transient plasmablasts (PBs) that localize to extrafollicular regions and mature into predominantly short-lived plasma cells (SLPCs). These antibody secreting cells (ASCs) typically produce an initial wave of low-affinity antigen-specific antibodies[1]. In comparison, primary follicular B cells activated by a T cell dependent (TD) antigen at the T:B border zone can rapidly expand within B cell follicles to form germinal centers (GCs). GC B cells undergo both extensive proliferation and antigen-driven affinity maturation resulting in the formation of plasma cells (PCs) that secrete high-affinity isotype-switched antibodies. These cells can then migrate to the bone marrow and become long-lived PCs (LLPCs)[2]. Antibody quality and the duration of antibody production are major determinants of protection against target pathogens and maintenance of long-term humoral immunity[3]. Unfortunately, the production of pathogenic PCs can also generate autoantibodies that participate in a range of autoimmune disorders[4]. Identifying factors that regulate PC differentiation, function, and survival could improve vaccine design and uncover potential strategies to eliminate the production and/or maintenance of pathogenic PCs.

To generate ASCs, extensive epigenetic, transcriptional, and metabolic remodeling must occur to terminate B cell and GC B cell specification and maintenance programs, coupled with induction of ASC differentiation[5, 6, 7]. Differing in their ontogeny, localization, function, and lifespan, ASCs are present as a heterogenous and diverse population. RNA expression profiling of splenic PCs that are enriched for SLPCs and bone marrow PCs that are enriched for LLPCs failed to identify wholesale transcriptional changes that could explain phenotypic differences in SLPC and LLPC longevity[8]. Instead, LLPCs were shown to develop a unique metabolic program that results in enhanced glucose import as well as increased pyruvate utilization for mitochondrial oxidative metabolism during times of stress[9]. How this metabolic program is

initiated and maintained in LLPCs is currently unknown. The lack of candidate gene expression differences between SLPCs and LLPCs that underlie differences in survival or longevity may suggest non-transcriptional or extrinsic factors. However, because of heterogeneity in the ASC population, meaningful mRNA transcript differences may actually exist that are muted within this heterogeneity and therefore overlooked.

Identified over a decade ago, a family of three cAMP response element binding protein (CREB)-regulated transcription coactivators (CRTC1 – 3) control gene expression and several additional biological processes[10, 11, 12]. Extracellular and intracellular signals phosphorylate CRTC family proteins, which influences their subcellular localization[13, 14]. CRTC proteins lacking phosphorylation at specific residues localize in the nucleus where they can bind to CREB and additional bZIP transcription factors to regulate gene expression for processes such as energy homeostasis, metabolism, and lifespan[11, 12]. Previously, we showed that CRTC2 phosphorylation in an *in vitro* B cell differentiation model caused CRTC2 inactivation by cytoplasmic re-localization, which triggered B cells to lose their GC-like identity and differentiate into ASCs[15]. Using isolated B cells, DNA damage during *immunoglobulin* (*Ig*) class switch recombination (CSR) initiated a signaling cascade involving ATM, LKB1, and an AMPK family member protein that phosphorylated and inactivated CRTC2 to down-regulate its gene regulatory network. Failed CRTC2 inactivation caused GC B cell biomarkers to remain elevated and inhibited ASC biomarker acquisition and antibody secretion. However, it remains unknown when CRTC2 inactivation is critical for ASC formation because activation, proliferation, and PC differentiation are plausible regulatory nodes. Additionally, whether CRTC2 plays a critical role in ASC formation *in vivo* has not been investigated.

To examine CRTC2 in B cell physiology, we generated transgenic (TG) mice that express constitutively active, nucleus-localized CRTC2 throughout B cell development. Here, we report on this unique CRTC2 TG mouse model and the unexpected result that CRTC2

inactivation in PCs is required for ASC survival, yielding at least a partial mechanism to explain the longevity of the humoral immune response.

**Results**

***Crtc2* expression in B cells is repressed during PC differentiation.** Initially, we examined the expression of CRTC2 in isolated, naïve splenic B cells from wild-type (WT) C57BL/6 mice stimulated with CD40L and IL-4, conditions that resemble a TD immune response[16, 17]. At early timepoints post-stimulation, CRTC2 lacked phosphorylation. By 24h post-stimulation, approximately half of the CRTC2 protein was phosphorylated, followed by a progressive reduction of total CRTC2 protein through day 5 of stimulation (**Fig. 1a**). Consistent with progressively reduced CRTC2 protein, *Crtc2* mRNA expression was repressed over the differentiation assay time course (**Fig. 1b**). At day 5, when CRTC2 expression was at its lowest, we observed the robust differentiation of activated B cells into $B220^{-}$ $CD138^{+}$ PCs as identified by flow cytometry (**Fig. 1c**). Additionally, we observed a 6-fold induction of *Prdm1*, encoding the ASC master regulator protein BLIMP1, in this bulk differentiation assay (**Fig. 1d**). These results show that CRTC2 inactivation by protein phosphorylation and transcriptional repression occurs during the transition from early B cell activation through PC formation.

**Generation of an *in vivo* model to study *Crtc2* repression in PCs.** To study potential roles for CRTC2 in mature B cells *in vivo*, we generated a TG mouse model that expresses a nucleus-localized, constitutively active form of CRTC2, generated with S171A and S275A amino acid substitutions in the transgene (*Crtc2-AA*)[14, 15, 18]. The *Crtc2-AA* transgene is under *B29* (*Ig*$\beta$) minimal promoter and *IgH* intronic enhancer (*E*$\mu$) control (**Supplementary Fig. 1a**). Previously, we showed that this promoter-enhancer combination enables transgene expression from pro-B through PC stages of B cell differentiation[19, 20]. Three founder mice were generated with a range of *Crtc2-AA* transgene expression. Two founder lines (F2 and F3) reproducibly showed 3-fold

higher levels of *Crtc2-AA* expression in the bone marrow than the third founder line (F1) (**Supplementary Fig. 1b**). We analyzed bone marrow B lymphocyte development using flow cytometric analysis of the cell surface markers B220, CD43, and IgM. Founder line F1, with modest total (endogenous and transgene) *Crtc2* overexpression in the bone marrow (1.4-fold compared to WT) (**Fig. 2a**), demonstrated normal production of pro-B ($B220^+$ $IgM^-$ $CD43^+$), pre-B ($B220^+$ $IgM^-$ $CD43^-$), immature ($B220^+$ $IgM^+$), and mature $B220^{hi}$ $IgM^+$ B lymphocytes compared to WT mice (**Fig. 2b**). In contrast, founders F2 and F3 demonstrated a significant reduction in bone marrow B lymphopoiesis (**Supplementary Fig. 1c**). While interesting, F2 and F3 founder lines were not examined further because of this impairment in early B cell development. F1 lineage mice showed total *Crtc2* expression that was 3.4-fold higher in the spleen compared to WT mice (**Fig. 2a**), and F1 lineage spleens possessed similar total numbers of follicular ($B220^+$ $CD19^+$ $CD23^+$ $CD21^-$) and marginal zone ($B220^+$ $CD19^+$ $CD23^-$ $CD21^+$) B cells as WT controls (**Fig. 2c**). Finally, low level Igβ (encoded by *B29*) expression was reported in early thymocyte development[21]. However, total *Crtc2* expression was not significantly increased in F1 thymocytes (**Fig. 2a**) and T lineage cell numbers in F1 thymus and spleen were similar to WT controls (**Fig. 2d,e**). Thus, B and T cell development appeared similar between F1 TG and WT mice.

To exclude transgene insertion site issues in F1 lineage mice, we performed whole genome sequencing and identified two distinct *Crtc2-AA* genome integration sites. One integration site was in a region of the mouse genome lacking any genes and the second site was in a large intronic region of a gene (*1110051M20Rik*) with no functional annotation (**Supplementary Fig. 1d**). This second transgene integration had no affect on the expression of the annotated gene as determined by RNA sequencing (RNA-seq) of TG and WT B cells (**Supplementary Table 1**).

Next, we examined the level of *Crtc2* expression in activated B cells. We stimulated naïve, isolated splenic B cells with CD40L, IL-4, and IL-5 for 5 days to increase the number of PCs obtained[17]. On day 5, stimulated B cells were sorted into early division (0-3), late division (5 or more), and PC subpopulations based on CFSE dye dilution and expression of the ASC cell surface marker CD138[22] (**Supplementary Fig. 1e**). We further validated the identity of our *in-vitro* derived and sorted PCs by comparing expression profiles to *in vivo* derived PC gene signatures[22] (data not shown). RNA-seq of naïve B cell controls and sorted, stimulated B cell subpopulations revealed stable endogenous *Crtc2* expression in naïve, early, and late division B cell subsets, along with robust *Crtc2* repression in WT PCs (**Supplementary Fig. 1f**). By contrast, *Crtc2-AA* TG B cells showed minimally elevated total *Crtc2* expression in naïve and early division B cell subsets, with 1.4-fold and 4.4-fold increased expression in late division and PC subpopulations, respectively (**Supplementary Fig. 1f)**. Induced expression of total *Crtc2* in TG PCs is consistent with increased enhancer activity known to elevate *Ig* gene expression at the PC stage of B cell differentiation[23]. These data validate our *Crtc2-AA* TG model that replicates expected transgene expression throughout B cell differentiation and provides sustained, over-expressed *Crtc2-AA* transcripts specifically in PCs, the stage in differentiation where endogenous *Crtc2* is strongly repressed.

**CRTC2 repression enables PC survival and humoral immune responses.** Our prior *in vitro* studies showed that aberrantly sustained CRTC2 activity following B cell activation caused a defect in ASC differentiation[15]. However, this pure B cell model left open the key question about the main role(s) for CRTC2 repression during an *in vivo* immune response. Analysis of the ASC population in naïve unimmunized mice revealed a significant decrease in the splenic PC population, while the PB population was unaffected in TG mice compared to WT controls (**Fig. 3a**). Further analysis of the serum of naïve mice revealed lower Ig titers in TG compared to WT

mice for all isotypes, except for IgA (**Fig. 3b**). Next, we immunized mice with TNP-Ficoll to induce a T cell independent (TI) immune response. TNP-specific IgM titers in the serum were 7-fold lower in TG compared to WT mice 7 days post-immunization (**Fig. 3c**). Mice were also immunized with NP-CGG in alum to induce a TD immune response. At 14 days post-immunization, NP-specific IgM and IgG1 titers were 2.7- and 6-fold lower in the serum of TG compared to WT mice, respectively (**Fig. 3d**). At 35 days, NP-specific serum IgG1 levels remained significantly lower in TG compared to WT mice, revealing that reduced Ig levels are not due to slower ASC differentiation in TG B cells (**Fig. 3d**). We also infected mice with the acute Armstrong strain of lymphocytic choriomeningitis virus (LCMV) to analyze the antiviral B cell response. This viral strain produces a vigorous T cell response that clears the infection 8 – 10 days post-infection but also elicits a robust TD B cell response, which generates LLPCs[24, 25]. Analysis of the spleen 8 days post-infection revealed a sharp reduction in the percentage of PCs in TG mice (**Fig. 3e**), along with a marked reduction in Ig titers for both total and LCMV-specific IgG compared to WT control mice (**Fig. 3f,g**).

We then performed ELISPOT assays to enumerate ASC frequencies, where each spot within an assay well represents an ASC whose spot intensity and/or size indicates the amount of antibody secreted. Consistent with reduced splenic PC numbers in naïve mice and reduced Ig titers, splenic ASCs generated from TI immunizations were reduced over time in TG compared to WT mice (**Supplementary Fig. 2a,b**). Of note, although there is no statistical difference in ASC numbers at day 7, a difference in spot intensities, with blue spots being most intense, was detected between WT and TG ASCs (**Supplementary Fig 2a,b**). By day 14 however, only blue spots are left remaining, resulting in a reduction in splenic ASCs in TG compared to WT mice (**Supplementary Fig 2a,b**). In ASCs generated from a TD response, there was also a dependence on time and spot intensity in ASC results. IgM specific ASCs were reduced in number from the spleen of TG compared to WT mice (**Supplementary Fig. 2c,d**).

For IgG1-secreting ASCs however, although statistically similar in number between TG and WT mice, TG IgG1 ASCs exhibited less intense spots than WT IgG1 ASCs (**Supplementary Fig. 2c,d**). For more mature ASCs, those representing PCs that have migrated into the bone marrow, both IgM- and IgG1-secreting PCs were reduced in number in TG compared to WT mice (**Supplementary Fig. 2e,f**). Interestingly, a recent report showed that LLPCs imported more glucose and secreted more antibodies than SLPCs, linking antibody secretion levels to length of PC survival[9, 26]. Observations of spots with varying intensities indicated heterogeneous populations of ASCs with different levels of antibody secretion and potentially different levels of glucose import. Thus, the data show that CRTC2 inactivation and repression in PCs supports the function and maintenance and by extension, possibly the length of PC survival.

To determine whether sustained *Crtc2-AA* expression effects were cell intrinsic, isolated naïve splenic B cells were activated *in vitro* with CD40L, IL-4, and IL-5. A time-course analysis of PC formation and/or persistence revealed that the reduction in ASC numbers and humoral immune responses were cell intrinsic, as TG PCs decreased over the course of stimulation, ending with a reduction from 37.3 to 18.4 percent PCs at day 5 (**Fig. 3h**). The decrease in TG compared to WT PCs is not related to changes in B cell activation, proliferation, GC formation, or CSR during B cell differentiation (**Supplementary Fig. 3**). Instead, we found that CRTC2 inactivation supported the survival of B cells in an advanced stage of differentiation, as the number of stimulated TG B cells were reduced in a division dependent manner compared to WT controls (**Fig. 3i**). Quantification of cell numbers by flow cytometry gating on early divisions, late divisions, and PC subpopulations revealed a significant decrease in cell numbers only for PCs, indicating that the difference in cell death occurs at a differentiation stage where CRTC2 is markedly repressed but is instead sustained in active form by the *Crtc2-AA* transgene (**Supplementary Fig. 1f** and **Fig. 3j**). Consistent with increased cell death detected by flow cytometry, immunoblot analysis with band densitometry also showed an increase in expression

of the pro-apoptotic biomarkers cleaved PARP and cleaved caspase-3 in TG compared to WT stimulated B cells (**Fig. 3k**). With the loss of *in vitro* generated PCs (**Fig. 3h**) and a reduction in splenic and bone marrow ASCs over time (**Supplementary Fig. 2**), TG PCs exhibit an intrinsic survival defect. Thus, physiologic CRTC2 inactivation and repression is required for PC survival in the spleen and bone marrow, directly affecting the generation of a robust, long-lived (**Supplementary Fig. 2**) humoral immune response.

**CRTC2 regulates mature B cell mRNA transcription and splicing.** To gain insight into reduced PC survival with sustained *Crtc2-AA* expression, we performed RNA-seq on naïve and sorted early division, late division, and PC TG and WT B cell subpopulations (**Supplementary Fig. 1e**). Principle-component analysis (PCA) of the RNA-seq data showed that each replicate within a given subpopulation clustered together, as expected, and that TG and WT B cell subsets were similar until modest separation occurred in the PC subpopulation (**Fig. 4a**). In concordance, *Crtc2-AA* induced the largest number of transcript differences for TG versus WT cells at the PC stage, with 767 differentially expressed genes (p-adj $< 0.05$). Most differential genes were up-regulated (502/767, 65%), consistent with the established role of CRTCs as transcription coactivators (**Fig. 4b, Supplementary Table 1**)[11]. By contrast, 38, 54, and 26 genes were differentially-expressed in naïve, early division, and late division subpopulations, respectively (p-adj $< 0.05$) (**Fig. 4b, Supplementary Table 1**). Of the differentially-expressed genes within the PC subpopulation, 192 had >|2|-fold ($Log_2$ fold > |1|) changes in expression (**Fig. 4c**). Key regulators of B cell fate and survival, such *as Prdm1*, *Irf4*, and *Mcl1* showed no significant differences in TG compared to WT PCs [22, 27, 28, 29] (**Fig. 4d**). However, *Cd28*, a costimulatory protein expressed in activated T cells and ASCs, was repressed 2.6-fold in TG compared to WT PCs[30, 31, 32] (**Fig. 4d**). CD28 regulates mitochondrial metabolism in T cells and while being a pro-survival factor for LLPCs in the bone marrow, is dispensable for the survival of

splenic SLPCs[33]. Gene set variation analysis (GSVA) also showed no differences between TG and WT subpopulations for BLIMP1 and IRF4 target genes, unfolded protein response (UPR) genes, and canonical early activation, GC, and ASC gene signatures (**Fig. 4e**) [27, 29]. In addition, analysis of all *Ig* transcripts between TG and WT B cell subpopulations were similar, indicating that the observed reduction in Ig secretion in TG ASCs by ELISPOT assay was not from changes in transcript levels (**Supplementary Table 1**).

To identify candidate biological processes influenced by CRTC2 in PCs, we examined differentially expressed genes in the PC subpopulation by KEGG pathway analysis. The top three significantly enriched pathways were DNA replication, cell cycle, and spliceosome genes (**Fig. 4f**). Recent reports show a role for alternative splicing in B cell fate, prompting an assessment of CRTC2 in alternative splicing during B cell differentiation[34, 35, 36, 37]. CRTCs do not contain conserved RNA binding domains, although one *in vitro* study in non-immune cells suggests that CRTCs may regulate mRNA splicing[11, 38]. It remains unknown, however, whether CRTC2 impacts mRNA splicing in activated B cells maturing into PCs. Analysis of the RNA-seq data revealed significant alterations (by >10%) in the splicing of 604 TG versus WT genes, most of which occurred in the PC subpopulation that favored skipped exons (SE) (**Fig. 4g and Supplementary Table 2**). Of note, only 33 (2.3%) of gene transcripts were altered by both expression and splicing between TG and WT B cells (**Fig. 4h**). Alternatively spliced genes were enriched for those that modify histones, contain methyltransferase activity, and those involved in organelle biogenesis (**Fig. 4i**). Genes including *Cep89*, *Ndufaf7*, and *Sirt3* have known roles in regulating mitochondrial metabolism while epigenetic modifiers such as *Dnmt3b* regulate B cell differentiation[39, 40, 41, 42]. Thus, CRTC2 independently regulates gene expression and mRNA splicing and its repression mediates the fidelity of these processes at the PC stage of B cell differentiation.

***Crtc2* repression increases oxidative metabolism.** CRTCs have established roles in energy homeostasis and mitochondrial metabolism [43, 44] and our data shows that CRTC2 controls mRNA expression and splicing associated with mitochondrial metabolism (e.g. *Cd28, Cep89, Ndufaf7, Sirt3* transcripts) in PCs. A selective GSVA for metabolism regulating genes revealed that TG PCs show a metabolic gene expression profile similar to late dividing WT and TG PC precursors that clustered distinctly from WT PCs (**Fig. 5a**). To determine whether TG and WT PCs were metabolically distinct, we measured the cellular oxygen consumption rate (OCR) and extracellular acidification rate (ECAR) as surrogates for mitochondrial respiration and glycolysis using a Seahorse Extracellular Flux Analyzer. OCR measurements on sorted *in vitro* derived $CD138^+$ PCs revealed similar basal respiration with reduced maximal respiration and reduced spare respiratory capacity (SRC) for TG compared to WT PCs (**Fig. 5b**,**c**,**d**,**e**). Cells utilize SRC during conditions of increased work or stress and LLPCs show increased SRC[45]. Interestingly, suppressed pyruvate generation and/or mitochondrial pyruvate import also reduces SRC, which leads to progressive loss of LLPCs in the bone marrow[9]. ECAR measurements in TG PCs also trend lower than the WT control, suggesting less available pyruvate for glycolysis or oxidative metabolism (**Fig. 5f**).

Consistent with reduced ECAR, steady-state metabolomics of bulk day 5 *in vitro* stimulated TG and WT B cells showed a decrease in the glycolytic metabolites fructose 1,6-bisphoshate (F16BP) and dihydroxyacetone phosphate (DHAP), and a reduction in the end product of the hexosamine biosynthetic pathway, UDP-GlcNAc, which is required for Ig glycosylation (**Fig. 5g**). TG B cells also showed an increase in $\alpha$-ketoglutarate and succinate compared to WT PCs (**Fig. 5g**). These data indicate that CRTC2 repression is required for increased oxidative metabolism and may regulate metabolic pathway activities in PCs, which could impact PC survival and function.

## Discussion

Our results demonstrate the requirement for physiologic *Crtc2* repression in PCs in order to maintain a humoral immune response. Elevated expression of a *Crtc2-AA* transgene at this stage in differentiation reduced the survival of PCs, resulting in humoral immune deficits against model antigens and an acute viral infection. Differentiation into PBs, however, is unaffected by CRTC2-AA, as naïve TG mice have similar numbers of splenic PBs as WT mice. In addition, similar numbers and frequencies of ASCs generated by immunizations and *in vitro* differentiation, respectively, at early timepoints further shows that the defect in survival lies within the more mature PC population. Our results were not specific to a particular type of immune stimulus as both TI and TD immune responses required the inactivation of CRTC2 for establishment of the mature PC pool. This suggests a generalized and critical need to suppress CRTC2 to generate PCs regardless of eliciting antigen. Perhaps this is not surprising as both TI and TD responses have been shown to generate LLPCs in the bone marrow[46].

The metabolic requirements of PCs differ from those of activated B cells and differentiating PBs. Instead of using energy and biosynthetic pathways for nucleotide synthesis and organelle biogenesis, PCs switch their metabolism to support antibody production[7]. Interestingly, our studies showed that repression of *Crtc2* in PCs is necessary for fidelity of PC gene expression and mRNA alternative-splicing programs. When these processes are altered by sustained CRTC2-AA activity, TG PCs show reductions in antibody secretion, glycolysis, oxidative phosphorylation, and SRC essentially adopting a SLPC-like phenotype[26]. Combined, the data suggest that CRTC2, and/or its affected non-overlapping gene and splicing targets, control metabolic programs required for mature PC survival and establishment of LLPCs in the bone marrow to sustain a long-term humoral immune response.

CD28, which is expressed in PCs and is critical for LLPC survival, is repressed nearly 2.6-fold in TG PCs[33]. In T cells, CD28 activation establishes SRC and increases glycolysis and

oxidative phosphorylation in memory T cells[47]. Similar phenotypic effects observed in WT PCs may suggest that CD28 controls similar functions in PCs to regulate LLPC survival. Reduced oxidative phosphorylation in TG PCs may also be associated with a 2-fold reduction in the expression of *Aldoc*, a key glycolytic enzyme necessary for generating mitochondrial pyruvate. TG PCs show a 3.5-fold over-expression of the solute carrier *Slc1a2*, which has high affinity for glutamate. In addition, *Glud1,* the mitochondrial glutamate dehydrogenase that converts L-glutamate into $\alpha$-ketoglutarate, is aberrantly spliced in TG PCs. These changes imply that reduced pyruvate generation through the glycolytic pathway in TG PCs is partially compensated through glutamine anaplerosis with incomplete recovery of respiration as shown by our OCR studies. TG PCs also aberrantly splice mRNA transcripts compared to WT PCs that associate with electron transport chain (ETC) complex activity and formation, suggesting that alterations in ETC activity may also contribute to impaired oxidative phosphorylation and reduced SRC in TG PCs, which would inhibit the previously demonstrated metabolic changes required to generate LLPCs.

Based on reductions in survival, antibody secretion, glycolysis, and oxidative phosphorylation in TG ASCs, we speculate that WT SLPCs might express more *Crtc2* transcripts than WT LLPCs because of strong similarities to the *Crtc2-AA* mouse model. Consistent with this prediction, independent RNA-seq profiling of PC subsets with different half-lives[26] showed highest *Crtc2* expression in the shortest half-life PC subset and the lowest expression in the longest half-life PC subset (**Fig. 6a**). Unfortunately, this data mining difference in *Crtc2* mRNA transcripts trended but was not statistically significant between PC subsets. Of note, the PC subsets analyzed were not pure populations because of current technical limitations in identifying PC heterogeneity and isolating these populations, and thus may account for the lack of statistical significance in *Crtc2* expression despite a clear trend [26]. Our prior signaling studies showed that CRTC2 inactivation by phosphorylation and cytoplasmic re-

localization in B cells initiates through engagement of the B cell antigen receptor (BCR) and/or through DNA double-stranded breaks during *IG* CSR[15, 48]. These prior results, coupled with reduced *Crtc2* expression during PC generation shown here, yields a conceptual framework in which the level of CRTC2 activity in PCs helps to establish a metabolic profile supporting PC function and longevity through numerous, modest but essential effects on gene expression and mRNA transcript splicing (**Fig. 6b**).

In prior studies, we showed that CRTC2-AA over-expression in isolated and stimulated human B cells blocked ASC differentiation by maintaining activated B cells in a GC-like state. The difference in outcome between those results and our report here may relate to differential biological functions of CRTC2 at different stages of B cell development. This is similar to BCL6, which regulates self-renewal in pre-B cells but functions to regulate survival in GC B cells[49]. We speculate that when CRTC2-AA expression is enforced in early activated human B cells, ASC differentiation is blocked, whereas enforced CRTC2-AA expression in mouse PCs results in altered metabolism and a survival defect. Interestingly, IRF4, which also has multiple roles in B cells[29, 50], was recently shown to be required in PCs to maintain mitochondrial homeostasis; providing a potential explanation for the requirement for IRF4 in PC survival[51]. In our TG model, the major ASC transcriptional regulators including IRF4 are unaffected, suggesting that factors downstream or independent of these major regulators are necessary to regulate PC metabolism.

Although discovered over a decade ago, new roles in physiology and disease are being attributed to the CRTC family[12, 43]. Our study shows that *Crtc2* repression is critical for PC function, survival, and lifespan. The impact of CRTC2 activity on PC metabolism and its role in regulating ASC survival and longevity may open new avenues for modulating humoral immune responses.

## Methods

### Reagents, antibodies, and oligonucleotides

This information is provided in **Supplementary Table 4**.

### Mice and animal procedures

*Crtc2-AA* transgenic mice were derived by pronuclear injection of C57BL/6 mouse embryos at the UCLA and UCI transgenic mouse facilities. Briefly, the mouse *Crtc2* coding sequence with introduced S171A and S275A alterations was cloned into a *B29* minimal promoter, *IgH* intronic enhancer ($E\mu$) expression plasmid[20]. The plasmid was injected into the pronucleus of mouse embryos and then implanted in a surrogate dam for gestation. F0 generation pups were selected for transgene integration through tail biopsy and PCR analysis and three founder lines were identified. For *in vivo* experiments, mice were immunized by intraperitoneal administration of 2 x $10^8$ sheep red blood cells (Colorado Serum Company), 25 ug of 2,4,6-Trinitrophenyl (TNP)-aminoethylcarboxymethyl-ficoll (AECM-Ficoll) (Biosearch Technologies), or 50 ug of alum-precipitated 4-Hydroxy-3-nitrophenylacetyl (NP)-chicken gamma globulin (CGG) (Biosearch Technologies). For viral infections, mice were inoculated intravenously with 2 x $10^6$ plaque forming units of the LCMV Armstrong strain. Virus stocks were prepared and viral titers were quantified as described[52]. Mouse experiments were conducted on mixed-sex mice between 8-12 weeks of age. No animals were excluded due to a lack of responsiveness to immunization or infection. Randomization, but not experimental blinding to sample identity was used for these studies. All animals were housed in a pathogen-free animal facility at UCLA and all procedures were performed with approval from the UCLA Animal Research Committee (#1998-113-63).

### Enzyme-linked immunosorbent (ELISA) & enzyme-linked immunospot (ELISPOT) assays

Serum Ig and TNP- and NP-specific antibodies were detected by ELISA as described[53]. TNP- and NP-specific ASCs were detected by ELISPOT assay. Briefly, MultiScreen HTS-HA filter plates (Millipore) for ELISPOT assays were prepared with 35% ethanol and then coated overnight at 4 °C with TNP-BSA or NP-BSA (Biosearch Technologies). Plates were washed and subsequently blocked at 37 °C with complete culture media prior to plating and culturing splenocytes or bone marrow cells for 18 h at 37 °C. Plates were washed with PBS-Tween (0.05%) and double-distilled water to remove cells before being incubated with alkaline phosphatase-conjugated anti-mouse IgM or anti-mouse IgG1 (Southern Biotech) for 2 h at room temperature. Plates were then washed with PBS-Tween (0.05%) and PBS before developing with BCIP/NBT blue substrate (Southern Biotech). Spots were imaged with an ImmunoSpot Analyzer (Cellular Technologies Ltd.) and quantified using ImageJ.

**B cell isolation and cell culture**

Whole spleens were mechanically disassociated through a 40 μm filter followed by red blood cell lysis with ammonium-chloride-potassium lysing buffer. Naïve mature B cells were isolated from spleen cells by immunomagnetic negative selection with anti-CD43 (Miltenyi Biotec). B cells were cultured in RPMI-1640 medium (Corning) supplemented with 10% FBS (Gibco), 1% penicillin/streptomycin (Corning), 1% MEM non-essential amino acids (Gibco), 1% sodium-pyruvate (Corning), 1% L-glutamine (Gibco), and β-mercaptoethanol (50 μM). B cells were stimulated with 1 ug/ml CD40L (BD Pharmingen) and 25 ng/ml IL-4 (R&D Systems) or with 0.1 ug/ml CD40L, 10 ng/ml IL-4, and 5 ng/ml IL-5 (R&D Systems) to monitor B cell processes during B cell differentiation or to monitor differentiation with increased plasma cell (PC) frequency, respectively[22]. For isolation of *in vitro* generated PCs, cultures stimulated for 5 days with CD40L, IL-4, and IL-5 were enriched for live cells using a dead cell removal kit (Miltenyi Biotec)

followed by CD138-APC (BD Pharmingen) staining. $CD138^+$ PCs were enriched by positive immunomagnetic enrichment of APC (Miltenyi Biotec).

**Flow cytometry**

Single cell suspensions were stained with conjugated antibodies and data were obtained on a BD LSR II (BD Biosciences) and analyzed with FlowJo software (Treestar). Cell sorting was performed on a BD FACSAria (BD Biosciences). B and T cell populations, B cell class-switching, and B cell activation were analyzed with anti-B220, anti-IgM, anti-IgG1, anti-CD4, anti-CD8, anti-CD19, anti-CD21, anti-CD23, anti-CD25, anti-CD43, anti-CD69, anti-CD86, anti-CD93, anti-CD95(FAS) anti-CD138, and anti-GL7 (**Supplementary Table 4**). Cell populations analyzed were as follows: pro-B cells, $B220^+IgM^-CD43^+$; pre-B cells, $B220^{int}IgM^-CD43^-$; immature B cells, $B220^{int}IgM^+CD43^-$; mature B cells, $B220^{hi}IgM^+CD43^-$; follicular B cells, $B220^+CD19^+CD93^-CD23^+CD21^{-/int}$; and marginal zone B cells, $B220^+CD19^+CD93^-CD23^-CD21^+$; germinal center B cells, $B220^+GL7^+CD95^+$; plasmablast (PB), $B220^+CD138^+$; plasma cell (PC), $B220^-CD138^+$; double negative T cells (DN), $CD19^-CD4^-CD8^-$; double positive T cells (DP), $CD19^-CD4^+CD8^+$; CD4 T cells, $CD19^-CD4^+$; and CD8 T cells, $CD19^-CD8^+$. Representative flow cytometry gating strategies are provided in **Supplementary Fig. 4**. DAPI was used for assessment of cell viability and *in vitro* B cell proliferation was assessed by flow cytometry after labeling of isolated $CD43^-$ naive mature B cells with CellTrace carboxyfluorescein succinimidyl ester (CFSE) (Invitrogen).

**Protein separation and immunoblot analysis**

Total whole cell extracts were prepared by incubating cells in lysis buffer containing 50 mM Tris HCl pH 7.4, 100 mM NaCl, 1 mM EDTA, and 1% Triton X-100 supplemented with protease and phosphatase inhibitors (Sigma Aldrich). Cell extracts were quantified and loaded onto

polyacrylamide SDS gels before separating by gel electrophoresis and transferring onto nitrocellulose membranes. CRTC2, cleaved PARP, cleaved caspase-3, β-actin, and β-tubulin proteins were detected by immunoblot analysis with rabbit polyclonal anti-CRTC2, anti-PARP, anti-caspase-3, anti-β-actin, and mouse monoclonal anti-β-tubulin antibodies (**Supplementary Table 4**). Protein bands were visualized by chemiluminescence or IRDye detection at 680 or 800 nm using an autoradiograph film developer or the Odyssey Fc imaging system (LI-COR).

**RNA extraction and RT-PCR assays**

Total RNA for quantitative RT-PCR assays were extracted using Trizol reagent (Invitrogen). Assays were performed with Kapa SYBR Fast qPCR master mix (Roche) and mRNA expression levels of *Crtc2* and *Prdm1* were quantified with standard curves and results were normalized to the expression of *Rps18*. RT-PCR primer sequences are provided in **Supplementary Table 4**. RNA for sequencing were extracted using the RNeasy Mini Kit (Qiagen) and RNase-free DNase (Qiagen). All samples showed an A260/280 ratio > 1.99. Prior to library preparation, quality control of the RNA was performed using the Advanced Analytical Technologies Fragment Analyzer (Advanced Analytical Technologies, now Agilent Technologies) and analyzed using PROSize 2.0.0.51 software. RNA Quality Numbers were computed per sample between 8.7 and 10, indicating intact total RNA per sample prior to library preparation.

**RNA-seq library preparation**

Strand-specific ribosomal RNA depleted RNA-seq libraries were prepared from 1 µg of total RNA using the KAPA Stranded RNA-seq Kit with Ribo-Erase (Roche). Samples were prepared in at least triplicate for analysis. Briefly, rRNA was depleted from total RNA samples, the remaining RNA was heat fragmented, and strand-specific cDNA was synthesized using a first

strand random priming and second strand dUTP incorporation approach. Fragments were then A-tailed, adapters were ligated, and libraries were amplified using high-fidelity PCR. All libraries were prepared in technical duplicates per sample and resulting raw sequencing reads merged for downstream alignment and analysis. Libraries were paired-end sequenced at 2x150 bp on an Illumina NovaSeq 6000.

**RNA-seq data processing**

Raw sequencing runs were filtered for low quality reads and adapter contamination using FastQC (http://www.bioinformatics.babraham.ac.uk/projects/fastqc), SeqTK (https://github.com/lh3/seqtk), and Cutadapt[54]. Filtered reads were quantified and quasi-mapped to the *Mus musculus* Gencode M17 (GRCm38.p6) reference transcriptome using the alignment-free transcript level quantifier Salmon v.0.9.1[55, 56, 57]. The resulting estimated transcript counts were summarized into normalized gene level transcripts per million (TPM) and estimated count matrices using R (v. 3.4.0) Bioconductor (v. 3.5) package tximport (v. 1.4)[58].

The resulting sample gene count matrix was normalized and analyzed for differential gene expression using R (v. 3.4.0) Bioconductor (v. 3.5) package DESeq2 v1.16.0[59, 60]. Significance testing was performed using the Wald test, testing for the significance of deviance in a full design “Batch + GenotypeStage”, modeling the genotype effect at each division and unstimulated time point while accounting for batch variance between matched stimulation replicates. Resulting *P* values were adjusted for multiple testing using the Benjamini-Hochberg procedure[61]. Differentially expressed genes (DEGs) were filtered using an adjusted false discovery rate (FDR) *P* value < 0.05 and an absolute $\log_2$(Fold Change) > 0.5 in either the stimulated or unstimulated paired conditions.

Volcano plots were made with ggplot2 as described above, using the DESeq2 output adjusted *P* values and $\log_2$-fold changes per TG/WT comparison at each timepoint. Division

course kinetic plots were made using ggplot2 with DESeq2 size factor normalized counts using function plotCounts(). Gene expression heat maps were prepared using pheatmap() with row Z-scores calculated as the variance stabilized transform (VST) subtracted by the row mean. PCA was plotted using VST values with function plotPCA() with parameter “ntop = 100000”.

Pathway-level signature gene set enrichment analysis was performed using R Bioconductor package GSVA v1.26.0 function gsva() with parameters “method = gsva, rnaseq = FALSE, abs.ranking = FALSE, min.sz = 5, max.sz = 500” using a $\log_2$(TPM + 1) transformed gene expression matrix[62]. GSVA pathway enrichment scores per sample were extracted and assessed for significance using R Bioconductor package limma v3.34.9, as described above except with a Benjamini-Hochberg adjusted *P* value threshold = 0.01. Differentiation signature gene sets was obtained for 24 hr CD40L plus IL-4 activated B cells[22, 63], GC B cells[22, 64], ASCs[22, 64], BLIMP1 activated and repressed targets[65], and IRF4 activated-B cell and plasma cell targets[50].

Alternative splicing analysis was performed using rMATS v4.0.2[66]. Alternative splicing events were selected using an inclusion level difference greater than 0.1 with an FDR < 0.05 for any event comparison between Naive, Early, Late, and PC stages. RNA binding motif analysis was performed using rMAPS[67] using JCEC counts and standard web server settings. Gene ontology (GO) term overrepresentation analysis was performed using the combined ASE lists at any event comparison, with R packages and parameters as previous described [68].

Lists of transcript/gene-level expression values and differentiation signature GSVA results are included in supplemental excel file **Table S1**. Lists of alternative splicing events and associated GO terms are provided in supplemental excel file **Table S2**.

**Transgene insertion analysis**

Identification of the transgene insertion site following founder selection was performed using BBMap (v.June 11, 2018) (BBtools - sourceforge.net/projects/bbmap/). Following WGS of the TG and WT litter-matched mates, sequences were first aligned to the transgene sequence cassette using parameters “bbmap.sh in1=jh_wt[tg]_fixedmate_1.fastq.gz in2=jh_wt[tg]_fixedmate_2.fastq.gz outm=eitherMapped_jh_wt[tg]_fixedmate.fq ref=insertionsequence.fasta”. The resulting aligned sequences were then remapped to the Mus musculus mm10 reference genome (NCBI38/mm10, December 2011) to identify sites spanning transgene and native genome sequence, using parameters “bbmap.sh in=eitherMapped_jh_wt[tg]_fixedmate.fq ref=mm10.fasta out=genomeMapped_jh_wt[tg]_fixedmate.sam bs=bs.sh”. The resulting bam files were converted into bigWig format and visualized using IGV v2.3.81[69].

**Metabolomics**

Metabolite extraction and processing of day 5 *in vitro* stimulated TG and WT B cells were performed as previously described[53]. Data analysis, including principal components analysis and clustering, was performed using the statistical language R v3.4.4 and Bioconductor v3.6.0 packages. Metabolite abundance was normalized per µg of protein content per metabolite extraction, and metabolites not detected were set to zero. Metabolite normalized amounts were scaled and centered into Z-scores for relative comparison using R base function scale() with parameters “scale = TRUE, center = TRUE”. Volcano plots were prepared using R package ggplot2 v. 2.2.1; adjusted P values were calculated using R base functions t.test() and p.adjust() with parameter “method = ‘BH’” using corrected isotopomer distribution (MID) values.

**Statistical analyses**

All metabolomics and transcriptomics statistical analyses are described in the above methods. Values represent mean ± S.D. or S.E.M. Data were analyzed with Prism 8 (GraphPad) (**Figures 1, 2, 3, 5** and **Supplementary Figs. 1, 2, 3**) or R (**Figure 4** and **Supplementary Fig. 1**). Parametric data were analyzed using two-tailed, unpaired Student's *t*-tests, or 2-way ANOVA with Bonferroni correction for multiple comparisons. Transcriptomic volcano and kinetic time course expression plots were analyzed using DESeq2 Wald tests with Benjamini-Hochberg FDR correction for multiple comparisons. For all data sets, $P \leq 0.05$ was considered significant. *$P \leq 0.05$, **$P \leq 0.01$, ***$P \leq 0.001$, ****$P \leq 0.0001$.

**Data and code availability**

All raw RNA-Seq and WGS reads, transcript abundance values, and processed gene count matrices are in submission to the NCBI Gene Expression Omnibus (GEO). Accession numbers will be provided upon request prior to publication. All RNA-seq, metabolomics, and WGS datasets have been provided as supplemental material in this study (**Supplementary Tables 1**, **2**, and **3**). All custom code used for analyses are available on Atlassian BitBucket at https://bitbucket.org/ahsanfasih/crtc2bcell/src. All other relevant data are available from the corresponding author on request.

**Acknowledgements**

We thank the UCLA Flow Cytometry Core, Immuno/Biospot Core, Mitochondria and Metabolism Core, and Metabolomics Center for technical support. We thank Drs. Douglas Black, Jessica Fowler, Nicole Walsh, Rani Najdi, Tara TeSlaa, Laura Jimenez, and Alexander Patananan, along with Alexander Sercel and Vivian Lu for technical assistance and helpful discussions. Supported by NIH awards R01CA90571, R01CA156674, R01GM073981, R21CA227480, and P30CA016042, and the Air Force Office of Scientific Research FA9550-15-1-0406.

**Author information**

**Affiliations**

*Department of Pathology and Laboratory Medicine, David Geffen School of Medicine, University of California, Los Angeles, CA, USA*

Jason S. Hong, Fasih M. Ahsan, Peter D. Pioli, and Michael A. Teitell

*Department of Molecular and Medical Pharmacology, David Geffen School of Medicine, University of California, Los Angeles, CA, USA*

Min-sub Lee

*Department of Bioengineering, University of California, Los Angeles, CA, USA*

Thang L. Nguyen and Michael A. Teitell

*Department of Microbiology, Immunology, and Molecular Genetics, David Geffen School of Medicine, University of California, Los Angeles, CA, USA*

David G. Brooks

*NantOmics, LLC, Culver City, CA, USA*

Justin Golovato

*ImmunityBio, Culver City, CA, USA*

Kayvan R. Niazi

*Jonsson Comprehensive Cancer Center, Molecular Biology Interdepartmental Program, California NanoSystems Institute, Department of Pediatrics, and Broad Center for Regenerative Medicine and Stem Cell Research, University of California, Los Angeles, CA, USA*

Michael A. Teitell

*Current address: Program in Biological and Biomedical Sciences, Harvard Medical School, Boston, MA, 02215, USA*

Fasih M. Ahsan

*Current address: Department of Biomedical Sciences, Center for Immunobiology, Homer Stryker M.D. School of Medicine, Kalamazoo, MI 49007, USA*

Peter D. Pioli

*Current address: Princess Margaret Cancer Center, University Health Network, Toronto, ON, M5G 2M9 Canada*

David G. Brooks

## Author Contributions

J.S.H., F.M.A., P.D.P. and M.A.T. designed experiments; J.S.H., F.M.A., P.D.P., M.-S.L., T.L.N., D.G.B., and J.G. performed experiments and/or analyzed data; F.M.A. carried out computational analysis; K.R.N. provided resources for RNA and whole genome sequencing; J.S.H. and M.A.T. wrote the manuscript with input and editing from F.M.A., P.D.P., D.G.B., and K.R.N.

## Corresponding author

Correspondence to Michael A. Teitell.

## Ethics Declaration

## Competing interests

The authors declare no competing financial interests.

**References**


1. MacLennan, I.C. *et al.* Extrafollicular antibody responses. *Immunol Rev* **194**, 8-18 (2003).

2. De Silva, N.S. & Klein, U. Dynamics of B cells in germinal centres. *Nat Rev Immunol* **15**, 137-148 (2015).

3. Amanna, I.J., Carlson, N.E. & Slifka, M.K. Duration of humoral immunity to common viral and vaccine antigens. *N Engl J Med* **357**, 1903-1915 (2007).

4. Brink, R. & Phan, T.G. Self-Reactive B Cells in the Germinal Center Reaction. *Annu Rev Immunol* **36**, 339-357 (2018).

5. Nutt, S.L., Hodgkin, P.D., Tarlinton, D.M. & Corcoran, L.M. The generation of antibody-secreting plasma cells. *Nat Rev Immunol* **15**, 160-171 (2015).

6. Barwick, B.G., Scharer, C.D., Bally, A.P.R. & Boss, J.M. Plasma cell differentiation is coupled to division-dependent DNA hypomethylation and gene regulation. *Nat Immunol* **17**, 1216-1225 (2016).

7. Boothby, M. & Rickert, R.C. Metabolic Regulation of the Immune Humoral Response. *Immunity* **46**, 743-755 (2017).

8. Lam, W.Y. *et al.* Metabolic and Transcriptional Modules Independently Diversify Plasma Cell Lifespan and Function. *Cell Rep* **24**, 2479-2492 e2476 (2018).

9. Lam, W.Y. *et al.* Mitochondrial Pyruvate Import Promotes Long-Term Survival of Antibody-Secreting Plasma Cells. *Immunity* **45**, 60-73 (2016).

10. Conkright, M.D. *et al.* TORCs: transducers of regulated CREB activity. *Mol Cell* **12**, 413-423 (2003).

11. Altarejos, J.Y. & Montminy, M. CREB and the CRTC co-activators: sensors for hormonal and metabolic signals. *Nat Rev Mol Cell Biol* **12**, 141-151 (2011).

12. Tasoulas, J., Rodon, L., Kaye, F.J., Montminy, M. & Amelio, A.L. Adaptive Transcriptional Responses by CRTC Coactivators in Cancer. *Trends Cancer* **5**, 111-127 (2019).

13. Koo, S.H. *et al.* The CREB coactivator TORC2 is a key regulator of fasting glucose metabolism. *Nature* **437**, 1109-1111 (2005).

14. Jansson, D. *et al.* Glucose controls CREB activity in islet cells via regulated phosphorylation of TORC2. *Proc Natl Acad Sci U S A* **105**, 10161-10166 (2008).

15. Sherman, M.H. *et al.* AID-induced genotoxic stress promotes B cell differentiation in the germinal center via ATM and LKB1 signaling. *Mol Cell* **39**, 873-885 (2010).

16. Maliszewski, C.R. *et al.* Recombinant CD40 ligand stimulation of murine B cell growth and differentiation: cooperative effects of cytokines. *Eur J Immunol* **23**, 1044-1049 (1993).

17. Hasbold, J., Corcoran, L.M., Tarlinton, D.M., Tangye, S.G. & Hodgkin, P.D. Evidence from the generation of immunoglobulin G-secreting cells that stochastic mechanisms regulate lymphocyte differentiation. *Nat Immunol* **5**, 55-63 (2004).

18. Screaton, R.A. *et al.* The CREB coactivator TORC2 functions as a calcium- and cAMP-sensitive coincidence detector. *Cell* **119**, 61-74 (2004).

19. Hermanson, G.G., Eisenberg, D., Kincade, P.W. & Wall, R. B29: a member of the immunoglobulin gene superfamily exclusively expressed on beta-lineage cells. *Proc Natl Acad Sci U S A* **85**, 6890-6894 (1988).

20. Hoyer, K.K. *et al.* Dysregulated TCL1 promotes multiple classes of mature B cell lymphoma. *Proc Natl Acad Sci U S A* **99**, 14392-14397 (2002).

21. Wang, H., Diamond, R.A. & Rothenberg, E.V. Cross-lineage expression of Ig-beta (B29) in thymocytes: positive and negative gene regulation to establish T cell identity. *Proc Natl Acad Sci U S A* **95**, 6831-6836 (1998).

22. Shi, W. *et al.* Transcriptional profiling of mouse B cell terminal differentiation defines a signature for antibody-secreting plasma cells. *Nat Immunol* **16**, 663-673 (2015).

23. Ong, J., Stevens, S., Roeder, R.G. & Eckhardt, L.A. 3' IgH enhancer elements shift synergistic interactions during B cell development. *J Immunol* **160**, 4896-4903 (1998).

24. Ahmed, R., Salmi, A., Butler, L.D., Chiller, J.M. & Oldstone, M.B. Selection of genetic variants of lymphocytic choriomeningitis virus in spleens of persistently infected mice. Role in suppression of cytotoxic T lymphocyte response and viral persistence. *J Exp Med* **160**, 521-540 (1984).

25. Hao, Y., Li, Z., Wang, Y., Liu, X. & Ye, L. Analyzing Mouse B Cell Responses Specific to LCMV Infection. *Methods Mol Biol* **1707**, 15-38 (2018).

26. Lam, W.Y. & Bhattacharya, D. Metabolic Links between Plasma Cell Survival, Secretion, and Stress. *Trends Immunol* **39**, 19-27 (2018).

27. Shapiro-Shelef, M., Lin, K.I., Savitsky, D., Liao, J. & Calame, K. Blimp-1 is required for maintenance of long-lived plasma cells in the bone marrow. *J Exp Med* **202**, 1471-1476 (2005).

28. Peperzak, V. *et al.* Mcl-1 is essential for the survival of plasma cells. *Nat Immunol* **14**, 290-297 (2013).

29. Tellier, J. *et al.* Blimp-1 controls plasma cell function through the regulation of immunoglobulin secretion and the unfolded protein response. *Nat Immunol* **17**, 323-330 (2016).

30. Guo, M. *et al.* EZH2 Represses the B Cell Transcriptional Program and Regulates Antibody-Secreting Cell Metabolism and Antibody Production. *J Immunol* **200**, 1039-1052 (2018).

31. Linsley, P.S. & Ledbetter, J.A. The role of the CD28 receptor during T cell responses to antigen. *Annu Rev Immunol* **11**, 191-212 (1993).

32. Kozbor, D., Moretta, A., Messner, H.A., Moretta, L. & Croce, C.M. Tp44 molecules involved in antigen-independent T cell activation are expressed on human plasma cells. *J Immunol* **138**, 4128-4132 (1987).

33. Rozanski, C.H. *et al.* Sustained antibody responses depend on CD28 function in bone marrow-resident plasma cells. *J Exp Med* **208**, 1435-1446 (2011).

34. Chang, X., Li, B. & Rao, A. RNA-binding protein hnRNPLL regulates mRNA splicing and stability during B-cell to plasma-cell differentiation. *Proc Natl Acad Sci U S A* **112**, E1888-1897 (2015).

35. Litzler, L.C. *et al.* PRMT5 is essential for B cell development and germinal center dynamics. *Nat Commun* **10**, 22 (2019).

36. Diaz-Munoz, M.D. *et al.* The RNA-binding protein HuR is essential for the B cell antibody response. *Nat Immunol* **16**, 415-425 (2015).

37. Monzon-Casanova, E. *et al.* The RNA-binding protein PTBP1 is necessary for B cell selection in germinal centers. *Nat Immunol* **19**, 267-278 (2018).

38. Amelio, A.L., Caputi, M. & Conkright, M.D. Bipartite functions of the CREB co-activators selectively direct alternative splicing or transcriptional activation. *EMBO J* **28**, 2733-2747 (2009).

39. van Bon, B.W. *et al.* CEP89 is required for mitochondrial metabolism and neuronal function in man and fly. *Hum Mol Genet* **22**, 3138-3151 (2013).

40. Zurita Rendon, O., Silva Neiva, L., Sasarman, F. & Shoubridge, E.A. The arginine methyltransferase NDUFAF7 is essential for complex I assembly and early vertebrate embryogenesis. *Hum Mol Genet* **23**, 5159-5170 (2014).

41. Ahn, B.H. *et al.* A role for the mitochondrial deacetylase Sirt3 in regulating energy homeostasis. *Proc Natl Acad Sci U S A* **105**, 14447-14452 (2008).

42. Barwick, B.G. *et al.* B cell activation and plasma cell differentiation are inhibited by de novo DNA methylation. *Nat Commun* **9**, 1900 (2018).

43. Escoubas, C.C., Silva-Garcia, C.G. & Mair, W.B. Deregulation of CRTCs in Aging and Age-Related Disease Risk. *Trends Genet* **33**, 303-321 (2017).

44. Wu, Z. *et al.* Transducer of regulated CREB-binding proteins (TORCs) induce PGC-1alpha transcription and mitochondrial biogenesis in muscle cells. *Proc Natl Acad Sci U S A* **103**, 14379-14384 (2006).

45. van der Windt, G.J. *et al.* Mitochondrial respiratory capacity is a critical regulator of CD8+ T cell memory development. *Immunity* **36**, 68-78 (2012).

46. Bortnick, A. *et al.* Long-lived bone marrow plasma cells are induced early in response to T cell-independent or T cell-dependent antigens. *J Immunol* **188**, 5389-5396 (2012).

47. Klein Geltink, R.I. *et al.* Mitochondrial Priming by CD28. *Cell* **171**, 385-397 e311 (2017).

48. Kuraishy, A.I. *et al.* TORC2 regulates germinal center repression of the TCL1 oncoprotein to promote B cell development and inhibit transformation. *Proc Natl Acad Sci U S A* **104**, 10175-10180 (2007).

49. Duy, C. *et al.* BCL6 is critical for the development of a diverse primary B cell repertoire. *J Exp Med* **207**, 1209-1221 (2010).

50. Ochiai, K. *et al.* Transcriptional regulation of germinal center B and plasma cell fates by dynamical control of IRF4. *Immunity* **38**, 918-929 (2013).

51. Low, M.S.Y. *et al.* IRF4 Activity Is Required in Established Plasma Cells to Regulate Gene Transcription and Mitochondrial Homeostasis. *Cell Rep* **29**, 2634-2645 e2635 (2019).

52. Elsaesser, H., Sauer, K. & Brooks, D.G. IL-21 is required to control chronic viral infection. *Science* **324**, 1569-1572 (2009).

53. Waters, L.R. *et al.* Ampk regulates IgD expression but not energy stress with B cell activation. *Sci Rep* **9**, 8176 (2019).

54. Martin, M. Cutadapt removes adapter sequences from high-throughput sequencing reads. *2011* **17** (2011).

55. Harrow, J. *et al.* GENCODE: the reference human genome annotation for The ENCODE Project. *Genome Res* **22**, 1760-1774 (2012).

56. Mudge, J.M. & Harrow, J. Creating reference gene annotation for the mouse C57BL6/J genome assembly. *Mamm Genome* **26**, 366-378 (2015).

57. Patro, R., Duggal, G., Love, M.I., Irizarry, R.A. & Kingsford, C. Salmon provides fast and bias-aware quantification of transcript expression. *Nat Methods* **14**, 417-419 (2017).

58. Soneson, C., Love, M.I. & Robinson, M.D. Differential analyses for RNA-seq: transcript-level estimates improve gene-level inferences. *F1000Res* **4**, 1521 (2015).

59. Love, M.I., Huber, W. & Anders, S. Moderated estimation of fold change and dispersion for RNA-seq data with DESeq2. *Genome Biol* **15**, 550 (2014).

60. Huber, W. *et al.* Orchestrating high-throughput genomic analysis with Bioconductor. *Nat Methods* **12**, 115-121 (2015).

61. Benjamini, Y. & Hochberg, Y. Controlling the False Discovery Rate - a Practical and Powerful Approach to Multiple Testing. *Journal of the Royal Statistical Society Series B-Methodological* **57**, 289-300 (1995).

62. Hanzelmann, S., Castelo, R. & Guinney, J. GSVA: gene set variation analysis for microarray and RNA-seq data. *BMC Bioinformatics* **14**, 7 (2013).

63. Stein, M. *et al.* A defined metabolic state in pre B cells governs B-cell development and is counterbalanced by Swiprosin-2/EFhd1. *Cell Death Differ* **24**, 1239-1252 (2017).

64. Gloury, R. *et al.* Dynamic changes in Id3 and E-protein activity orchestrate germinal center and plasma cell development. *J Exp Med* **213**, 1095-1111 (2016).

65. Minnich, M. *et al.* Multifunctional role of the transcription factor Blimp-1 in coordinating plasma cell differentiation. *Nat Immunol* **17**, 331-343 (2016).

66. Shen, S. *et al.* rMATS: robust and flexible detection of differential alternative splicing from replicate RNA-Seq data. *Proc Natl Acad Sci U S A* **111**, E5593-5601 (2014).

67. Park, J.W., Jung, S., Rouchka, E.C., Tseng, Y.T. & Xing, Y. rMAPS: RNA map analysis and plotting server for alternative exon regulation. *Nucleic Acids Res* **44**, W333-338 (2016).

68. Shimada, E. *et al.* PNPase knockout results in mtDNA loss and an altered metabolic gene expression program. *PLoS One* **13**, e0200925 (2018).

69. Robinson, J.T. *et al.* Integrative genomics viewer. *Nat Biotechnol* **29**, 24-26 (2011).

Figure 1

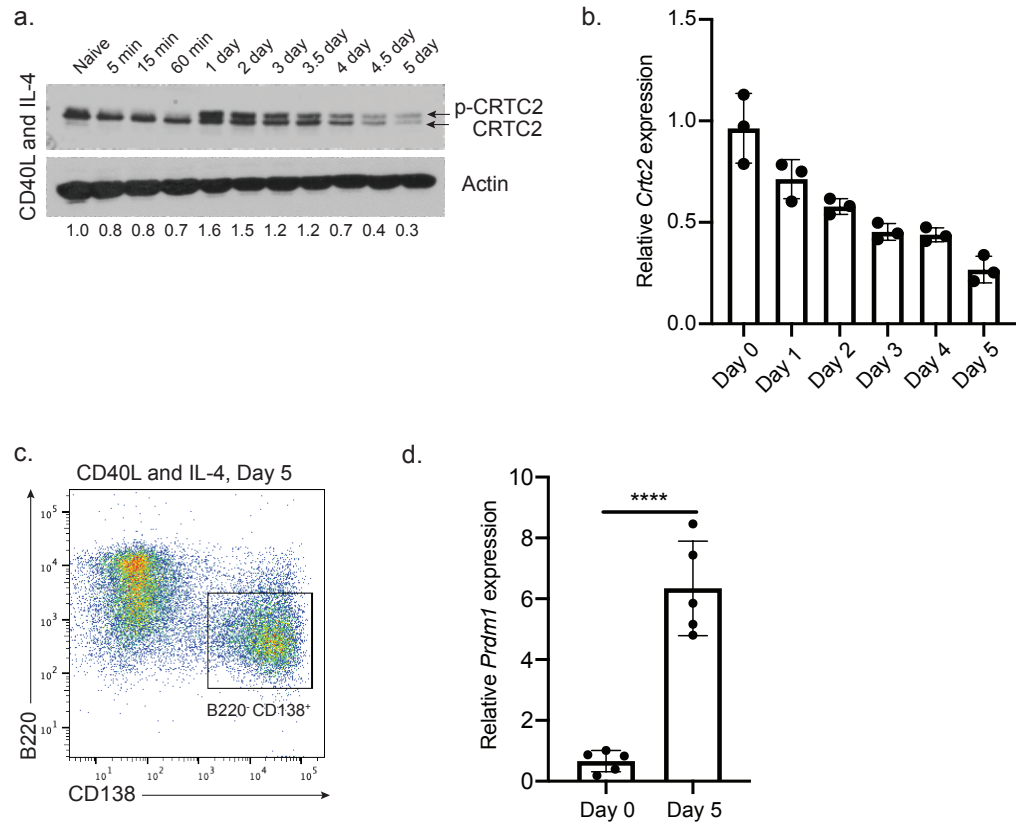
a.
Naive
5 min
15 min
60 min
1 day
2 day
3 day
3.5 day
4 day
4.5 day
5 day
CD40L and IL-4
p-CRTC2
CRTC2
Actin
1.0 0.8 0.8 0.7 1.6 1.5 1.2 1.2 0.7 0.4 0.3
b.
Relative Crtc2 expression
1.5
1.0
0.5
0.0
Day 0
Day 1
Day 2
Day 3
Day 4
Day 5
c.
CD40L and IL-4, Day 5
B220
CD138
B220- CD138+
d.
Relative Prdm1 expression
10
8
6
4
2
0
****
Day 0
Day 5

**Figure 1** CRTC2 expression in B cells is repressed during PC differentiation. (**a**) Immunoblot of a representative time-course analysis of phosphorylated and unphosphorylated CRTC2 protein expression in naïve splenic B cells stimulated with CD40L and IL-4 over 5 days. Actin was used as a loading control. Numbers indicate CRTC2 band intensities normalized to actin and were quantified by ImageJ analysis ($n$ = 3 WT and 3 TG). (**b**) Time-course analysis of *Crtc2* mRNA expression from naïve splenic B cells stimulated with CD40L and IL-4 by quantitative RT-PCR ($n$ = 3 WT and 3 TG). (**c**) Representative flow cytometry plot at day 5 of CD40L and IL-4 stimulation showing PC differentiation (boxed region). (**d**) Quantification of *Prdm1* expression at day 5 of CD40L and IL-4 induced differentiation by quantitative RT-PCR analysis ($n$ = 5 WT and 5 TG). Data represent mean ± s.d. (**b**,**c**). $P$ values determined by two-tailed, unpaired Student's $t$-test (**b**), $^{****}P \leq 0.0001$.

Figure 2

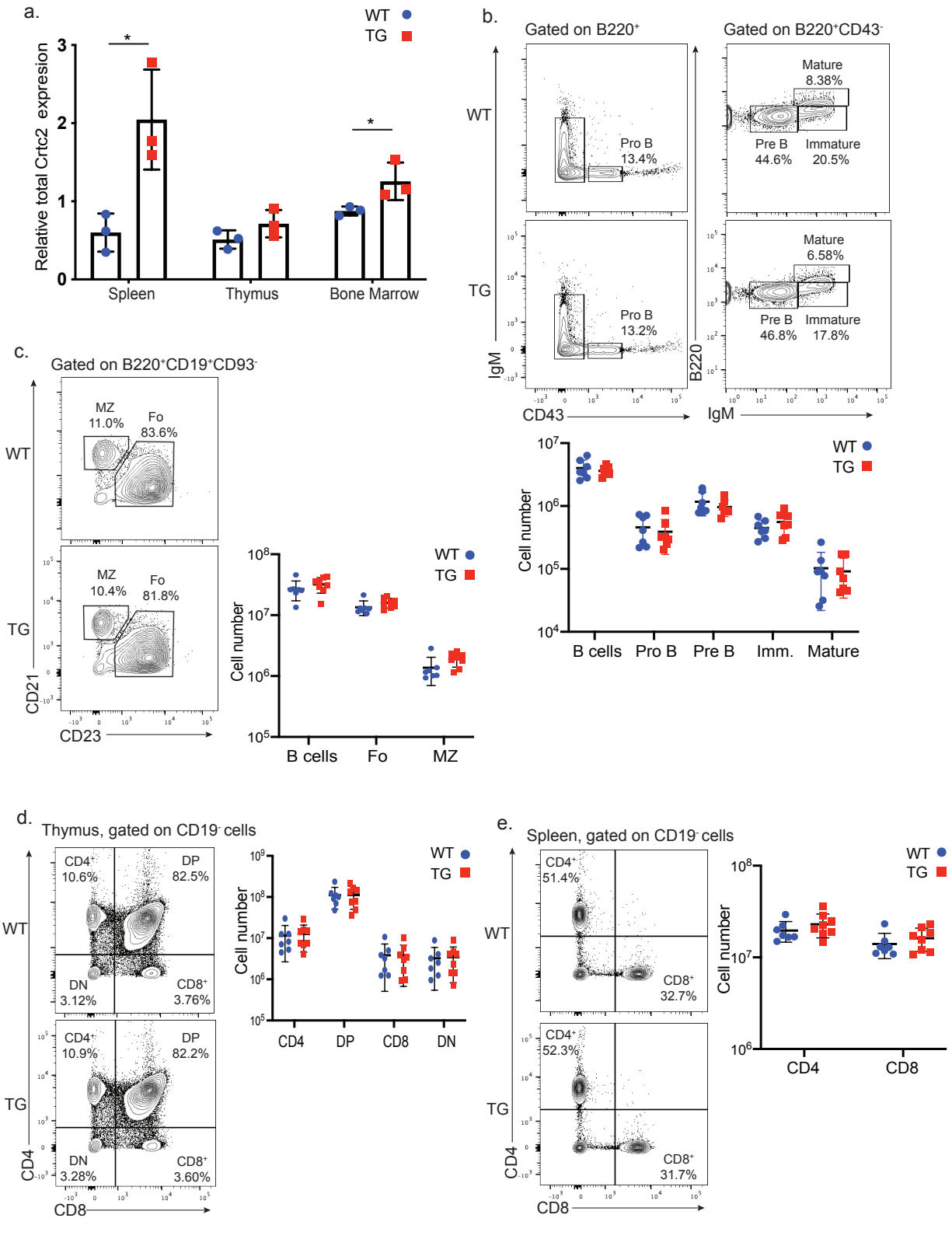
a.
WT
TG
Relative total Crtc2 expresion
Spleen
Thymus
Bone Marrow
b.
Gated on B220+
Gated on B220+CD43-
WT
TG
Pro B
13.4%
Pro B
13.2%
Mature
8.38%
Pre B
44.6%
Immature
20.5%
Mature
6.58%
Pre B
46.8%
Immature
17.8%
IgM
CD43
B220
IgM
Cell number
B cells
Pro B
Pre B
Imm.
Mature
c.
Gated on B220+CD19+CD93-
MZ
11.0%
Fo
83.6%
MZ
10.4%
Fo
81.8%
CD21
CD23
Cell number
B cells
Fo
MZ
d.
Thymus, gated on CD19- cells
CD4+
10.6%
DP
82.5%
DN
3.12%
CD8+
3.76%
CD4+
10.9%
DP
82.2%
DN
3.28%
CD8+
3.60%
CD4
CD8
Cell number
CD4
DP
CD8
DN
e.
Spleen, gated on CD19- cells
CD4+
51.4%
CD8+
32.7%
CD4+
52.3%
CD8+
31.7%
CD4
CD8
Cell number
CD4
CD8

**Figure 2** B cell development is unaffected in *Crtc2-AA* F1 TG mice. (**a**) Total *Crtc2* mRNA expression (endogenous and transgene) from mouse cells isolated from the spleen, thymus, and bone marrow by quantitative RT-PCR analysis ($n$ = 3 WT and 3 TG). (**b**) Representative flow cytometry plots of B cell populations in the bone marrow of WT and TG mice (top) and quantification of absolute numbers of total, pro-B, pre-B, immature, and mature B cells in the bone marrow (bottom). (**c**) Representative flow cytometry plots of B cell populations in the spleen of WT and TG mice (left) and quantification of absolute numbers of total, FO, and MZ B cells in the spleen (right). (**d**) Representative flow cytometry plots of T cells in the thymus of WT and TG mice (left) and quantification of absolute numbers of subpopulations in the thymus (right). (**e**) Representative flow cytometry plots of T cells in the spleen of WT and TG mice (left) and quantification of absolute numbers of T cell subpopulations in the spleen (right). Each symbol (**b,c,d,e**) represents an individual mouse ($n$ = 7 WT and 8 TG). Data represent mean $\pm$ s.d. (**a**,**b**,**c**,**d,e**). $P$ values determined by two-tailed, unpaired Student's $t$-test (**a**), *$P \leq 0.05$.

Figure 3

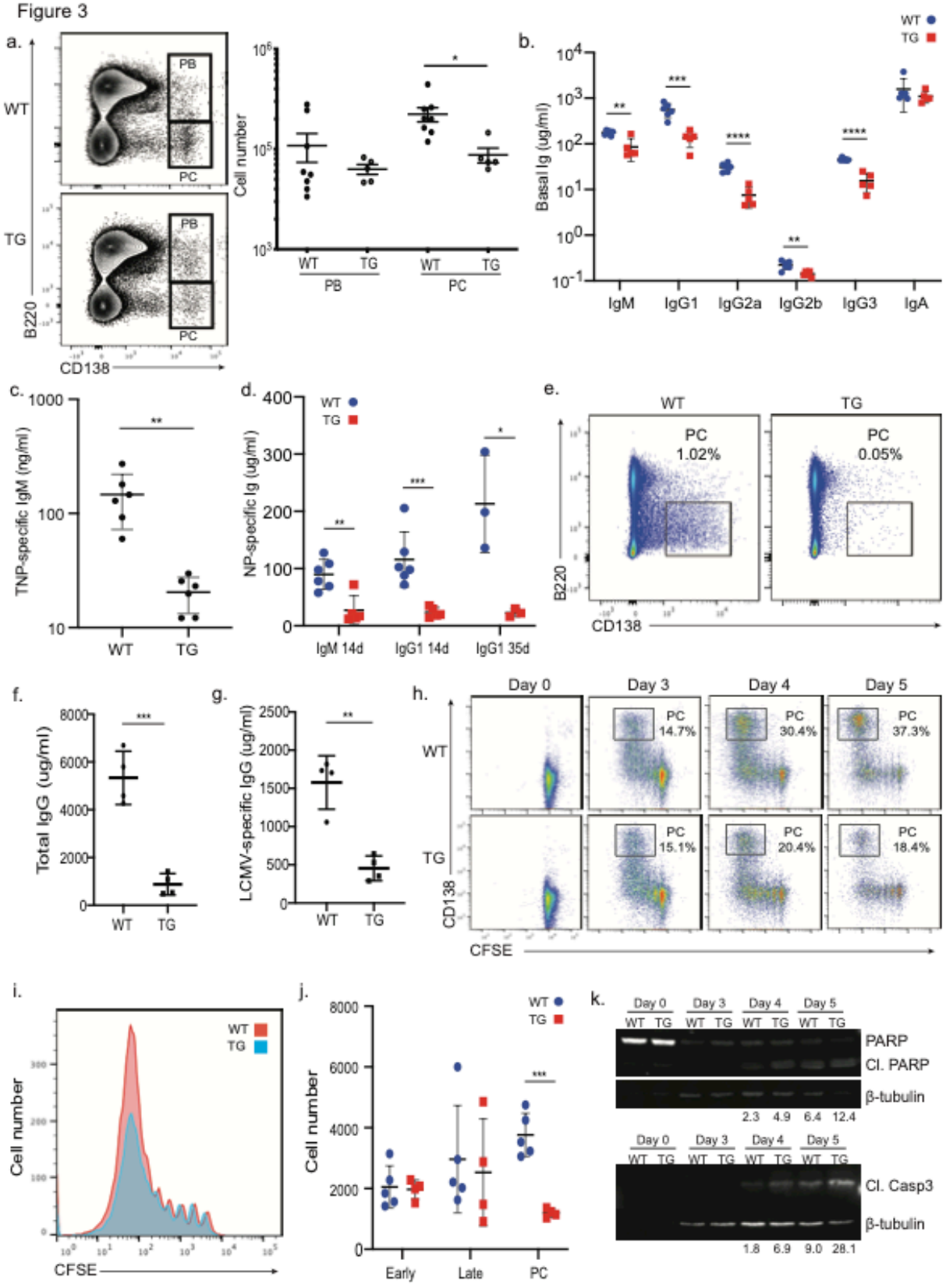
a.
WT
TG
PB
PC
B220
CD138
Cell number
WT
TG
PB
PC
b.
WT
TG
Basal Ig (ug/ml)
IgM
IgG1
IgG2a
IgG2b
IgG3
IgA
c.
TNP-specific IgM (ng/ml)
d.
NP-specific Ig (ug/ml)
IgM 14d
IgG1 14d
IgG1 35d
e.
PC 1.02%
PC 0.05%
f.
Total IgG (ug/ml)
g.
LCMV-specific IgG (ug/ml)
h.
Day 0
Day 3
Day 4
Day 5
PC 14.7%
PC 30.4%
PC 37.3%
PC 15.1%
PC 20.4%
PC 18.4%
CD138
CFSE
i.
Cell number
CFSE
j.
Cell number
Early
Late
PC
k.
Day 0
Day 3
Day 4
Day 5
PARP
Cl. PARP
β-tubulin
2.3 4.9 6.4 12.4
Cl. Casp3
β-tubulin
1.8 6.9 9.0 28.1

**Figure 3** Impaired humoral immune response in TG mice linked to increased PC death. (**a**) Representative flow cytometry plots of plasmablasts (PBs) and plasma cells (PCs) in the spleen of unimmunized naïve mice (left) and quantification of PB and PC numbers (right) (*n*= 8 WT and 5 TG). (**b**) Quantification of serum immunoglobulin (Ig) titers from unimmunized WT and TG mice (*n* = 6 WT and 5 TG). (**c**) Quantification of TNP-specific IgM serum titers from WT and TG mice 7 days post-immunization with TNP-Ficoll (*n* = 6 WT and 6 TG). (**d**) Quantification of NP-specific IgM and IgG1 serum titers from WT and TG mice 14 days post-immunization (*n* = 6 WT and 5 TG) and NP-specific IgG1 serum titers from WT and TG mice 35 days post-immunization with NP-CGG (*n*= 3 WT and 3 TG). (**e**) Representative flow cytometry plots of PCs in the spleen of mice infected with Armstrong strain LCMV 8 days post-infection (dpi) (*n* = 4 WT and 4 TG). (**f**) Quantification of total IgG serum titers from LCMV infected mice 8 dpi. (**g**) Quantification of LCMV-specific IgG serum titers from LCMV infected mice 8 dpi. (**h-k**) Naïve splenic mouse B cells from WT and TG mice were labeled with CFSE and then stimulated with CD40L, IL-4, and IL-5. Cells were collected and analyzed at days 0, 3, 4, and 5 of stimulation (*n* = 5 WT and 4 TG). (**h**) Representative flow cytometry plots of WT and TG PC differentiation. Boxed areas indicate the percentage of $CD138^+$ PCs. (**i**) Representative flow cytometry plots showing number of cell divisions by TG and WT B cells at day 5 of stimulation by CFSE dye dilution assay. (**j**) Live cells ($DAPI^-$) were gated into early divisions, late divisions, and PC subpopulations and the number of cells for each quantified by flow cytometry. (**k**) Representative immunoblot of cleaved PARP and cleaved caspase-3 in WT and TG B cells. Numbers beneath lanes indicate the expression of the cleaved forms of PARP and caspase-3 normalized to β-tubulin and as arbitrary fluorescence units. Data represent mean ± s.e.m. (**a**), ± s.d. (**b**,**c**,**d**,**f**,**g**,**j**). *P* values were determined by two-tailed, unpaired Student's *t*-test (**a**,**b**,**c**,**d**,**f**,**g**,**j**), $*P \leq 0.05$, $**P \leq 0.01$, $***P \leq 0.001$, $****P \leq 0.0001$.

Figure 4

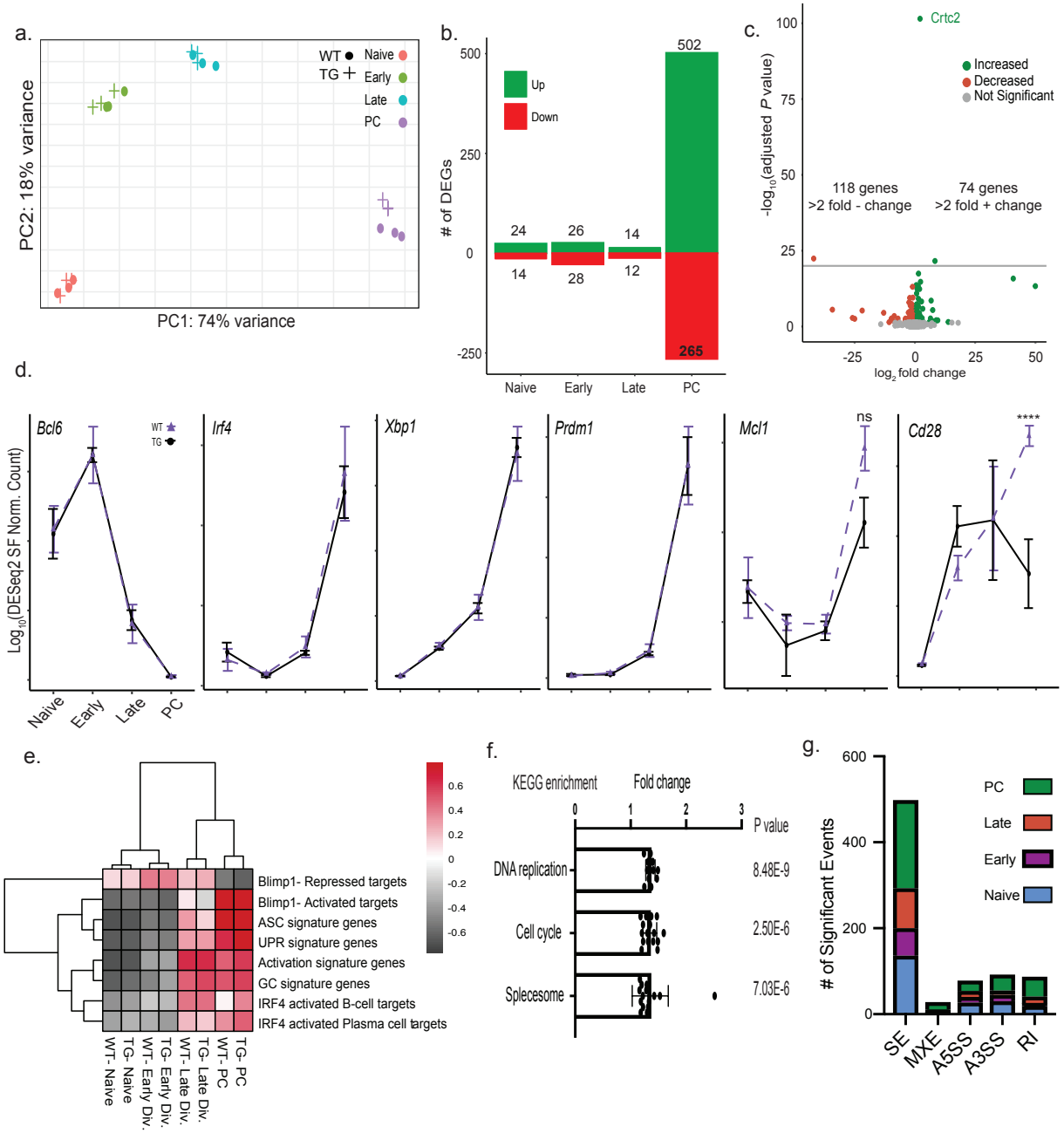


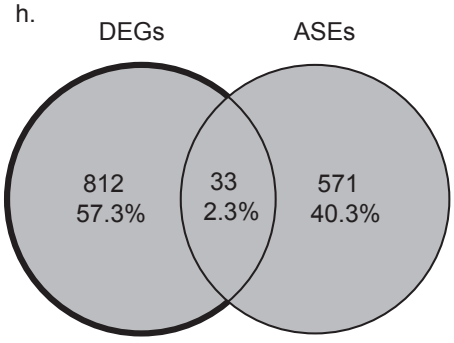


i.

| Enrichment of SE events | # of genes | Adj. *p* value |
|---|---|---|
| Lysine modifications | 18 (Gene ontology) | 0.003 |
| Histone modifications | 21 (Gene ontology) | 0.003 |
| Methyltransferase activity | 21 (Gene ontology) | 0.01 |
| Organelle biogenesis | 12 (Reactome) | 0.01 |

**Figure 4** CRTC2 regulates mRNA expression and alternative splicing in mature B cells. (**a**) Principal component analysis of bulk transcriptomes derived from CD138 and CFSE dye-dilution FACS sorted populations described in **Supplementary Fig. 1f**. Points represent replicates of n = 3 independent experiments for WT and TG pairs. PC1 and PC2 scores are plotted on the x- and y-axes, respectively. (**b**) List of differentially expressed genes (DEGs) between WT and TG cells at each stage of PC fate specification derived from bulk transcriptomics. Numbers represent the number of up-regulated and down-regulated DEGs in each subpopulation. (**c**) Volcano plot of WT and TG cell fold change differences during the PC stage of differentiation. Green dots indicate genes up-regulated in the TG population during the PC stage of differentiation, whereas red dots indicate down-regulated genes. The adjusted *P* value cutoff represents values < 0.05 calculated using the Wald test following DESeq2 normalization. (**d**) Stage-course expression plots for transcripts of canonical B cell differentiation, PC formation, and PC survival markers *Bcl6, Irf4, Xbp1, Prdm1, Mcl1, and Cd28*. Data represent $\log_2$ transformed DESeq2 normalized counts. (**e**) Gene set variation analysis (GSVA) results for *Blimp1* target, *Irf4* target, unfolded protein response (UPR) signature, and canonical early activation/GC/ASC formation signatures in WT and TG cell populations at each assessed stage of differentiation. Data represent *n* = 3 independent experiments. (**f**) KEGG overrepresentation analysis (ORA) plots indicating pathways enriched in WT versus TG cell differentially expressed genes at the PC stage. (**g**) mRNA alternative splicing events (detected by rMATS 4.0.2) at each stage of PC differentiation. Events are split into skipped exon (SE), mutually exclusive exon (MXE), alternative 5' (A5SS) or 3' (A3SS) splice sites, and retained intron (RI) events. Events are detected at an inclusion level difference of 0.10 and an FDR < 0.05 at all stages of differentiation between WT and TG cells. (**h**) Venn diagram displaying the intersection of all DEGs from (**b**) and all mRNA alternative splicing events (ASEs) from (**g**). (**i**) Table with selected

gene-ontology (GO) and Reactome terms containing genes with significantly affected SE events in TG PCs. Adjusted *P* values were determined by Wald test **(d)**, ****$P \leq 0.0001$

Figure 5

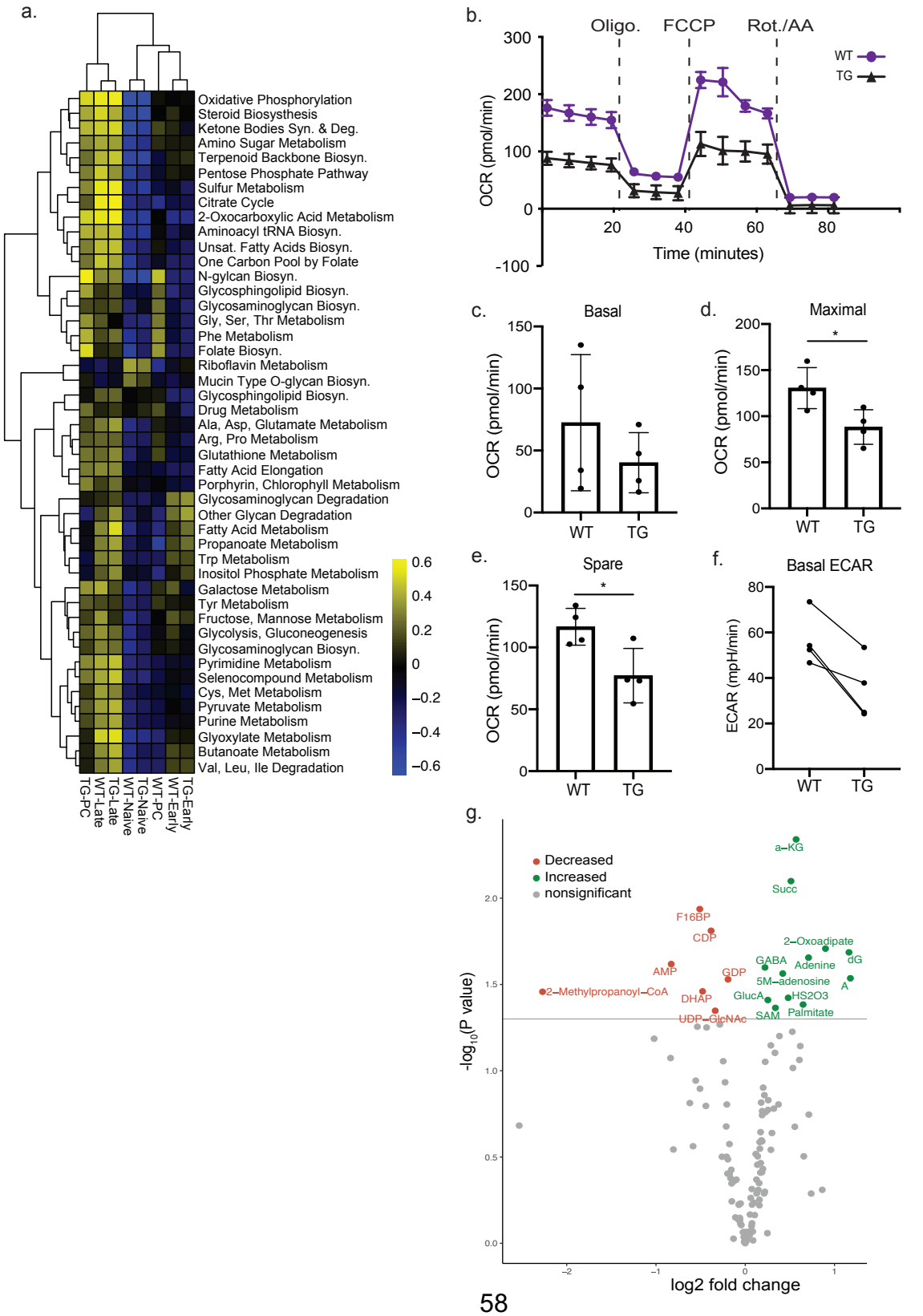
a.
Oxidative Phosphorylation
Steroid Biosysthesis
Ketone Bodies Syn. & Deg.
Amino Sugar Metabolism
Terpenoid Backbone Biosyn.
Pentose Phosphate Pathway
Sulfur Metabolism
Citrate Cycle
2-Oxocarboxylic Acid Metabolism
Aminoacyl tRNA Biosyn.
Unsat. Fatty Acids Biosyn.
One Carbon Pool by Folate
N-gylcan Biosyn.
Glycosphingolipid Biosyn.
Glycosaminoglycan Biosyn.
Gly, Ser, Thr Metabolism
Phe Metabolism
Folate Biosyn.
Riboflavin Metabolism
Mucin Type O-glycan Biosyn.
Glycosphingolipid Biosyn.
Drug Metabolism
Ala, Asp, Glutamate Metabolism
Arg, Pro Metabolism
Glutathione Metabolism
Fatty Acid Elongation
Porphyrin, Chlorophyll Metabolism
Glycosaminoglycan Degradation
Other Glycan Degradation
Fatty Acid Metabolism
Propanoate Metabolism
Trp Metabolism
Inositol Phosphate Metabolism
Galactose Metabolism
Tyr Metabolism
Fructose, Mannose Metabolism
Glycolysis, Gluconeogenesis
Glycosaminoglycan Biosyn.
Pyrimidine Metabolism
Selenocompound Metabolism
Cys, Met Metabolism
Pyruvate Metabolism
Purine Metabolism
Glyoxylate Metabolism
Butanoate Metabolism
Val, Leu, Ile Degradation
0.6
0.4
0.2
0
−0.2
−0.4
−0.6
TG-PC
WT-Late
TG-Late
WT-Naive
TG-Naive
WT-PC
WT-Early
TG-Early
b.
Oligo.
FCCP
Rot./AA
WT
TG
OCR (pmol/min)
300
200
100
0
-100
20
40
60
80
Time (minutes)
c.
Basal
OCR (pmol/min)
150
100
50
0
WT
TG
d.
Maximal
*
OCR (pmol/min)
200
150
100
50
0
WT
TG
e.
Spare
*
OCR (pmol/min)
150
100
50
0
WT
TG
f.
Basal ECAR
ECAR (mpH/min)
80
60
40
20
0
WT
TG
g.
Decreased
Increased
nonsignificant
a−KG
Succ
F16BP
CDP
2−Oxoadipate
dG
GABA
Adenine
AMP
GDP
5M−adenosine
A
2−Methylpropanoyl−CoA
DHAP
GlucA
HS2O3
SAM
Palmitate
UDP−GlcNAc
-log10(P value)
2.0
1.5
1.0
0.5
0.0
−2
−1
0
1
log2 fold change

**Figure 5** *Crtc2* repression increases oxidative metabolism. (**a**) Gene set variation analysis (GSVA) results for metabolic signature genes derived from the KEGG database. Results represent metabolic gene sets passing a Benjamini Hochberg adjusted P value threshold < 0.01. Data represent the mean of $n = 3$ independent experiments. (**b**) Representative extracellular flux analysis of WT and TG PCs. Oxygen consumption rate (OCR) before and after treatment with indicated pharmacological inhibitors. Each point represents the mean ± s.d. of $n = 4$ independent experiments. (**c**) Quantification of basal oxygen consumption rate. (**d**) Quantification of maximal oxygen consumption rate. (**e**) Quantification of spare respiratory capacity. (**f**) Quantification of basal extracellular acidification rate (ECAR) from extracellular flux assay in (**b**). (**g**) Volcano plot of steady state metabolite abundances from WT and TG cells at day 5 of stimulation with CD40L and IL-4. Plotted are *P* values for WT and TG cell amounts of specific metabolites. Data represent $n = 3$ independent experiments. *P* values were determined by two-tailed, unpaired Student's *t*-test (**d**,**e**), $^*P \leq 0.05$.

Figure 6

a.

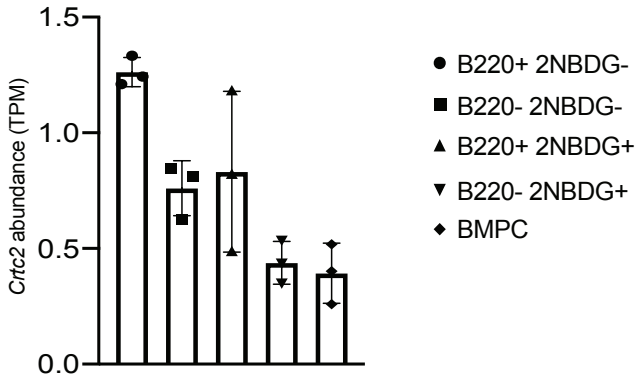
1.5
1.0
0.5
0.0
Crtc2 abundance (TPM)
B220+ 2NBDG-
B220- 2NBDG-
B220+ 2NBDG+
B220- 2NBDG+
BMPC

b.

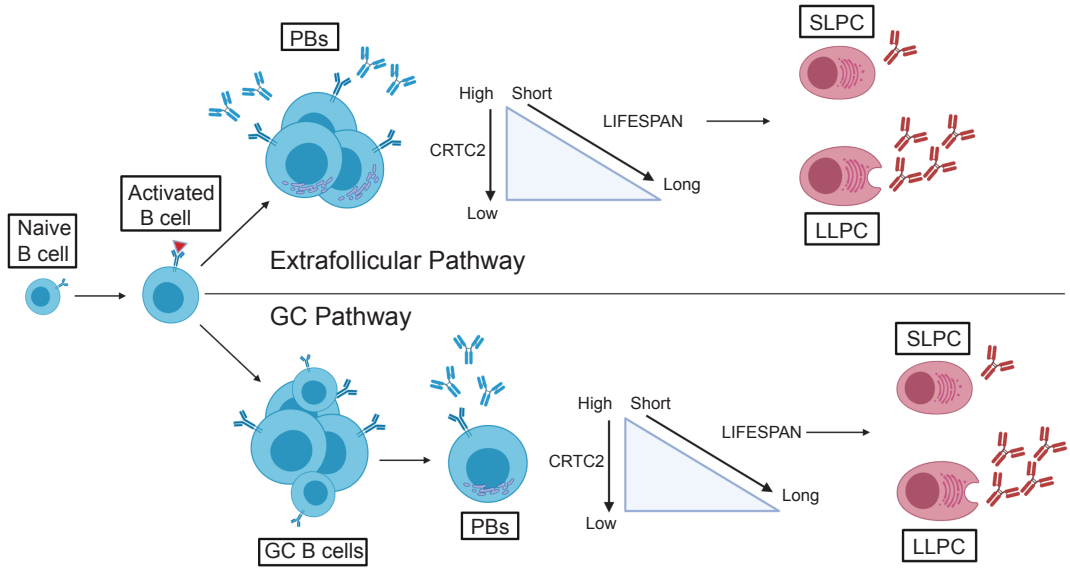
PBs
Activated B cell
Naive B cell
High
Short
CRTC2
LIFESPAN
Long
Low
SLPC
LLPC
Extrafollicular Pathway
GC Pathway
GC B cells
PBs
High
Short
CRTC2
LIFESPAN
Long
Low
SLPC
LLPC

**Figure 6** *Crtc2* expression levels trend with ASC longevity. (**a**) Abundance of *Crtc2* transcripts, measured in transcripts per million (TPM) in sorted PC subsets from the spleen and bone marrow. RNA-seq data from Lam et al., 2018, was re-analyzed to determine transcript abundance. The half-life of sorted PC subsets increases from left to right as previously determined by Lam et al., 2018. Data represents the mean ± s.d. of $n = 3$ independent experiments. (**b**) Model in which the level of CRTC2 activity in differentiated ASCs contributes to PC longevity. Details are provided in the text.

Supplementary Figure 1

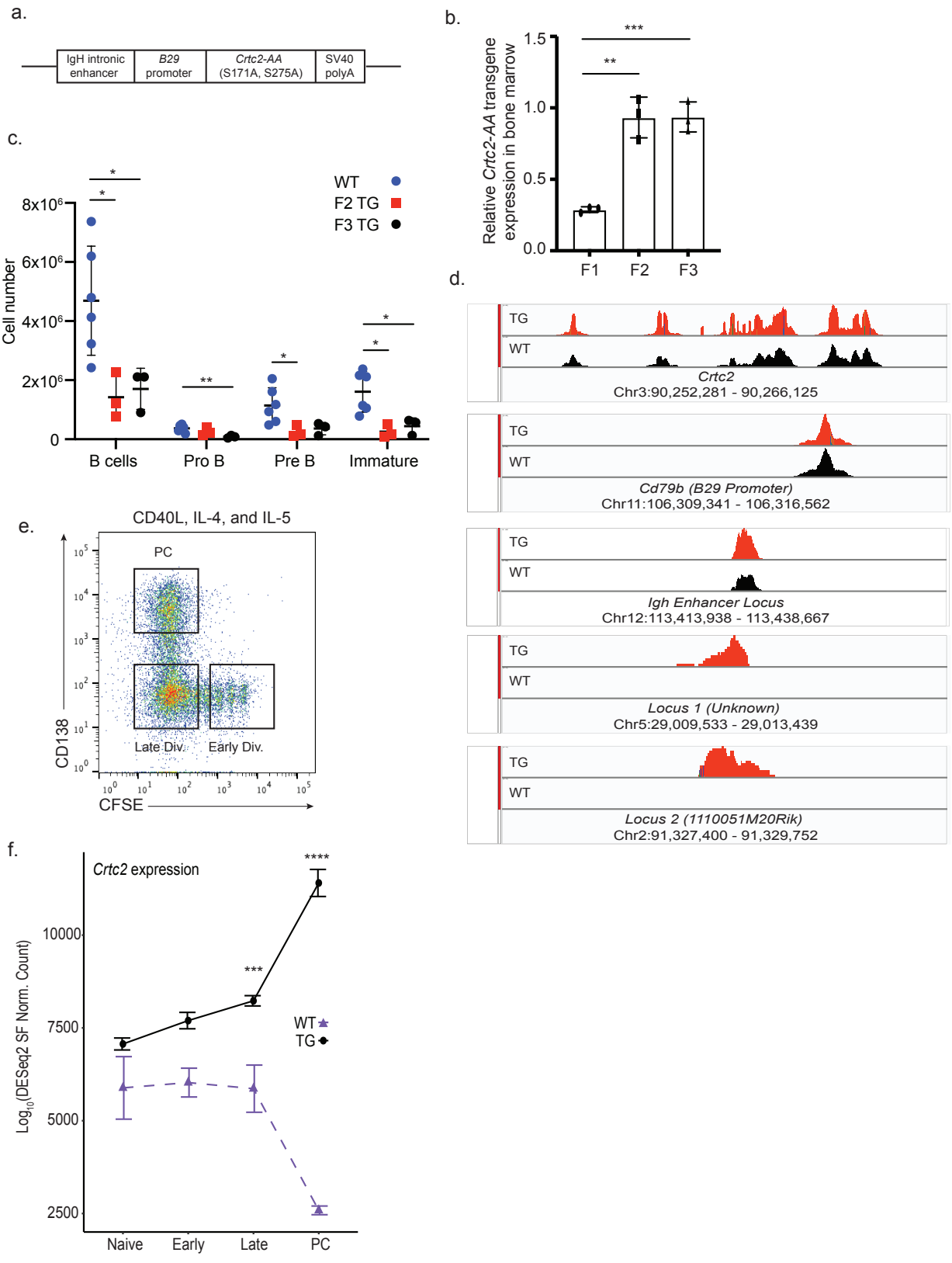

**Supplementary Figure 1** Transgenic founder lines, transgene expression, and transgene integration analysis. (**a**) Schematic of the *Crtc2-AA* transgenic construct used to generate TG mouse founder lines. (**b**) *Crtc2-AA* transgene expression in bone marrow cells of each TG founder line by quantitative RT-PCR analysis ($n$= 3 for each founder line). (**c**) Quantification of absolute cell numbers from bone marrow B cell subpopulations in TG founder lines F2 and F3 compared to WT controls ($n$ = 6 WT and 3 each F2, F3 TG). (**d**) Paired-end whole genome sequencing (WGS) of the F1 TG founder mouse to identify transgene integration site(s). Genome browser tracks depict mapping of reads to the mouse genome with integration sites determined by accumulation of reads that partially align to both the genome and the transgene insertion cassette. Data are plotted relative to WT WGS results analyzed in the same pipeline. (**e**) Representative flow cytometry plot of naïve splenic B cells stimulated with CD40L, IL-4, and IL-5 used for cell sorting and RNA-seq. At day 5 of stimulation, cells were sorted into early division, late division, and PC subpopulations as indicated by boxed areas based on CFSE dye dilution assay and CD138 staining. (**f**) *Crtc2* mRNA expression from sorted cell populations as outlined in (**e**). Expression represented as normalized counts for 3 independent RNA-seq experiments of WT and TG pairs. Data represent mean ± s.d. (**b**,**c**,**f**). *P* values were determined by two-tailed, unpaired Student's *t*-test (**b**,**c**), adjusted *P* values were determined by Wald test (**f**), $*P \leq 0.05$, $**P \leq 0.01$, $***P \leq 0.001$, $****P \leq 0.0001$.

Supplementary Figure 2

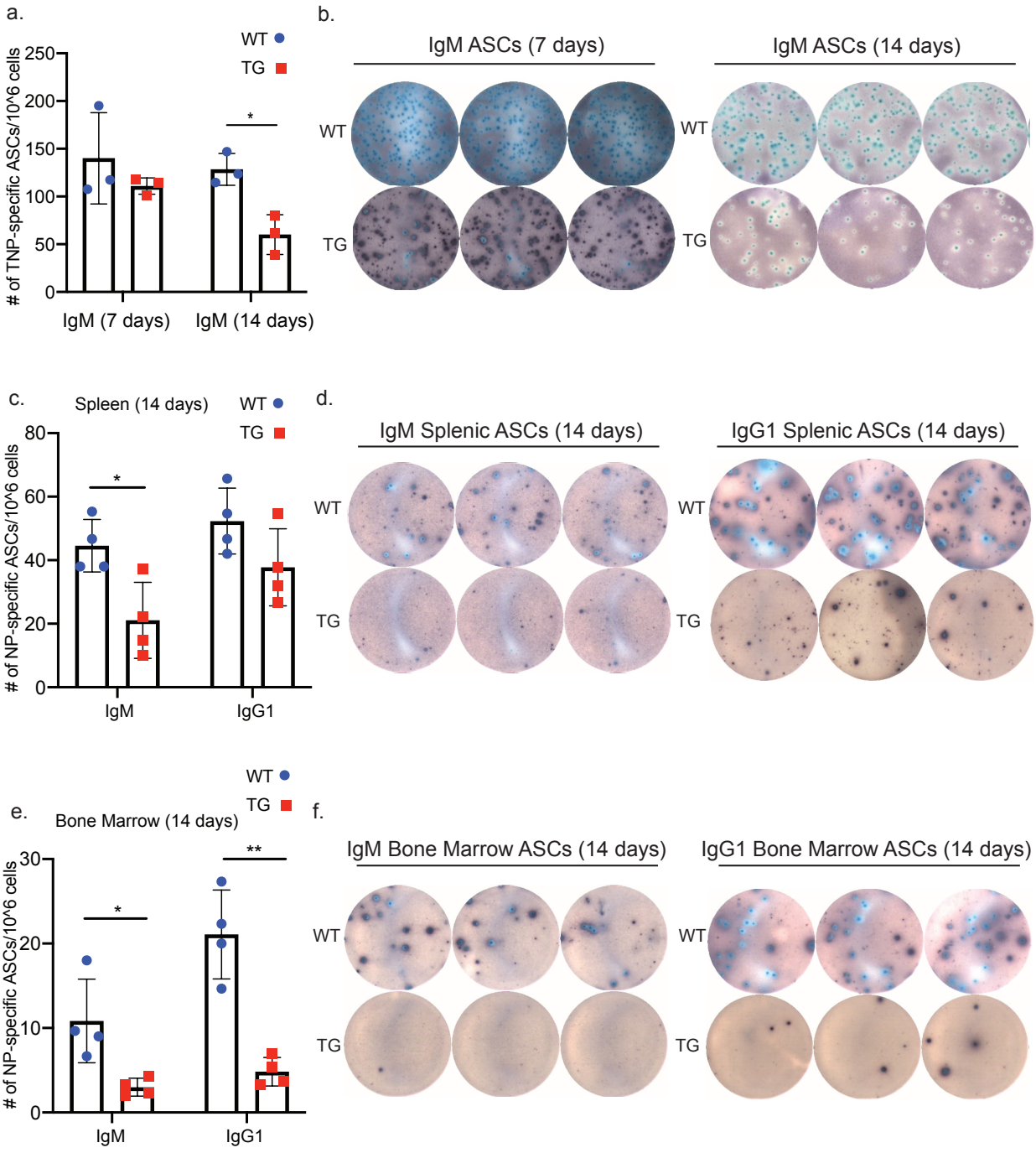

**Supplementary Figure 2** ELISPOT images documenting reduction in ASC numbers with PC maturation. (**a**) Quantification of TNP-specific IgM ASCs from the spleen 7 and 14 days post-immunization with TNP-Ficoll by ELISPOT (*n* = 3 WT and 3 TG for each 7 and 14 day experiment). (**b**) Representative images of ELISPOT wells in triplicate revealing IgM secreting ASCs at 7 days (left) and at 14 days (right) post TNP-Ficoll immunizations in WT and TG splenic cells. (**c**) Quantification of NP-specific IgM and IgG1 ASCs from the spleen 14 days post-immunization with NP-CGG plus alum by ELISPOT (*n* = 4 WT and 4 TG). (**d**) Representative images of ELISPOT wells in triplicate revealing IgM and IgG1 secreting ASCs at 14 days post NP-CGG immunizations in alum for WT and TG splenic cells. (**e**) Quantification of NP-specific IgM and IgG1 ASCs from the bone marrow 14 days post-immunization with NP-CGG plus alum by ELISPOT (*n* = 4 WT and 4 TG). (**f**) Representative images of ELISPOT wells in triplicate revealing IgM and IgG1 secreting ASCs 14 days post NP-CGG immunizations in alum for WT and TG bone marrow cells. Data represent mean ± s.d. (**a**,**c**,**e**). *P* values were determined by two-tailed, unpaired Student's *t*-test (**a**,**c**,**e**), $*P \leq 0.05$, $**P \leq 0.01$.

Supplementary Figure 3

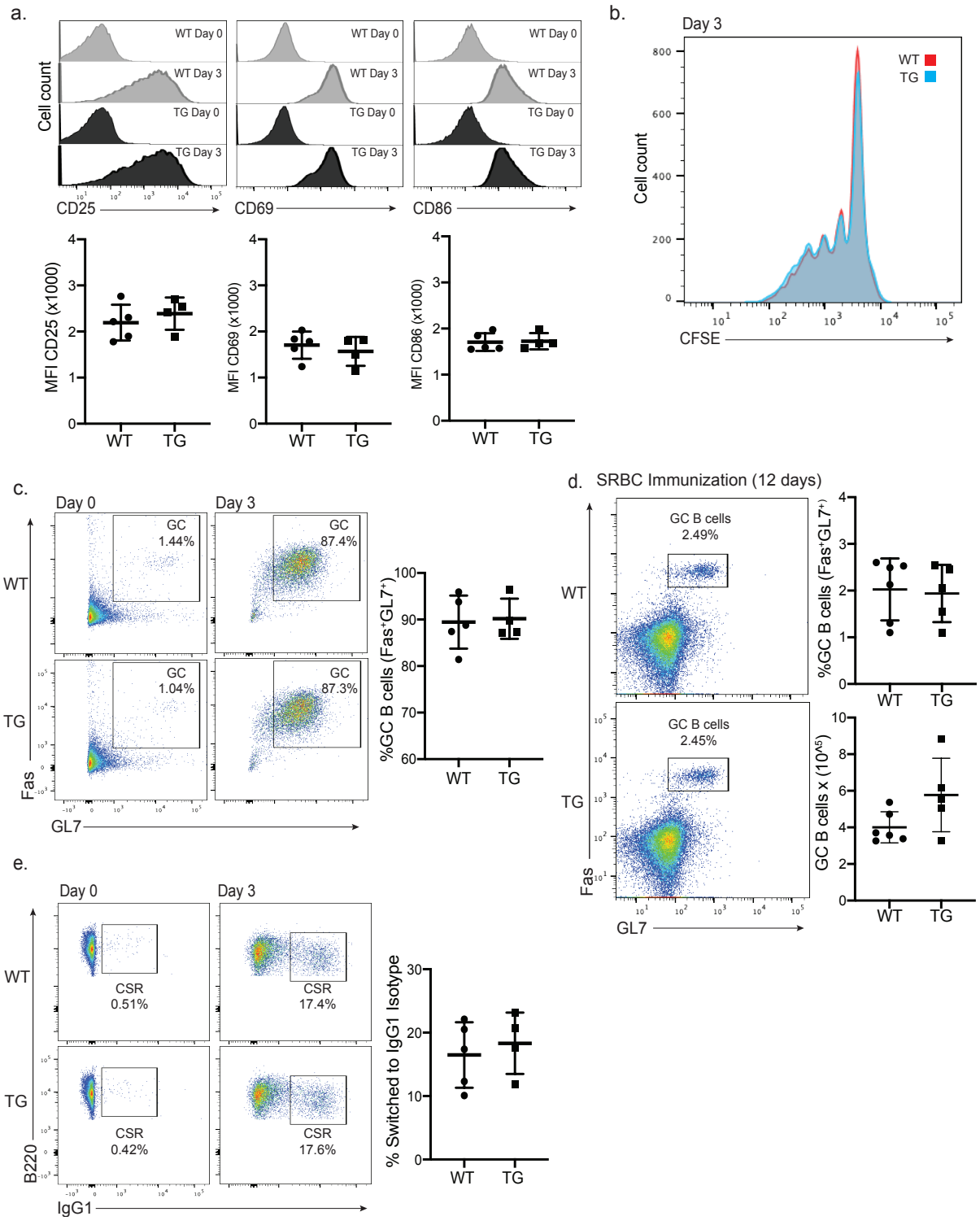

**Supplementary Figure 3** Unaffected B cell activation, proliferation, GC formation, and CSR in TG B cells. (**a**,**b**,**c**,**e**) Naïve splenic mouse B cells from WT and TG mice were stimulated with CD40L and IL-4. Data represents *n* = 5 WT and 4 TG (**a**) Representative flow cytometry plots depicting activation marker expression at day 3 of stimulation (top) and quantification of activation marker expression by mean fluorescence intensity (MFI) (bottom). (**b**) Representative flow cytometry plots depicting cell division measured using CFSE dye dilution assay at day 3 of stimulation. (**c**) Representative flow cytometry plots depicting differentiation of GC-like B cells at day 3 of stimulation (left) and quantification of the percentage of GC-like B cells (right). (**d**) Representative flow cytometry plots depicting differentiation of GC B cells (left) and quantification of the percentage and absolute number of GC B cells in the spleen of mice 12 days post SRBC immunization (*n* = 6 WT and 5 TG). (**e**) Representative flow cytometry plots depicting class switch recombination (CSR) to the IgG1 isotype at day 3 of stimulation (left) and quantification of the percentage of CSR (right). Data represent mean ± s.d. (**a**,**c**,**d**,**e**).

Supplementary Figure 4

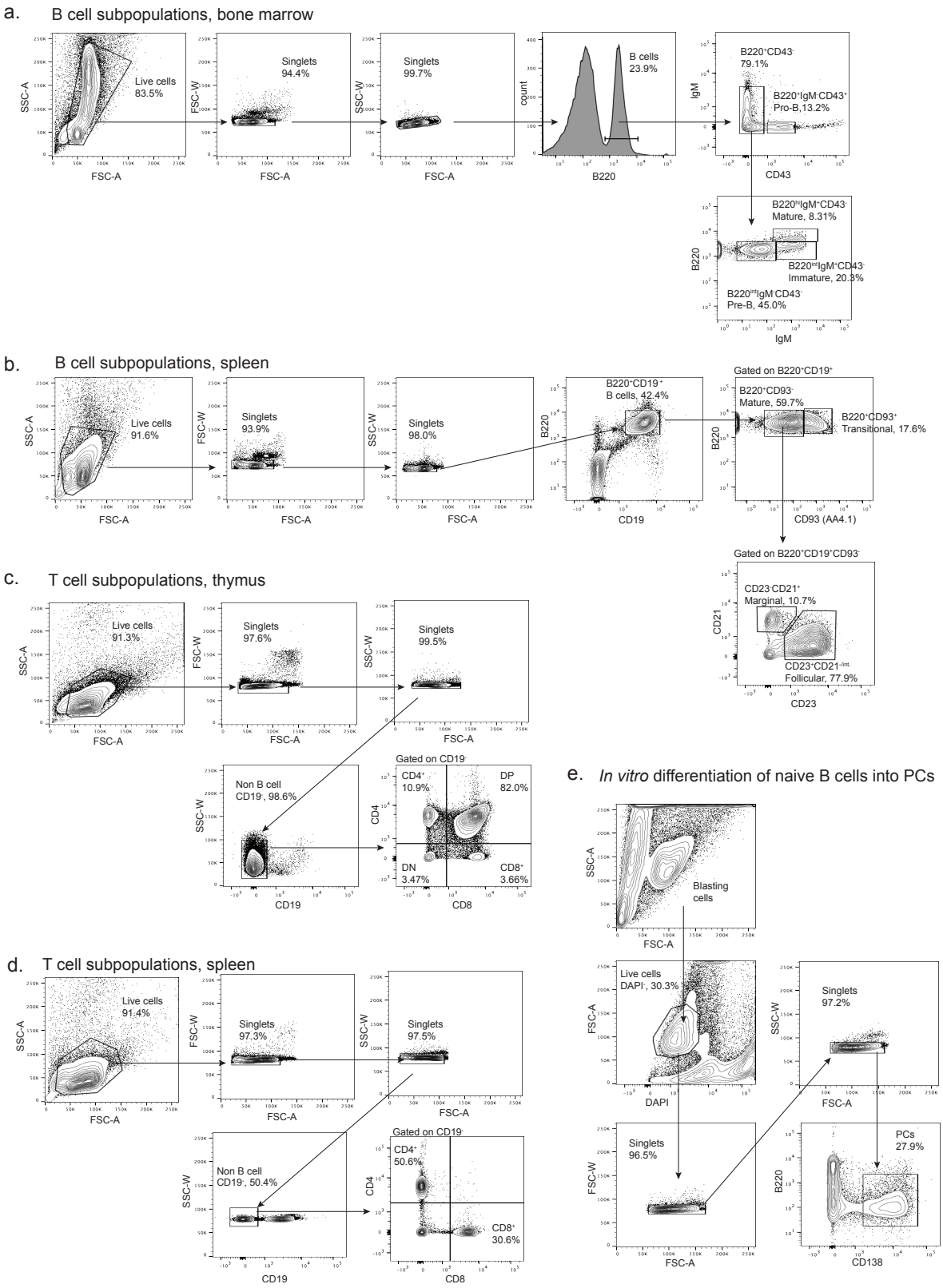

**Supplementary Figure 4** Representative gating strategy for flow cytometry analysis. (**a**) Representative gating strategy for analyzing the B cell subpopulations in the bone marrow. (**b**) Representative gating strategy for analyzing the B cell subpopulations in the spleen. (**c**) Representative gating strategy for analyzing the T cell subpopulations in the thymus. (**d**) Representative gating strategy for analyzing the T cell subpopulations in the spleen. (**e**) Representative gating strategy for analyzing the *in vitro* differentiation of naïve splenic B cells into PCs with either CD40L and IL-4 or CD40L, IL-4, and IL-5 stimulations.

**Supplementary Table 1** List of transcript and gene-level expression values, GO term overrepresentation results, and signature differentiation pathway scores from RNA-seq datasets for WT and *Crtc2-AA* TG B cells during the differentiation stage-course.

**Supplementary Table 2** List of mRNA alternative splicing events, differential expression overlaps, and GO term overrepresentation analysis of significantly spliced genes.

**Supplementary Table 3** List of relative amounts and statistical testing for LC-MS metabolomics steady-state abundances between WT and *Crtc2-AA* TG B cells at day 5 of differentiation.

**Supplementary Table 4** List of reagents, antibodies, and oligonucleotides used in this study.

# Chapter 3:

# Conclusions

Newly generated ASCs are mostly short-lived, as the frequency of antigen-specific ASCs drop exponentially during the primary antibody response[1]. However, the question of what regulates the survival and longevity of these cells has not been well characterized. Further, the size and capacity of survival niches in the bone marrow and other niches in the periphery, appear to be limited, as repeated booster immunizations have been shown to release mature PCs that secrete antibodies to alternate antigens into the blood stream[2]. Due to size limitations in these niches, it appears necessary for mechanisms to exist which limit the survival of PCs with lower antigen affinity while selecting for PCs with higher affinities[3]. Transcriptional profiling studies of LLPCs and SLPCs however, have failed to identify unique transcriptional signatures which could aid in elucidating such mechanisms.

In our study, we generated a TG mouse model to study the *in vivo* role of CRTC2 in B cell development, differentiation, and the humoral immune response. In doing so, we generated mice with two interesting phenotypes. The first mouse, which we did not study beyond initial characterization, exhibits B cell developmental defects in the bone marrow which result in spleens that are smaller in size compared to WT controls. The second mouse, the subject of this dissertation, exhibits normal B cell development and differentiation, but exhibits a defect in PC survival. We further showed that during differentiation, *Crtc2* expression remained stable in early and late dividing B cell populations, but was repressed in the PC population. Remarkably, whereas WT B cells repress endogenous *Crtc2* expression, TG B cells over-expressed the constitutively active and nucleus-localized mutant of *Crtc2* (*Crtc2-AA*) predominantly in the PC population. Further characterization of TG B cells revealed no defects in B cell

activation, proliferation, or other B cell fates such as CSR, and GC formation. We thus generated a mouse model that we can use to study the effects of CRTC2 dysregulation in PCs without the confounding factors that upstream defects in B cell responses and B cell fates may introduce.

The most interesting and impactful outcome of our study is that CRTC2 levels upon ASC differentiation may dictate the longevity of the ASC pool through its regulation of PC metabolism. From our previous and current data, CRTC2 can be inactivated and presumably be repressed at the mRNA level by BCR engagement[4, 5]. If proven that the strength of BCR signaling affects the level of *Crtc2* repression, we can begin to validate our model showing that antigen affinity and *Crtc2* expression dictates the longevity of PCs. This model attempts to address the question of how newly generated PCs in the bone marrow with varying degrees of antigen affinity are selected. In our model, PCs with the lowest *Crtc2* levels would be longer-lived because of increased oxidative metabolism. With increased survival, these PCs may have more time to access survival niches and acquire extrinsic survival signals, at which point the long-term survival of these cells may then become CRTC2-independent.

We tested this hypothesis by reanalyzing the RNA sequencing data by Lam *et al.* where they sorted and sequenced mouse splenic and bone marrow PC subsets based on B220 expression and 2NBDG import[6]. In our reanalysis, we confirmed a trend existed between PC subsets with longer half-lives and decreased *Crtc2* transcript levels. Differential gene expression analysis found no statistical significance between the sorted PC subsets. However, analysis of the makeup of each sorted PC subset revealed a high degree of contamination with other PC subsets, indicating that the

sorting purity was low. Perhaps because of this fact, Lam *et al.* also performed single cell RNA-seq of these sorted populations but *Crtc2* transcripts dropped out and were not counted[6]. Although not definitive, the data suggests further efforts should be pursued in 1) determining that BCR signal strength can directly affect *Crtc2* levels and 2) potentially performing our own single cell RNA sequencing of sorted PC subsets to analyze *Crtc2* transcript levels. Unfortunately, due to the low abundance and limitations in identifying PCs of varying half-lives and then sorting them, further studies may prove difficult without new methodologies[7].

Metabolic regulation of B cells is clearly important for B cell development, differentiation, and function. PBs differentiated by the TI antigen LPS, upregulate oxidative metabolism genes in a BLIMP1 dependent manner in order to support the production of antibodies[8]. In addition, PCs have been shown to increase import of glucose and amino acids and upregulate glycolysis and oxidative metabolism[9]. Further, a recent study of IRF4 which is critical for PC survival, found IRF4 regulated genes associated with metabolic pathways and maintained mitochondrial homeostasis[10]. As the CRTC family of co-activators have been associated with energy metabolism, mitochondria, and longevity, it perhaps was expected CRTC2 would affect metabolism[11, 12, 13]. Although we were unable to establish a direct mechanism for the deficiency in oxidative metabolism in TG PCs, GSVA of metabolic programs suggested a potential defect in metabolic reprogramming as TG PCs were shown to be metabolically more similar to WT and TG late dividing cells than WT PCs . Since we did not perform metabolic flux analysis with heavy isotope labeled glucose or glutamine, we were unable to determine how carbons were used in TG and WT PCs and therefore

cannot confirm a defect in metabolic reprogramming. However, gene expression and steady state metabolite profiling data does suggest a defect in the glycolytic pathway in TG PCs which would lead to a reduction in pyruvate synthesis. Additionally, it appears that TG PCs compensate for this defect by utilizing glutamine to fuel the TCA cycle. Both steady state metabolite profiling coupled with metabolic flux analysis will give us a clearer picture of how CRTC2 is affecting PC metabolism. Furthermore, determining the levels of TCA metabolites, such as $\alpha$-ketoglutarate and succinate, which regulate epigenetic modifiers may provide insights into whether there is also an impairment in epigenetic regulation of gene programs in TG compared to WT PCs[14, 15].

Additionally, Lam *et al.* established that the mitochondrial morphology of SLPCs and LLPCs were similar[16]. Much of the mitochondria's function can be determined by its size and morphology. Fused mitochondria are associated with increased oxidative metabolism, whereas fragmented mitochondria show inhibition of oxidative metabolism[17]. High-resolution confocal microscopy of TG and WT PCs revealed that there were no intrinsic differences in mitochondrial morphology, size, and abundance (data not shown). However, although TG PCs appear to compensate for the lack of pyruvate synthesis with glutamine anaplerosis, TG PCs still exhibit defects in oxidative metabolism. One explanation for this is that TG PCs may have defects in the individual electron transport chain (ETC) protein activity or supercomplex formation which would result in oxidative metabolism defects. TG PCs do in fact exhibit aberrant splicing of *Cep89, Ndufaf7,* and *Sirt3* which all have known roles in regulating ETC complex activity and formation[18, 19, 20]. It will be important to perform biochemical studies to

analyze ETC complex activity and to determine the extent of CRTC2 mediated metabolic defects in TG PCs.

We also observed that CD28, which is expressed in PCs and is critical for LLPC survival[21], is repressed 2.6-fold in TG PCs. CD28 activation establishes SRC and increases glycolysis and OXPHOS in memory T cells[22]. A previous study claimed that the pro-survival effect mediated by CD28 is through the translational upregulation of ATG5, increased autophagy activity, and elevated oxidative metabolism[23]. Interestingly, the study by Lam *et al.* also revealed an increase in autophagy staining in their sorted PC subsets. However, the increase in autophagy staining in PC subsets with longer half-lives was stated to be modest and subtle with unclear significance[7]. In our study, the transcriptional levels of *Atg5* were unchanged between TG and WT B cells, but we did not assess ATG5 protein levels, nor did we analyze autophagy. It will be interesting to see whether TG B cells are deficient in autophagy to determine another potential mechanism that could explain the reduced levels of oxidative metabolism and reduced survival in TG B cells. Additionally, CD28 has also been shown to regulate at the translational level, the expression of the anti-apoptotic factor BCL-$X_L$[24]. The lack of transcriptional differences between LLPCs and SLPCs suggests the potential for alternative means of regulation and requires analyses beyond mRNA expression quantification. Performing Western blot analysis on a selection of important factors that regulate differentiation and survival may be warranted to confirm that critical factors are unchanged at the translational levels in TG and WT PCs. Further, performing proteomics studies on TG and WT PCs to determine differential protein expression may uncover relevant factors and pathways that could regulate survival and longevity.

Surprisingly, we found CRTC2 inactivation and repression was required for the fidelity of mRNA alternative splicing programs. Although a previous study had shown over-expression of CRTC family members affect exon usage of *in vitro* splicing reporter assays, our study is the first to show in a physiologically relevant system that a CRTC family member can regulate alternative splicing. Since we did not perform CRTC2 ChIP-sequencing analysis of the PC population, it is unknown whether CRTC2 directly binds to the genes with alternative splicing events. Differential gene expression analysis did reveal numerous spliceosome related genes that were differentially expressed in TG PCs. However, whether these small magnitude changes in gene expression could account for the observed changes in alternative splicing events in TG compared to WT cells is unknown and perhaps unlikely. Interestingly, motif analysis of all genes that exhibited alternative splicing events, revealed an enrichment for the RNA binding motif protein 47 (RBM47).

RBM47 has been shown to regulate alternative splicing, stability, and abundance of several mRNAs. High-throughput sequencing and cross-linking immunoprecipitation (HITS-CLIP) analysis, which generates genome-wide protein-RNA interaction maps revealed that RBM47 bound predominantly to intronic and 3'UTRs of mRNAs[25]. In lung cancer cell lines, RBM47 bound genes were shown to regulate oxidative metabolism related genes. When RBM47 was knocked down in these lung cancer cell lines, oxidative metabolism was increased[26]. This suggests that RBM47, which was over-expressed by more than 4-fold in TG PCs may directly affect the splicing of many of the genes that exhibit aberrant splicing. Further work establishing RBM47 binding sites and direct target genes in TG and WT PCs by performing HITS-CLIP analysis should reveal

an important and previously unrecognized role for RBM47 in regulating PC metabolism and survival.

The study covered in this dissertation highlights a new and exciting role for CRTC2 in B cell biology. We show that by regulating both gene expression and mRNA alternative splicing programs in PCs, CRTC2 repression is required to regulate oxidative metabolism and survival of PCs. Over the course of this study, we were surprised to realize that TG PCs exhibited characteristics that mirrored the phenotype associated with SLPCs[16]. Therefore, we proposed a model where CRTC2 levels in differentiated ASCs could potentially regulate the ability of PCs to survive and establish long-term residency in survival niches. We were able to establish a trend between reduced *Crtc2* transcript levels and increased PC longevity, but further work will be required to validate this model. By beginning to delineate the molecular basis for PC metabolism and survival, we may be able in the future to modulate metabolic pathways in PCs for therapeutic means, either to enhance the efficacy of immunizations or to inhibit PCs that secrete pathogenic autoantibodies.

## References


1. Sze, D.M., Toellner, K.M., Garcia de Vinuesa, C., Taylor, D.R. & MacLennan, I.C. Intrinsic constraint on plasmablast growth and extrinsic limits of plasma cell survival. *J Exp Med* **192**, 813-821 (2000).

2. Odendahl, M. *et al.* Generation of migratory antigen-specific plasma blasts and mobilization of resident plasma cells in a secondary immune response. *Blood* **105**, 1614-1621 (2005).

3. Xiang, Z. *et al.* FcgammaRIIb controls bone marrow plasma cell persistence and apoptosis. *Nat Immunol* **8**, 419-429 (2007).

4. Kuraishy, A.I. *et al.* TORC2 regulates germinal center repression of the TCL1 oncoprotein to promote B cell development and inhibit transformation. *Proc Natl Acad Sci U S A* **104**, 10175-10180 (2007).

5. Sherman, M.H. *et al.* AID-induced genotoxic stress promotes B cell differentiation in the germinal center via ATM and LKB1 signaling. *Mol Cell* **39**, 873-885 (2010).

6. Lam, W.Y. *et al.* Metabolic and Transcriptional Modules Independently Diversify Plasma Cell Lifespan and Function. *Cell Rep* **24**, 2479-2492 e2476 (2018).

7. Lam, W.Y. & Bhattacharya, D. Metabolic Links between Plasma Cell Survival, Secretion, and Stress. *Trends Immunol* **39**, 19-27 (2018).

8. Price, M.J., Patterson, D.G., Scharer, C.D. & Boss, J.M. Progressive Upregulation of Oxidative Metabolism Facilitates Plasmablast Differentiation to a T-Independent Antigen. *Cell Rep* **23**, 3152-3159 (2018).

9. Akkaya, M. & Pierce, S.K. From zero to sixty and back to zero again: the metabolic life of B cells. *Curr Opin Immunol* **57**, 1-7 (2019).

10. Low, M.S.Y. *et al.* IRF4 Activity Is Required in Established Plasma Cells to Regulate Gene Transcription and Mitochondrial Homeostasis. *Cell Rep* **29**, 2634-2645 e2635 (2019).

11. Escoubas, C.C., Silva-Garcia, C.G. & Mair, W.B. Deregulation of CRTCs in Aging and Age-Related Disease Risk. *Trends Genet* **33**, 303-321 (2017).

12. Altarejos, J.Y. & Montminy, M. CREB and the CRTC co-activators: sensors for hormonal and metabolic signals. *Nat Rev Mol Cell Biol* **12**, 141-151 (2011).

13. Burkewitz, K. *et al.* Neuronal CRTC-1 governs systemic mitochondrial metabolism and lifespan via a catecholamine signal. *Cell* **160**, 842-855 (2015).

14. Lu, C. & Thompson, C.B. Metabolic regulation of epigenetics. *Cell Metab* **16**, 9-17 (2012).

15. Zan, H. & Casali, P. Epigenetics of Peripheral B-Cell Differentiation and the Antibody Response. *Front Immunol* **6**, 631 (2015).

16. Lam, W.Y. *et al.* Mitochondrial Pyruvate Import Promotes Long-Term Survival of Antibody-Secreting Plasma Cells. *Immunity* **45**, 60-73 (2016).

17. Galloway, C.A. & Yoon, Y. Mitochondrial dynamics in diabetic cardiomyopathy. *Antioxid Redox Signal* **22**, 1545-1562 (2015).

18. van Bon, B.W. *et al.* CEP89 is required for mitochondrial metabolism and neuronal function in man and fly. *Hum Mol Genet* **22**, 3138-3151 (2013).

19. Zurita Rendon, O., Silva Neiva, L., Sasarman, F. & Shoubridge, E.A. The arginine methyltransferase NDUFAF7 is essential for complex I assembly and early vertebrate embryogenesis. *Hum Mol Genet* **23**, 5159-5170 (2014).

20. Ahn, B.H. *et al.* A role for the mitochondrial deacetylase Sirt3 in regulating energy homeostasis. *Proc Natl Acad Sci U S A* **105**, 14447-14452 (2008).

21. Rozanski, C.H. *et al.* Sustained antibody responses depend on CD28 function in bone marrow-resident plasma cells. *J Exp Med* **208**, 1435-1446 (2011).

22. Klein Geltink, R.I. *et al.* Mitochondrial Priming by CD28. *Cell* **171**, 385-397 e311 (2017).

23. Peng, P., Chavel, C., Utley, A., Carlson, L., and Lee, KP. CD28 Regulates Autophagy to Enhance Plasma Cells Survival. Journal of Immunology; 2019; 2019.

24. Wu, L.X. *et al.* CD28 regulates the translation of Bcl-xL via the phosphatidylinositol 3-kinase/mammalian target of rapamycin pathway. *J Immunol* **174**, 180-194 (2005).

25. Vanharanta, S. *et al.* Loss of the multifunctional RNA-binding protein RBM47 as a source of selectable metastatic traits in breast cancer. *Elife* **3** (2014).

26. Sakurai, T. *et al.* RNA-binding motif protein 47 inhibits Nrf2 activity to suppress tumor growth in lung adenocarcinoma. *Oncogene* **35**, 5000-5009 (2016).

# APPENDIX I:

## AID-induced genotoxic stress promotes B cell differentiation in the germinal center via ATM and LKB1 signaling

Molecular Cell
Article

# AID-Induced Genotoxic Stress Promotes B Cell Differentiation in the Germinal Center via ATM and LKB1 Signaling

Mara H. Sherman,[1,10] Ali I. Kuraishy,[2,10] Chetan Deshpande,[8] Jason S. Hong,[3] Nicholas A. Cacalano,[4] Richard A. Gatti,[3] John P. Manis,[9] Michael A. Damore,[8] Matteo Pellegrini,[1,5,6,7] and Michael A. Teitell[1,3,6,7,*]
[1]Molecular Biology Institute
[2]Department of Human Genetics
[3]Department of Pathology and Laboratory Medicine, David Geffen School of Medicine
[4]Department of Radiation Oncology
[5]Department of Molecular, Cell, and Developmental Biology
[6]California NanoSystems Institute and Jonsson Comprehensive Cancer Center
[7]Broad Center of Regenerative Medicine and Stem Cell Research
University of California, Los Angeles, Los Angeles, CA 90095, USA
[8]Department of Molecular Sciences, Amgen Inc., Thousand Oaks, CA 91320, USA
[9]Department of Pathology, Harvard Medical School, Boston, MA 02115, USA
[10]These authors contributed equally to this work
*Correspondence: mteitell@mednet.ucla.edu
DOI 10.1016/j.molcel.2010.08.019

## SUMMARY

**During an immune response, B cells undergo rapid proliferation and activation-induced cytidine deaminase (AID)-dependent remodeling of *immunoglobulin* (*IG*) genes within germinal centers (GCs) to generate memory B and plasma cells. Unfortunately, the genotoxic stress associated with the GC reaction also promotes most B cell malignancies. Here, we report that exogenous and intrinsic AID-induced DNA strand breaks activate ATM, which signals through an LKB1 intermediate to inactivate CRTC2, a transcriptional coactivator of CREB. Using genome-wide location analysis, we determined that CRTC2 inactivation unexpectedly represses a genetic program that controls GC B cell proliferation, self-renewal, and differentiation while opposing lymphomagenesis. Inhibition of this pathway results in increased GC B cell proliferation, reduced antibody secretion, and impaired terminal differentiation. Multiple distinct pathway disruptions were also identified in human GC B cell lymphoma patient samples. Combined, our data show that CRTC2 inactivation, via physiologic DNA damage response signaling, promotes B cell differentiation in response to genotoxic stress.**

## INTRODUCTION

DNA double-strand breaks (DSBs) are generated during the assembly and diversification of antigen receptor genes in developing lymphocytes. During early B cell maturation in the bone marrow, the recombinase activating gene (RAG) endonuclease generates complete antigen receptor genes by the process of *V(D)J* recombination (Fugmann et al., 2000; Tonegawa, 1983). The generation of a diverse repertoire of high-affinity antibodies (Abs) requires further modifications of the *immunoglobulin* (*IG*) genes (Rajewsky, 1996; Revy et al., 2000) in secondary lymphoid follicles within compartments known as germinal centers (GCs). GCs are sites within lymphoid tissues where mature B cells rapidly proliferate, modify *IG* gene sequences, and differentiate in response to a stimulating antigen. A key feature of *IG* remodeling is class switch recombination (CSR), a process that modifies the effector function of an Ab by replacing one constant region of the *IG* gene with another. CSR requires activation-induced cytidine deaminase (AID)-generated DSB intermediates (Chaudhuri et al., 2003; Muramatsu et al., 2000) and subsequent repair of distal severed ends. This genomic remodeling is critical for a robust Ab response, but genotoxic stress associated with the GC reaction also promotes most human lymphomas (Küppers and Dalla-Favera, 2001).

In order to preserve genomic integrity, mammalian cells undergoing genotoxic stress usually respond by activating a complex DNA damage response (DDR). This response, which is required to prevent tumor formation, includes inhibition of cellular proliferation and/or induction of apoptosis (Khanna and Jackson, 2001). In GC B cells, the DDR is coordinated by the ATM serine/threonine kinase, which senses DSBs in concert with the MRN (MRE11-RAD50-NBS1) complex (Kastan and Bartek, 2004). This response is critical for humoral immunity and evasion of tumorigenesis because defects in CSR and increased chromosomal lesions occur in activated mature B cells from mice lacking ATM (Lumsden et al., 2004; Reina-San-Martin et al., 2004) or its target proteins 53BP1 (Manis et al., 2004; Ward et al., 2004), H2AX (Franco et al., 2006), NBS1 (Kracker et al., 2005; Reina-San-Martin et al., 2005), and MDC1 (Lou et al., 2006).

During the GC reaction, B cells express the BCL6 oncoprotein, which functions as a transcriptional repressor of the *PRDM1* gene encoding BLIMP-1 (Shaffer et al., 2000), the master regulator of plasma cell differentiation (Turner et al., 1994). Importantly, BCL6 also suppresses key components of the DDR in the GC by repressing the expression of *ATR* (Ranuncolo et al., 2007), *TP53* (Phan and Dalla-Favera, 2004), and *CDKN1A* (*P21*) (Phan et al., 2005). This suppression may enable GC B cells to proliferate rapidly without triggering cellular senescence or apoptosis programs, although the resulting modified DDR increases the susceptibility of GC B cells to malignant transformation. Accordingly, BCL6 downregulation is required for post-GC B cell differentiation and evasion of tumorigenesis (Cattoretti et al., 2005).

ATM promotes and BCL6 represses the DDR, representing antagonistic forces in the life of a GC B cell. To terminate the GC reaction, rapidly proliferating B cells must tip this balance toward exiting the cell cycle to allow for terminal differentiation, although a mechanism initiating this shift has not been identified. Previously, we showed that B cell antigen receptor (BCR) engagement led to cytoplasmic sequestration and inactivation of the CREB transcriptional coactivator CRTC2 (TORC2), causing downregulation of the *TCL1* oncogene in GC B cells (Kuraishy et al., 2007). Studies of glucose metabolism regulation have shown that CRTC2 inactivation results from phosphorylation at S-171 (Screaton et al., 2004) and/or S-275 (Jansson et al., 2008) by members of the AMPK family, promoting a physical association between CRTC2 and the cytoplasmic chaperone 14-3-3. However, the physiologic event(s) that inactivate CRTC2 in GC B cells are unknown. Because GC B cells experience both DNA damage and CRTC2 inactivation-dependent *TCL1* repression, we hypothesized that CRTC2 is inhibited by the DDR and that CRTC2 controls an extended gene program beyond *TCL1*. Testing of this hypothesis led to the discovery of a DDR pathway in GC B cells, with exogenous or intrinsic AID-induced DSBs activating ATM signaling to LKB1, a master kinase for AMPK family member proteins (Lizcano et al., 2004), which then resulted in the inactivation of CRTC2. Suggesting a role as a key homeostatic regulator, changes in gene expression resulting from CRTC2 inactivation were essential for cessation of the GC reaction, plasma cell differentiation, and suppression of tumorigenesis.

## RESULTS

### DNA Double-Strand Breaks Inactivate CRTC2

To determine whether DNA damage inactivates CRTC2, we induced DSBs in the Ramos human GC B cell line by using etoposide (Eto) or γ-irradiation (IR), which are known to generate γ-H2AX foci (Phan et al., 2007). Subcellular fractionation showed that DSBs caused a shift in CRTC2 localization from the nucleus to the cytoplasm (Figure 1A). This change in CRTC2 location was accompanied by an increased association between CRTC2 and the cytoplasmic chaperone 14-3-3 (Figure 1B) (Jansson et al., 2008; Screaton et al., 2004). Chromatin immunoprecipitation (ChIP) showed a >4-fold reduction in the association between CRTC2 and the CRTC2-responsive *TCL1* promoter with DSBs (Figure 1C). DSBs also repressed expression of the *TCL1* promoter (Figure 1D and Figures S1A–S1C, available online). Combined, these data show that DSBs inactivate CRTC2, leading to repression of CRTC2-dependent gene expression.

### DSB-Induced CRTC2 Inactivation Requires Activation of ATM and LKB1

We next tried to identify a link between DSBs and CRTC2 inactivation. Since the DNA damage-sensing kinase ATM is required for CSR (Lumsden et al., 2004; Reina-San-Martin et al., 2004), we evaluated ATM for a role in CRTC2 inactivation. Induced DSBs in Ramos cells activated ATM (Figure S2A). ATM loss of function, using two different shRNA sequences targeting *ATM*, pharmacological inhibition with the ATM inhibitor Kudos, and the use of B cell lines from ATM-deficient ataxia-telangiectasia (A-T) patients showed a requirement for ATM in DSB-induced CRTC2 inactivation (Figures 2A–2D and Figures S2B–S2D). ATM phosphorylates multiple substrates during the DDR (Matsuoka et al., 2007), potentially including T366 of the tumor suppressor LKB1 (Fernandes et al., 2005; Sapkota et al., 2002). In turn, LKB1 phosphorylates and inactivates CRTC2 through AMPK family members (Fu and Screaton, 2008; Katoh et al., 2006; Shaw et al., 2005), suggesting a pathway from DSBs to CRTC2 inactivation. DSBs caused ATM-dependent phosphorylation of LKB1 T366 (Figures S2E and S2F). Similarly, DSBs induced LKB1 phosphorylation in primary B cells (Figure S2G). Metformin is an antidiabetic drug that promotes LKB1-dependent activation of AMPK (Shackelford and Shaw, 2009; Shaw et al., 2005). Ramos cells exposed to metformin showed reduced nuclear localization of CRTC2 and *TCL1* repression (Figures S2H–S2J). shRNA knockdown of *LKB1* with two different sequences lessened CRTC2 inactivation in response to DSBs in Nalm-6 pre-B cells (Figures S2K and S2L) and Ramos cells (Figures 2E–2G, Figures S2M and S2N). These data demonstrate that DSBs inactivate CRTC2 via ATM and LKB1 signaling, providing a gene regulation mechanism during the DDR.

### CRTC2 Inactivation Occurs during CSR in GC B Cells

To determine the role of CRTC2 in GC B cells, we evaluated changes in CRTC2 activity and direct target gene expression over the course of a GC reaction. For this, we modified an in vitro B cell differentiation system starting with naive human tonsil B cells (Figure 3A) (Arpin et al., 1995; Fluckiger et al., 1998). Rapid B cell expansion and correct modulation of established GC B and plasma cell markers (BCL6, MYC, OCA-B, and BLIMP-1) occurred over 7 days, as expected for a GC-like reaction (Figures 3B–3D) (Allman et al., 1996; Greiner et al., 2000; Shaffer et al., 2008). Though undetectable on day 3, soluble and membrane-bound IgG (32% of cells) was detected by day 7 (Figure 3E and Figure S3A), preceded by γ-H2AX focus formation by day 5 (Figure S3B) (Petersen et al., 2001). These results indicate that CSR followed by plasma cell differentiation was induced during a GC-like reaction between days 3 and 7 of culture.

CRTC2 activity was evaluated during the interval in which CSR occurred. Nuclear CRTC2 decreased between days 3 and 7 (Figure 3F) with a coinciding decrease in the association between CRTC2 and the *TCL1* promoter and decreased *TCL1* expression, as observed in vivo (Figures 3G and 3H) (Said

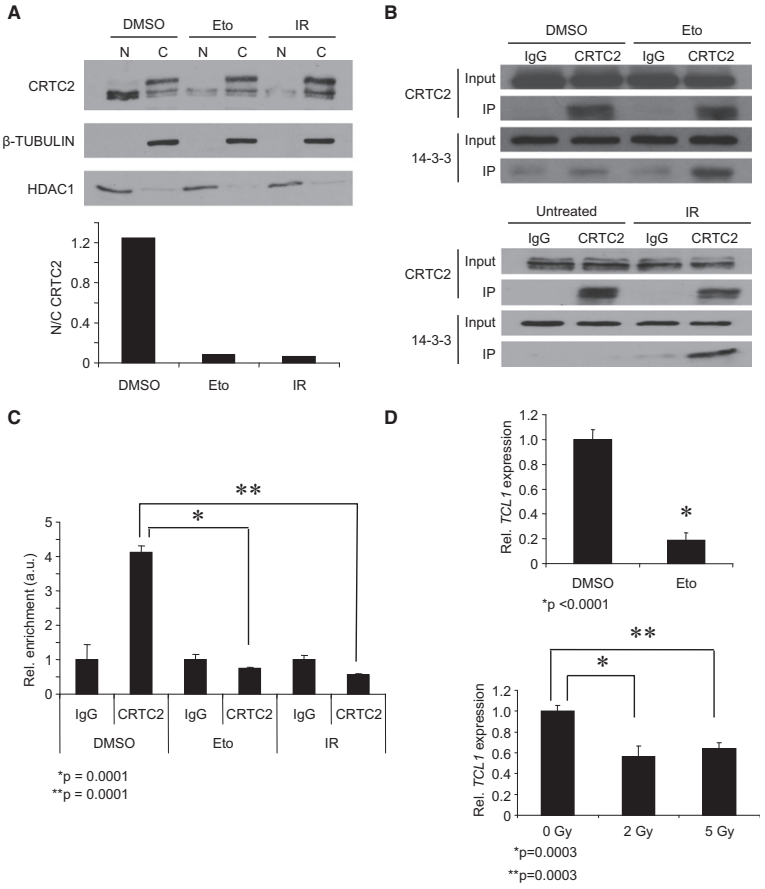


**Figure 1. DNA Double-Strand Breaks Inactivate CRTC2**

(A) Top: immunoblot showing CRTC2 protein expression in the nucleus (N) and cytoplasm (C) of Ramos B cells exposed to DMSO (control), Eto (20 μM, 1 hr), or IR (5 Gy). Upper bands in the cytoplasm lanes indicate phosphorylated CRTC2. β-TUBULIN (cytoplasm) and HDAC1 (nucleus) are loading controls. Bottom: nuclear/cytoplasmic ratios for CRTC2 are plotted from densitometry.

(B) Top: immunoprecipitation of CRTC2 or rabbit IgG from lysates of Ramos cells exposed to DMSO or Eto (20 μM, 1 hr). Bottom: untreated cells were compared to cells exposed to IR (5 Gy). Immunoblots for lysates (Input) and CRTC2 or 14-3-3 immunoprecipitates (IP) are shown.

(C) ChIP for CRTC2 or rabbit IgG using chromatin from Ramos cells after DMSO, Eto (20 μM, 1 hr), or IR (5Gy). Immunoprecipitates were analyzed by qPCR for the *TCL1* promoter. Values were normalized to the *ACTB* promoter and shown as arbitrary units (a.u.). Values are expressed as the mean ± SEM for three independent experiments.

(D) Top: qPCR for *TCL1* in Ramos cells after DMSO or Eto (20 μM, 6 hr). Bottom: untreated cells were compared to cells exposed to the indicated doses of IR. Values were normalized to *36B4*. Values are expressed as the mean ± SEM for three independent experiments.

et al., 2001; Teitell et al., 1999). Importantly, similar CRTC2 modulation was observed during GC B cell development in vivo (Figure S3C) (Klein et al., 2003; Said et al., 2001), with ~70% of plasma cells containing entirely cytoplasmic CRTC2 and ~30% negative for CRTC2 protein expression. Combined, these results strongly suggest that CRTC2 becomes phosphorylated and sequestered in the cytoplasm and inactivated during CSR in vivo, resulting in reduced expression of CRTC2-dependent target genes, such as *TCL1* (Figure S3D).

## AID-Dependent ATM to LKB1 Signaling in GC B Cells Inactivates CRTC2

The requirement for ATM and LKB1 as upstream regulators of CRTC2 inactivation was assessed in the modeled GC-like

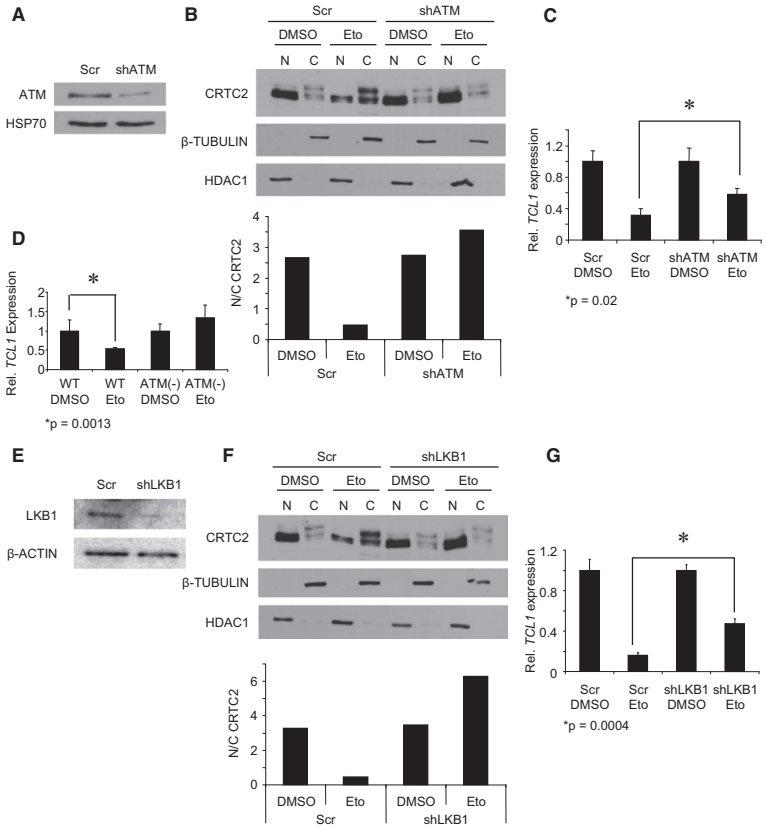


**Figure 2. DSB-Induced CRTC2 Inactivation Requires Activation of ATM and LKB1**

(A) Immunoblot showing ATM knockdown in Ramos cells 4 days after transduction. HSP70 is a loading control.

(B) Top: immunoblot showing CRTC2 protein expression in the nucleus (N) and cytoplasm (C) of Ramos cells transduced with control (Scr) shRNA or shATM after exposure to DMSO or Eto (20 μM, 1 hr). β-TUBULIN (cytoplasm) and HDAC1 (nucleus) are loading controls. Bottom: nuclear/cytoplasmic ratios for CRTC2 are plotted from densitometry.

(C) qPCR for *TCL1* in shATM or control (Scr) Ramos cells after DMSO or Eto (20 μM, 6 hr) exposure. Values were normalized to *36B4*. Values are expressed as the mean ± SEM for three independent experiments.

(D) qPCR for *TCL1* in WT or ATM-deficient lymphoblastoid cells exposed to DMSO or Eto (20 μM, 6 hr). Values were normalized to *36B4*. Values are expressed as the mean ± SEM for three independent experiments.

(E) Immunoblot showing LKB1 knockdown in Ramos cells 4 days after transduction. β-ACTIN is a loading control.

(F) Top: immunoblot showing CRTC2 protein expression in the nucleus (N) and cytoplasm (C) of Ramos cells transduced with control (Scr) shRNA or shLKB1 after exposure to DMSO or Eto (20 μM, 1 hr). β-TUBULIN (cytoplasm) and HDAC1 (nucleus) are loading controls. Bottom: nuclear/cytoplasmic ratios for CRTC2 are plotted from densitometry.

(G) qPCR for *TCL1* in shLKB1 or control (Scr) Ramos cells after DMSO or Eto (20 μM, 6 hr) exposure. Values were normalized to *36B4*. Values are expressed as the mean ± SEM for three independent experiments.

reaction. An increase in phospho-ATM S1981 was detected by day 7 (Figure 4A), coinciding with DSB generation during CSR. ATM knockdown (Figure 4B) resulted in increased CRTC2 nuclear localization during B cell differentiation compared to control cells (Figure 4C). Similar results were obtained for LKB1 (Figures 4D–4F). These data strongly suggest that GC-like B cells responding to physiologic DSBs activate ATM to LKB1 signaling to inactivate CRTC2. This pathway is engaged during the period of CSR, further suggesting a link to Ab production and B cell maturation.

To directly determine whether CSR drives CRTC2 inactivation, we compared the subcellular localization of CRTC2 in B cells from wild-type (WT) and *AID* knockout mice. AID-deficient B cells cannot produce DSBs at *IG* loci and therefore CSR does

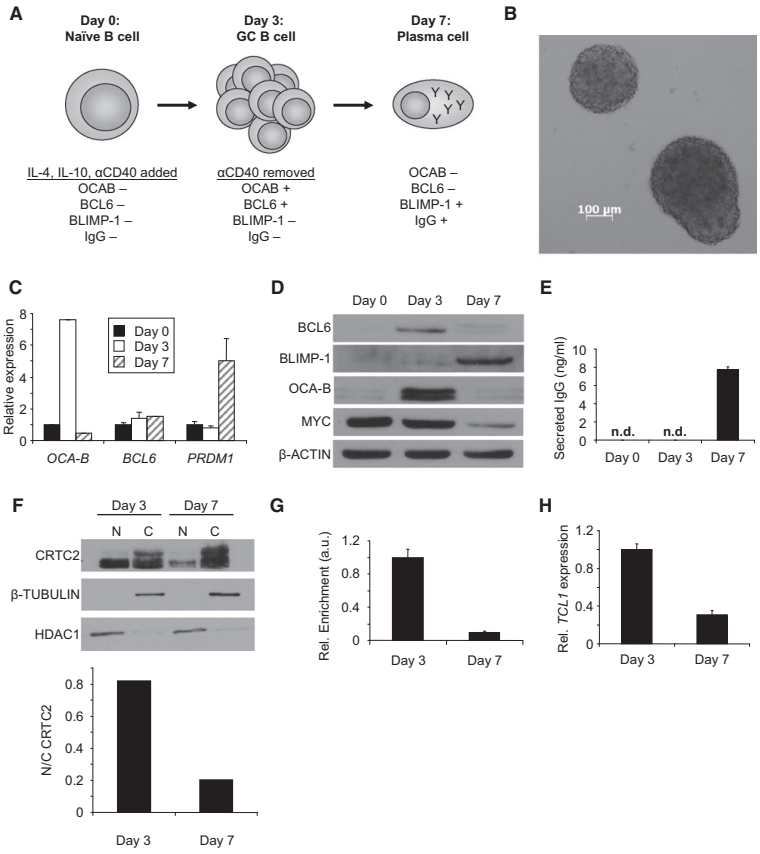


**Figure 3. CRTC2 Inactivation Occurs during CSR in GC B Cells**

(A) Schematic of primary human B cell differentiation system.

(B) Phase-contrast image of expanding human B cell clusters 24 hr after stimulation (at a magnification of 5×).

(C) qPCR for *OCA-B*, *BCL6*, and *PRDM1* in human B cells at 0, 3, or 7 days of differentiation. Values are normalized to *36B4* and are expressed as the mean ± SEM for three independent experiments.

(D) Immunoblot for BCL6, BLIMP-1, OCA-B, and MYC in primary human B cells after 0, 3, or 7 days of differentiation. β-ACTIN is a loading control.

(E) ELISA for total IgG in human B cell culture media harvested after 0, 3, or 7 days of differentiation. n.d. = none detected. Values are expressed as the mean ± SEM for three independent experiments.

(F) Top: immunoblot showing CRTC2 protein expression in the nucleus (N) and cytoplasm (C) of primary human B cells on days 3 or 7 of differentiation. β-TUBULIN (cytoplasm) and HDAC1 (nucleus) are loading controls. Bottom: nuclear/cytoplasmic ratios for CRTC2 are plotted from densitometry.

(G) ChIP for CRTC2 using chromatin from human B cells after 3 or 7 days of differentiation. Immunoprecipitates were analyzed by qPCR for the *TCL1* promoter. Values are normalized to an intergenic region and shown as a.u. Values are expressed as the mean ± SEM for three independent experiments.

(H) qPCR for *TCL1* in human B cells after 3 or 7 days of differentiation. Values are normalized to *36B4*. Values are expressed as the mean ± SEM for three independent experiments.

not occur (Muramatsu et al., 2000). αCD40 and IL-4 induced CSR in ~43% of WT but not in *AID* knockout B cells (Figure S4). Most importantly, CRTC2 was retained in the nucleus of *AID* knockout B cells compared to its nuclear depletion in WT B cells (Figure 4G). This result strongly supports the requirement for physiologic DSBs induced by AID during CSR for ATM- and LKB1-dependent CRTC2 inactivation.

## CRTC2 Regulates Genes that Control B Cell Development

The effect of CRTC2 inactivation on global gene expression in GC B cells was evaluated. ChIP-on-chip for CRTC2 target genes in Ramos cells was performed with two Abs that recognize distinct CRTC2 epitopes (Figure S5A). The genomic DNA bound to CRTC2 and total input DNA were distinctly labeled and

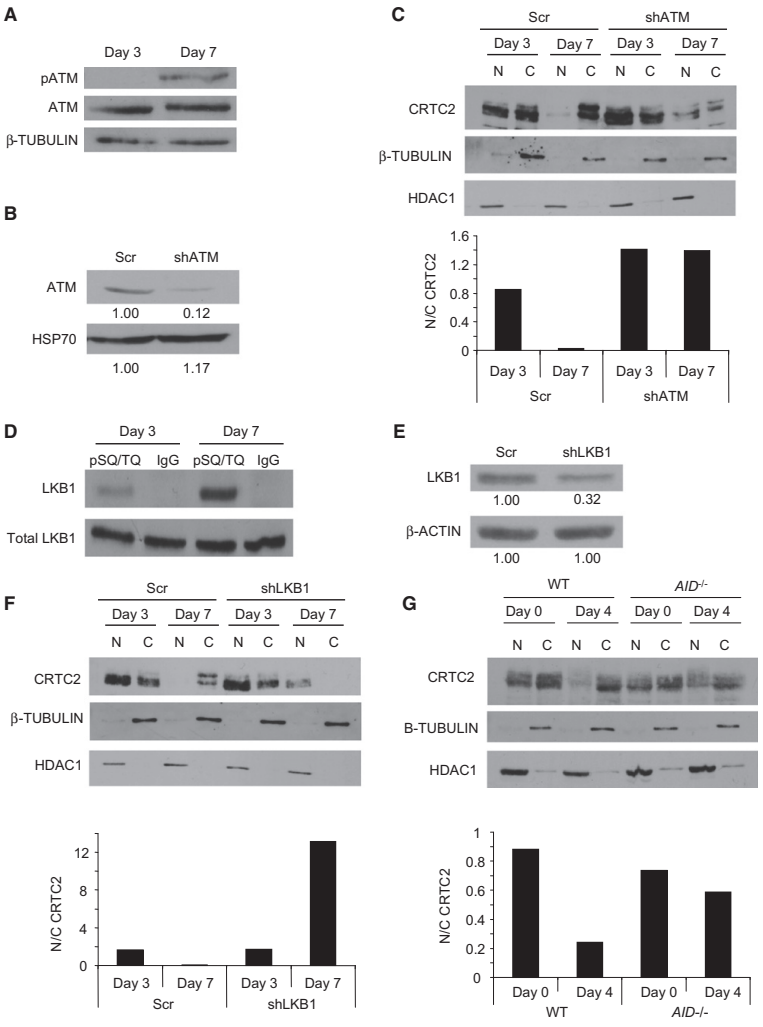


**Figure 4. AID-Dependent ATM to LKB1 Signaling in GC B Cells Inactivates CRTC2**

(A) Immunoblot of pATM (S1981) and ATM in human B cells after 3 or 7 days of differentiation. β-TUBULIN is a loading control.

(B) Immunoblot showing ATM knockdown in human B cells 3 days after shATM transduction. HSP70 is a loading control. Densitometric values are indicated below each band.

(C) Top: immunoblot showing CRTC2 protein expression in the nucleus (N) and cytoplasm (C) of primary human B cells, transduced with control (Scr) or shATM-expressing lentiviruses, on days 3 or 7 of differentiation. β-TUBULIN (cytoplasm) and HDAC1 (nucleus) are loading controls. Bottom: nuclear/cytoplasmic ratios for CRTC2 are plotted from densitometry.

(D) Immunoprecipitation of phosphorylated ATM/ATR substrates (pSQ/TQ) or a rabbit IgG control from lysates of human B cells after 3 or 7 days of differentiation. Lysates (Total LKB1) or immunoprecipitates (LKB1) are analyzed by immunoblot for LKB1.

(E) Immunoblot showing LKB1 knockdown in human B cells 3 days after shLKB1 transduction. β-ACTIN is a loading control. Densitometric values are indicated below each band.

(F) Top: immunoblot showing CRTC2 protein expression in the nucleus (N) and cytoplasm (C) of primary human B cells, transduced with control (Scr) or shLKB1-expressing lentiviruses, on days 3 or 7 of differentiation. β-TUBULIN (cytoplasm) and HDAC1 (nucleus) are loading controls. Bottom: nuclear/cytoplasmic ratios for CRTC2 are plotted from densitometry.

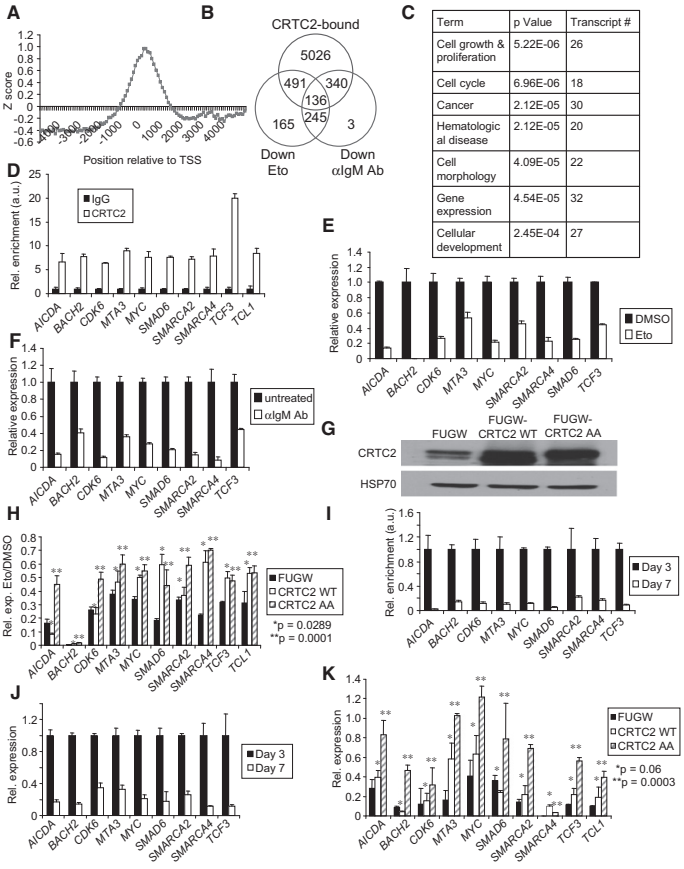


| Term | p Value | Transcript # |
|---|---|---|
| Cell growth & proliferation | 5.22E-06 | 26 |
| Cell cycle | 6.96E-06 | 18 |
| Cancer | 2.12E-05 | 30 |
| Hematological disease | 2.12E-05 | 20 |
| Cell morphology | 4.09E-05 | 22 |
| Gene expression | 4.54E-05 | 32 |
| Cellular development | 2.45E-04 | 27 |

**Figure 5. CRTC2 Regulates a Gene Program that Controls B Cell Development**

(A) Plotted z scores for CRTC2 binding to human promoter regions relative to the predicted transcriptional start sites (TSS).

(B) Venn diagram displaying putative CRTC2 direct target genes as defined by downregulation with exposure to α-IgM Ab and Eto and CRTC2 binding to the promoter region.

(C) Gene ontology (GO) analysis of candidate CRTC2 target genes. p values are based on a hypergeometric distribution.

(D) ChIP for CRTC2 or rabbit IgG in Ramos cells. Immunoprecipitates were analyzed by qPCR for the promoters of CRTC2 target genes. Values are normalized to intergenic regions and shown as a.u. Values are expressed as the mean ± SEM for three independent experiments.

(E) qPCR for CRTC2 target genes in Ramos cells after DMSO or Eto (20 μM, 6 hr) exposure. Values are normalized to *36B4* and are expressed as the mean ± SEM for three independent experiments.

(F) qPCR for CRTC2 target genes in Ramos cells with or without α-IgM (10 μg/ml, 6 hr) exposure. Values are normalized to *36B4*. Values are expressed as the mean ± SEM for three independent experiments.

(G) Immunoblot for CRTC2 protein expression in Ramos cells 48 hr after infection with the indicated lentivirus. HSP70 is a loading control.

(H) qPCR for CRTC2 target genes in Ramos cells transduced with the indicated lentivirus. DMSO or Eto (20 μM, 6 hr) exposures were initiated 48 hr after infection. Values are normalized to *36B4* and are expressed as the mean ± SEM for three independent experiments.

(I) ChIP for CRTC2 using chromatin from human B cells after 3 or 7 days of differentiation. Immunoprecipitates were analyzed by qPCR for the promoters of CRTC2 target genes. Values are normalized to intergenic regions, are shown as a.u., and are expressed as the mean ± SEM for three independent experiments.

(J) qPCR for CRTC2 target genes in human B cells after 3 or 7 days of differentiation. Values are normalized to *36B4* and are expressed as the mean ± SEM for three independent experiments.

(K) qPCR for CRTC2 target genes in human B cells transduced with the indicated lentivirus after 3 or 7 days of differentiation. Values are normalized to *36B4* and are expressed as the mean ± SEM for three independent experiments.

cohybridized to Agilent 244K human promoter microarrays that contained 60-mer oligonucleotide probes covering the region from −5.5 kb to +2.5 kb relative to the transcriptional start sites for ~17,000 annotated human genes. The vast majority of bound sequences were located within 1 kb of transcriptional start sites (Figure 5A), consistent with a previous global analysis of CREB promoter occupancy (Zhang et al., 2005). This approach revealed that CRTC2 occupied the promoters of 5993 genes (Figures S5B and S5C). Motif analysis among the bound sequences identified conventional CRE half-sites as the two most highly enriched of all possible 6-mers ($p = 10^{-22.5}$; Figure S5D), as anticipated for a coactivator of CREB. Gene expression profiling was also performed with Ramos cells treated with Eto or anti-IgM Ab, which was also shown to inactivate CRTC2 (Kuraishy et al., 2007). This screen identified 136 putative CRTC2-regulated genes (Figure 5B, Table S1) implicated in cellular growth and proliferation, the cell cycle, and cancer (Figure 5C).

To validate these findings, we selected ten candidate CRTC2 target genes that have functional relevance for GC B cell development and/or lymphomagenesis. Gene-specific ChIP demonstrated enrichment for promoter regions of these ten candidate

(G) Top: immunoblot showing CRTC2 protein expression in the nucleus (N) and cytoplasm (C) of spleen B cells from WT or *AID* knockout (*AID*$^{-/-}$) mice on days 0 and 4 of differentiation. β-TUBULIN (cytoplasm) and HDAC1 (nucleus) are loading controls. Bottom: nuclear/cytoplasmic ratios for CRTC2 are plotted from densitometry.

CRTC2 target genes with a CRTC2 Ab compared to an isotype control (Figure 5D). Gene expression changes were measured with Eto or anti-IgM treatment, with quantitative polymerase chain reaction (qPCR) validating the expression array results (Figures 5E and 5F). To determine a causal relationship between CRTC2 inactivation and downregulation of candidate CRTC2 target genes, we used a lentiviral expression system to transduce Ramos cells with WT or mutant CRTC2 in which serines 171 and 275 were mutated to alanines (CRTC2-AA; Figure 5G and Figure S5E). CRTC2-AA should remain in the nucleus because both serines require phosphorylation by AMPK to exclude CRTC2 from the nucleus (Jansson et al., 2008; Screaton et al., 2004). CRTC2-WT overexpression or continued activation by CRTC2-AA caused a derepression of the ten target genes with DSBs or with anti-IgM exposure (Figure 5H and Figure S5F), indicating that expression of these genes is dependent upon CRTC2 activity. Similar results were obtained from primary human B cells (Figures 5I–5K). Supporting the connection between genotoxic stress and CRTC2 target gene regulation, pretreatment of Ramos cells with the ATM inhibitor Kudos caused a significant depression of CRTC2 target genes with DSBs (Figure S5I). In addition, a significant derepression of CRTC2 target genes occurred when DSBs were induced in immortalized B cells from A-T patients, which lack functional ATM, compared to WT controls (Figure S5G). A-T cells also exhibited a striking retention of CRTC2 in the nucleus after Eto exposure compared to WT controls (Figure S5H).

### CRTC2 Inactivation Is Required for Plasma Cell Differentiation

To determine the effect of signaling that inactivates CRTC2 on B cell development, we stimulated naive tonsil B cells efficiently transduced with CRTC2-WT or CRTC2-AA to generate a GC-like reaction. Proliferating GC B cells, or centroblasts, are among the fastest proliferating cells in the body (Klein and Dalla-Favera, 2008), and plasma cell differentiation is characterized in part by repression of pro-proliferative gene expression (Shaffer et al., 2002). Hyperactive or overexpressed CRTC2 caused a marked increase in proliferation (Figure 6A), a decrease in soluble IgG production (Figure 6B), impaired induction of the plasma cell master regulator BLIMP-1 (Figure 6C), and sustained expression of the GC B cell master regulator BCL6 (Figure 6D) on day 7 of culture. Similar results were obtained when *ATM* or *LKB1* expression was decreased by shRNAs (Figures 6E–6H). Interestingly, transduced CRTC2 did not impair CSR, as equivalent levels of productive *IGG* transcripts were generated in CRTC2-overexpressing and control cells (Figures S6A and S6B). These data strongly suggest that the DDR pathway leading to CRTC2 inactivation is required for efficient termination of the GC reaction and Ab secretion.

### CRTC2 Inactivation Is Disrupted in GC-Derived B Cell Lymphomas

Since *TCL1* is often overexpressed in GC B cell lymphomas (Klein et al., 2001; Narducci et al., 2000; Said et al., 2001), we assessed this signaling pathway in human lymphoma samples. qPCR analysis revealed a 10-fold or greater loss of *ATM* expression in 6/17 (35%), or *LKB1* expression in 7/17 (41%), clinical samples (Figures 7A and 7B). *CRTC2* expression was not altered in these tumors (data not shown), so the *CRTC2* coding sequence was evaluated for alterations. A C→T missense mutation was identified in 10/17 tumor samples, compared with 0/14 normal tonsil samples ($p < 0.0005$, one-sided Fisher's exact test) (Figure 7C and Figure S7). This change results in a L→F amino acid substitution in the AMPK recognition sequence of the CRTC2 protein (Screaton et al., 2004). Although this alteration is conservative, it prevented inactivation of CRTC2 in Ramos B cells subjected to DSBs (Figures 7D and 7E), perhaps by disrupting AMPK-CRTC2 or CRTC2-14-3-3 interactions. Consistent with this result, *TCL1* expression was maintained in 11 of 13 B cell lymphomas that harbored disruptions in the ATM→LKB1→AMPK→CRTC2 signaling pathway (Figure 7F). These results provide evidence for aberrant CRTC2 activity in human lymphomas from multiple, distinct defects in a DDR pathway.

## DISCUSSION

Here, we describe a mechanism in which exogenous and physiologic DNA damage in GC B cells leads to CRTC2 inactivation, which is required for IG secretion and plasma cell differentiation. Although a prior study showed a BCR signaling requirement for Ab affinity-driven plasma cell development (Phan et al., 2006), the cues that cause GC B cells to differentiate into plasma cells are unknown. Previously, we showed that CRTC2 is also inactivated by BCR engagement (Kuraishy et al., 2007), suggesting that CRTC2 inactivation is a response to both genotoxic stress and BCR signaling, which terminates the GC reaction. More broadly, these results also implicate LKB1 as a central kinase with the potential to integrate metabolic and now AID-initiated genotoxic stress signaling in a pathway that can terminate with CRTC2 inactivation to drive terminal cell differentiation.

Our results, along with aspects of two recent studies, provide an important direction for the DDR by coupling genotoxic stress to non-DNA-repair-related physiologic or pathologic cellular maturation. One recent study in pre-B cells demonstrated that RAG-induced DSBs during *V(D)J* recombination activated transcription by NF-κB, leading to the expression of mature lymphocyte-specific genes (Bredemeyer et al., 2008). However, this study required genetically sustained RAG-induced DSBs to detect mature lymphocyte gene expression, leaving open the question of physiologic relevance. A second recent study showed that genotoxic stress opposed self-renewal in melanocyte stem cells (MSCs) and caused the MSCs to aberrantly differentiate into ectopically pigmented melanocytes, resulting in irreversible hair graying (Inomata et al., 2009). This form of abnormal differentiation resulted from pathologic DNA damage accumulation from the environment, which led to lineage degeneration and aging by an unknown mechanism. In contrast, our study shows a mechanism linking physiologic, AID-induced DSBs to ATM and LKB1 signaling in order to inactivate CRTC2, with CRTC2 inactivation required for the differentiation of plasma cells. This regulatory function exceeds the established response to DSBs that maintains genomic integrity, and it provides evidence that the DDR influences normal cell development and physiology. A potential ontologic reason for coupling genotoxic stress with differentiation is that the forced elimination

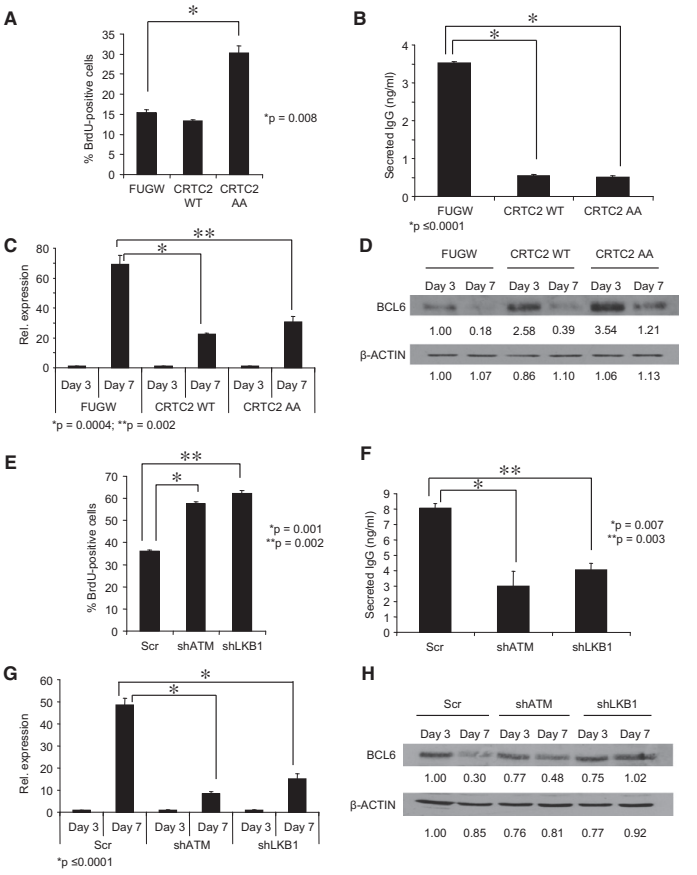


**Figure 6. CRTC2 Inactivation is Required for Plasma Cell Differentiation**

(A) BrdU incorporation in human B cells, transduced with the indicated lentivirus, on day 7 of differentiation. BrdU-FITC-positive cells were detected by flow cytometry. Values are expressed as the mean ± SEM for three independent experiments.

(B) ELISA for total secreted IgG in human B cell culture media harvested after day 7 of differentiation. Cells were transduced with the indicated lentivirus prior to the initiation of differentiation. Values are expressed as the mean ± SEM for three independent experiments.

(C) qPCR for *PRDM1* expression in human B cells transduced with the indicated lentivirus after 3 or 7 days of differentiation. Values are normalized to *36B4* and are expressed as the mean ± SEM for three independent experiments.

(D) Immunoblot for BCL6 in human B cells transduced with the indicated lentivirus after 3 or 7 days of differentiation. β-ACTIN is a loading control. Densitometric values are indicated below each band.

(E) BrdU incorporation in human B cells, transduced with the indicated lentivirus, on day 7 of differentiation. BrdU-FITC-positive cells were detected by flow cytometry. Values are expressed as the mean ± SEM for three independent experiments.

(F) ELISA for total secreted IgG in human B cell culture media harvested after day 7 of differentiation. Cells were transduced with the indicated lentivirus prior to the initiation of differentiation. Values are expressed as the mean ± SEM for three independent experiments.

(G) qPCR for *PRDM1* in human B cells transduced with the indicated lentivirus after 3 or 7 days of differentiation. Values are normalized to *36B4* and are expressed as the mean ± SEM for three independent experiments.

(H) Immunoblot for BCL6 in human B cells, transduced with the indicated lentivirus, after 3 or 7 days of differentiation. β-ACTIN is a loading control. Densitometric values are indicated below each band.

of damaged cells from stem or precursor cell pools, such as the GC, may be an intrinsic mechanism to preserve the integrity of preterminal cell types and prevent tumorigenesis.

A consistent theme that re-emerges from studies of hematopoietic development is that a block in differentiation seems to promote a malignancy that reflects the stage in development at which the block occurs. Here, we show that disruption of the signaling pathway leading to CRTC2 inactivation and plasma cell differentiation occurs in GC-derived lymphomas. Because ATM is required for CRTC2 inactivation, defects in this pathway may contribute in part to the IG deficiencies (Nowak-Wegrzyn et al., 2004; Staples et al., 2008) and increased susceptibility to lymphoma (Taylor et al., 1996) observed in patients with A-T. In addition to mutations, aberrant *ATM* repression in multiple B cell lymphoma subtypes has also been reported (Basso et al., 2005). Like ATM, the LKB1 tumor suppressor is inactivated in a number of human malignancies (Hezel and Bardeesy, 2008; Shaw, 2008). Furthermore, a small population-based case-control study showed that diabetics taking metformin, which activates LKB1 and results in CRTC2 inactivation, had a reduced risk of cancer (Evans et al., 2005). In mice, a hypomorphic mutation in *Lkb1* present on a *Pten* haploinsufficient background markedly accelerated the development of marginal-zone B cell lymphoma (Huang et al., 2008). Interestingly, PTEN deficiency is similar to aberrantly sustained TCL1 expression for mature B cells because both alterations hyperactivate AKT signaling (Teitell, 2005).

In summary, CRTC2 plays a powerful and previously unknown role in normal GC B cell differentiation, and its inactivation by the DDR is critical for downregulation of a genetic program that maintains the GC reaction. These findings place CRTC2 in a regulatory pathway that controls GC exit and plasma cell

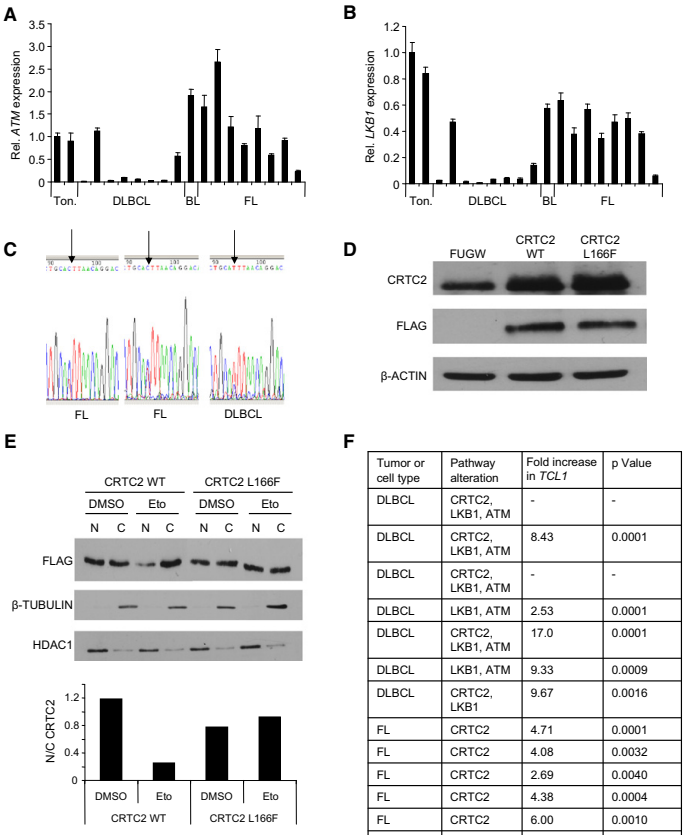


| Tumor or cell type | Pathway alteration | Fold increase in *TCL1* | p Value |
|---|---|---|---|
| DLBCL | CRTC2, LKB1, ATM | - | - |
| DLBCL | CRTC2, LKB1, ATM | 8.43 | 0.0001 |
| DLBCL | CRTC2, LKB1, ATM | - | - |
| DLBCL | LKB1, ATM | 2.53 | 0.0001 |
| DLBCL | CRTC2, LKB1, ATM | 17.0 | 0.0001 |
| DLBCL | LKB1, ATM | 9.33 | 0.0009 |
| DLBCL | CRTC2, LKB1 | 9.67 | 0.0016 |
| FL | CRTC2 | 4.71 | 0.0001 |
| FL | CRTC2 | 4.08 | 0.0032 |
| FL | CRTC2 | 2.69 | 0.0040 |
| FL | CRTC2 | 4.38 | 0.0004 |
| FL | CRTC2 | 6.00 | 0.0010 |
| FL | LKB1 | 3.78 | 0.0001 |
| GC B Cell | none | 2.29 | 0.0059 |

**Figure 7. CRTC2 Inactivation Is Disrupted in GC-Derived B Cell Lymphomas**

(A) qPCR for *ATM* in 17 human lymphoma samples and two tonsils. Values are normalized to *36B4* and are expressed as the mean ± SEM for three independent experiments. The following abbreviations are used: Ton., tonsil; DLBCL, diffuse large B cell lymphoma; BL, Burkitt lymphoma; FL, follicular lymphoma.

(B) qPCR for *LKB1* in 17 human lymphoma samples and two tonsils. Values are normalized to *36B4* and are expressed as the mean ± SEM for three independent experiments.

(C) Representative chromatograms showing a CRTC2 496 C→T alteration in human GC B cell lymphomas. Arrow indicates nucleotide 496 in the coding region of CRTC2.

(D) Immunoblot showing expression of CRTC2 and FLAG in Ramos cells 48 hr after infection with the indicated lentivirus. β-ACTIN is a loading control.

(E) Top: immunoblot showing exogenous CRTC2 localization in Ramos cells, transduced with the indicated lentivirus, after DMSO or Eto (20 μM, 1 hr) exposure. β-TUBULIN (cytoplasm) and HDAC1 (nucleus) are loading controls. Bottom: nuclear/cytoplasmic ratios for CRTC2 are plotted from densitometry.

(F) qPCR for *TCL1* expression in 13 human B cell lymphoma samples and in GC B cells at day 3 of culture. Values are normalized to *36B4* and compared to *TCL1* expression in differentiated plasma cells at day 7 of culture. Dashes indicate tumors with undetectable *TCL1* expression.

differentiation during terminal B cell development and herald future studies to interrogate the role of CRTC2 as a potential oncogenic factor and therapeutic target in B cell lymphoma.

## EXPERIMENTAL PROCEDURES

### Cell Culture, Tissues, and Reagents

Wild-type, *Atm*$^{-/-}$, *Lkb1(T366A)*, and *Lkb1*$^{-/-}$ MEFs (N. Bardeesy, Massachusetts General Hospital) were grown in Dulbecco's modified Eagle's medium (GIBCO, USA) with 20% fetal bovine serum (FBS) plus antibiotics. Nalm-6, Ramos, PBL, and ATM-deficient lymphoblastoid cells were grown in RPMI 1640 (GIBCO) with 10% FBS plus antibiotics. Fresh-frozen human tissues and fresh human tonsils were obtained from the University of California, Los Angeles (UCLA) Tissue Procurement Core Laboratory in accordance with institutional guidelines and Institutional Review Board approval. Reagents included etoposide, mitomycin C, and metformin (Sigma, USA) and the ATM inhibitor KU55933 (Kudos Pharmaceuticals, UK). α-CD40 (mouse anti-human IgG) was purified from a culture medium of G28-5 mouse hybridoma cells (K. Zhang, UCLA).

### Primary Human B Cell Culture System

Fresh tonsils were used to isolate naive B cells as described (Said et al., 2001). Tonsils were minced, and mononuclear cells (MCs) were isolated by Ficoll-Paque (GE Healthcare, USA) density centrifugation. MCs were incubated with α-IgD-PE (BD PharMingen, USA) on ice, washed, incubated with α-PE beads (Miltenyi Biotech), washed, and collected using the MidiMACS system (Miltenyi Biotec, Germany). Lentiviral transduction was performed at this stage, as indicated. Cells were seeded 5 × 10$^5$ cells/ml and cultured in complete RPMI 1640 plus 20 ng/ml IL-4, 20 ng/ml IL-10 (BD PharMingen), and 2 μg/ml α-CD40 Ab.

### ELISA

ELISA was performed with a human IgG ELISA quantification kit (Bethyl Laboratories, USA).

### RNA Analysis

Total RNA was extracted with Trizol (Life Technologies, USA). cDNA was made with the Superscript First-Strand Synthesis System (Invitrogen, USA). qPCR was performed as described previously (Kuraishy et al., 2007). Expression was normalized to a *36B4* mRNA control sequence.

### Immunoblot, Immunoprecipitation, and Antibodies

Immunoblots were performed as described (Kuraishy et al., 2007). Briefly, 20–50 μg whole-cell extract for each sample was separated by SDS-PAGE and transferred to a nitrocellulose membrane. Blocked membranes were incubated with primary Abs in TBS-Tween and 5% milk (or 5% BSA for phosphospecific Abs) overnight (Ab sources provided upon request). Immunoprecipitations were performed with whole-cell extracts and primary Ab overnight,

followed by precipitation of immune complexes with Protein G beads (Santa Cruz Biotechnologies, USA). Subcellular fractionations were performed with the NE-PER Nuclear and Cytoplasmic Extraction kit (Thermo Scientific, USA) according to the manufacturer's protocol.

### Chromatin Immunoprecipitation

ChIP assays were performed as described (Kuraishy et al., 2007).

### Immunofluorescence Microscopy

Ramos or primary B cells were plated on poly-L-lysine coverslips and used for immunofluorescence studies as described (Kuraishy et al., 2007).

### siRNA Electroporation

*LKB1* siRNA (2 μM; Dharmacon) or a scrambled control siRNA (2 μM) was electroporated into Nalm-6 cells with the Amaxa Nucleofector I (program C-05) and Nucleofector kit T (Amaxa, Germany).

### Retrovirus and Luciferase Assays

Luciferase assays were performed as described (Kuraishy et al., 2007). A *pBABE-FLAG-LKB1* retroviral construct, expressing FLAG-tagged LKB1, was generated by standard methods. Viral supernatant from HEK293T cells was collected 48 and 72 hr after transfection. PBL cells ($1 \times 10^5$/well) were incubated with 1 ml of virus supplemented with 2 μl polybrene and centrifuged at 2500 rpm for 1 hr at 30°C. One day after repeat infection, puromycin (0.5 μg/ml) was added to the media. FLAG-LKB1 expression was determined by western blot.

### Lentivirus

For shRNA, the *H1* promoter and RNAi sequences for *LKB1*, *ATM*, or scramble were subcloned into *FUGW* at the PacI site upstream of a ubiquitin promoter-driven *EGFP* sequence (Lois et al., 2002). For expression vectors, full-length *CRTC2* cDNA was cloned into *FUGW* downstream of the ubiquitin promoter. CRTC2 mutants were generated with the Quikchange site-directed mutagenesis kit (Stratagene, USA). Virus produced by HEK293T cells was concentrated by ultracentrifugation, resuspended in RPMI 1640, and used to spin-infect $2 \times 10^6$ cells/well in a 24-well plate for 2 hr.

### In Vitro Proliferation Assays

In vitro proliferative kinetics were assayed with the BrdU flow kit (BD PharMingen) according to the manufacturer's protocol.

### ChIP-on-Chip

ChIP was performed with two different Abs against CRTC2 (EMD Biosciences, USA; Cell Signaling, USA). Biological duplicate experiments were performed with each Ab. Array details are in the Supplemental Experimental Procedures.

### Gene Expression Arrays

RNA was isolated from Ramos cells without treatment or after 6 hr of Eto (20 μM) or α-IgM (10 μg/ml) exposure using Trizol, followed by clean-up with the QIAGEN RNeasy kit. Array details are in the Supplemental Experimental Procedures.

### Gene Ontology Analysis

Gene ontology analysis was performed with Ingenuity Pathways Analysis.

### Statistical Analyses

Data are presented as the mean ± standard error of the mean (SEM). A two-tailed t test was used for most comparisons, with $p < 0.05$ considered significant.

## ACCESSION NUMBERS

All ChIP-on-chip and gene expression microarray data have been deposited in the Gene Expression Omnibus (GEO) under the submission number GSE23171.

## SUPPLEMENTAL INFORMATION

Supplemental Information includes Supplemental Experimental Procedures, seven figures, and one table and can be found with this article online at doi:10.1016/j.molcel.2010.08.019.

## ACKNOWLEDGMENTS

The authors thank Reuben J. Shaw and Marc Montminy (Salk Institute) for discussions and reagents and Heather Christofk, Steve Bensinger, Randolph Wall, and Steven Smale (UCLA) for discussions and evaluation of the manuscript. This work was supported by National Institutes of Health Grants GM07185 (National Research Service Award to M.H.S. and A.I.K.), R01CA90571 (to M.A.T.), R01CA156674 (to M.A.T.), and by the National Institutes of Health Roadmap for Medical Research Nanomedicine Initiative (PNEY018228; to M.A.T.). M.A.T. is a recent Scholar of the Leukemia and Lymphoma Society.

Received: September 16, 2009
Revised: April 19, 2010
Accepted: July 28, 2010
Published: September 23, 2010

## REFERENCES

Allman, D., Jain, A., Dent, A., Maile, R.R., Selvaggi, T., Kehry, M.R., and Staudt, L.M. (1996). BCL-6 expression during B-cell activation. Blood *87*, 5257–5268.

Arpin, C., Déchanet, J., Van Kooten, C., Merville, P., Grouard, G., Brière, F., Banchereau, J., and Liu, Y.J. (1995). Generation of memory B cells and plasma cells in vitro. Science *268*, 720–722.

Basso, K., Margolin, A.A., Stolovitzky, G., Klein, U., Dalla-Favera, R., and Califano, A. (2005). Reverse engineering of regulatory networks in human B cells. Nat. Genet. *37*, 382–390.

Bredemeyer, A.L., Helmink, B.A., Innes, C.L., Calderon, B., McGinnis, L.M., Mahowald, G.K., Gapud, E.J., Walker, L.M., Collins, J.B., Weaver, B.K., et al. (2008). DNA double-strand breaks activate a multi-functional genetic program in developing lymphocytes. Nature *456*, 819–823.

Cattoretti, G., Pasqualucci, L., Ballon, G., Tam, W., Nandula, S.V., Shen, Q., Mo, T., Murty, V.V., and Dalla-Favera, R. (2005). Deregulated BCL6 expression recapitulates the pathogenesis of human diffuse large B cell lymphomas in mice. Cancer Cell *7*, 445–455.

Chaudhuri, J., Tian, M., Khuong, C., Chua, K., Pinaud, E., and Alt, F.W. (2003). Transcription-targeted DNA deamination by the AID antibody diversification enzyme. Nature *422*, 726–730.

Evans, J.M., Donnelly, L.A., Emslie-Smith, A.M., Alessi, D.R., and Morris, A.D. (2005). Metformin and reduced risk of cancer in diabetic patients. BMJ *330*, 1304–1305.

Fernandes, N., Sun, Y., Chen, S., Paul, P., Shaw, R.J., Cantley, L.C., and Price, B.D. (2005). DNA damage-induced association of ATM with its target proteins requires a protein interaction domain in the N terminus of ATM. J. Biol. Chem. *280*, 15158–15164.

Fluckiger, A.C., Sanz, E., Garcia-Lloret, M., Su, T., Hao, Q.L., Kato, R., Quan, S., de la Hera, A., Crooks, G.M., Witte, O.N., and Rawlings, D.J. (1998). In vitro reconstitution of human B-cell ontogeny: from CD34(+) multipotent progenitors to Ig-secreting cells. Blood *92*, 4509–4520.

Franco, S., Gostissa, M., Zha, S., Lombard, D.B., Murphy, M.M., Zarrin, A.A., Yan, C., Tepsuporn, S., Morales, J.C., Adams, M.M., et al. (2006). H2AX prevents DNA breaks from progressing to chromosome breaks and translocations. Mol. Cell *21*, 201–214.

Fu, A., and Screaton, R.A. (2008). Using kinomics to delineate signaling pathways: control of CRTC2/TORC2 by the AMPK family. Cell Cycle *7*, 3823–3828.

Fugmann, S.D., Lee, A.I., Shockett, P.E., Villey, I.J., and Schatz, D.G. (2000). The RAG proteins and V(D)J recombination: complexes, ends, and transposition. Annu. Rev. Immunol. *18*, 495–527.

Greiner, A., Müller, K.B., Hess, J., Pfeffer, K., Müller-Hermelink, H.K., and Wirth, T. (2000). Up-regulation of BOB.1/OBF.1 expression in normal germinal center B cells and germinal center-derived lymphomas. Am. J. Pathol. *156*, 501–507.

Hezel, A.F., and Bardeesy, N. (2008). LKB1; linking cell structure and tumor suppression. Oncogene *27*, 6908–6919.

Huang, X., Wullschleger, S., Shpiro, N., McGuire, V.A., Sakamoto, K., Woods, Y.L., McBurnie, W., Fleming, S., and Alessi, D.R. (2008). Important role of the LKB1-AMPK pathway in suppressing tumorigenesis in PTEN-deficient mice. Biochem. J. *412*, 211–221.

Inomata, K., Aoto, T., Binh, N.T., Okamoto, N., Tanimura, S., Wakayama, T., Iseki, S., Hara, E., Masunaga, T., Shimizu, H., and Nishimura, E.K. (2009). Genotoxic stress abrogates renewal of melanocyte stem cells by triggering their differentiation. Cell *137*, 1088–1099.

Jansson, D., Ng, A.C., Fu, A., Depatie, C., Al Azzabi, M., and Screaton, R.A. (2008). Glucose controls CREB activity in islet cells via regulated phosphorylation of TORC2. Proc. Natl. Acad. Sci. USA *105*, 10161–10166.

Kastan, M.B., and Bartek, J. (2004). Cell-cycle checkpoints and cancer. Nature *432*, 316–323.

Katoh, Y., Takemori, H., Lin, X.Z., Tamura, M., Muraoka, M., Satoh, T., Tsuchiya, Y., Min, L., Doi, J., Miyauchi, A., et al. (2006). Silencing the constitutive active transcription factor CREB by the LKB1-SIK signaling cascade. FEBS J. *273*, 2730–2748.

Khanna, K.K., and Jackson, S.P. (2001). DNA double-strand breaks: signaling, repair and the cancer connection. Nat. Genet. *27*, 247–254.

Klein, U., and Dalla-Favera, R. (2008). Germinal centres: role in B-cell physiology and malignancy. Nat. Rev. Immunol. *8*, 22–33.

Klein, U., Tu, Y., Stolovitzky, G.A., Mattioli, M., Cattoretti, G., Husson, H., Freedman, A., Inghirami, G., Cro, L., Baldini, L., et al. (2001). Gene expression profiling of B cell chronic lymphocytic leukemia reveals a homogeneous phenotype related to memory B cells. J. Exp. Med. *194*, 1625–1638.

Klein, U., Tu, Y., Stolovitzky, G.A., Keller, J.L., Haddad, J., Jr., Miljkovic, V., Cattoretti, G., Califano, A., and Dalla-Favera, R. (2003). Transcriptional analysis of the B cell germinal center reaction. Proc. Natl. Acad. Sci. USA *100*, 2639–2644.

Kracker, S., Bergmann, Y., Demuth, I., Frappart, P.O., Hildebrand, G., Christine, R., Wang, Z.Q., Sperling, K., Digweed, M., and Radbruch, A. (2005). Nibrin functions in Ig class-switch recombination. Proc. Natl. Acad. Sci. USA *102*, 1584–1589.

Küppers, R., and Dalla-Favera, R. (2001). Mechanisms of chromosomal translocations in B cell lymphomas. Oncogene *20*, 5580–5594.

Kuraishy, A.I., French, S.W., Sherman, M., Herling, M., Jones, D., Wall, R., and Teitell, M.A. (2007). TORC2 regulates germinal center repression of the TCL1 oncoprotein to promote B cell development and inhibit transformation. Proc. Natl. Acad. Sci. USA *104*, 10175–10180.

Lizcano, J.M., Göransson, O., Toth, R., Deak, M., Morrice, N.A., Boudeau, J., Hawley, S.A., Udd, L., Mäkelä, T.P., Hardie, D.G., and Alessi, D.R. (2004). LKB1 is a master kinase that activates 13 kinases of the AMPK subfamily, including MARK/PAR-1. EMBO J. *23*, 833–843.

Lois, C., Hong, E.J., Pease, S., Brown, E.J., and Baltimore, D. (2002). Germline transmission and tissue-specific expression of transgenes delivered by lentiviral vectors. Science *295*, 868–872.

Lou, Z., Minter-Dykhouse, K., Franco, S., Gostissa, M., Rivera, M.A., Celeste, A., Manis, J.P., van Deursen, J., Nussenzweig, A., Paull, T.T., et al. (2006). MDC1 maintains genomic stability by participating in the amplification of ATM-dependent DNA damage signals. Mol. Cell *21*, 187–200.

Lumsden, J.M., McCarty, T., Petiniot, L.K., Shen, R., Barlow, C., Wynn, T.A., Morse, H.C., 3rd, Gearhart, P.J., Wynshaw-Boris, A., Max, E.E., and Hodes, R.J. (2004). Immunoglobulin class switch recombination is impaired in Atm-deficient mice. J. Exp. Med. *200*, 1111–1121.

Manis, J.P., Morales, J.C., Xia, Z., Kutok, J.L., Alt, F.W., and Carpenter, P.B. (2004). 53BP1 links DNA damage-response pathways to immunoglobulin heavy chain class-switch recombination. Nat. Immunol. *5*, 481–487.

Matsuoka, S., Ballif, B.A., Smogorzewska, A., McDonald, E.R., 3rd, Hurov, K.E., Luo, J., Bakalarski, C.E., Zhao, Z., Solimini, N., Lerenthal, Y., et al. (2007). ATM and ATR substrate analysis reveals extensive protein networks responsive to DNA damage. Science *316*, 1160–1166.

Muramatsu, M., Kinoshita, K., Fagarasan, S., Yamada, S., Shinkai, Y., and Honjo, T. (2000). Class switch recombination and hypermutation require activation-induced cytidine deaminase (AID), a potential RNA editing enzyme. Cell *102*, 553–563.

Narducci, M.G., Pescarmona, E., Lazzeri, C., Signoretti, S., Lavinia, A.M., Remotti, D., Scala, E., Baroni, C.D., Stoppacciaro, A., Croce, C.M., and Russo, G. (2000). Regulation of TCL1 expression in B- and T-cell lymphomas and reactive lymphoid tissues. Cancer Res. *60*, 2095–2100.

Nowak-Wegrzyn, A., Crawford, T.O., Winkelstein, J.A., Carson, K.A., and Lederman, H.M. (2004). Immunodeficiency and infections in ataxia-telangiectasia. J. Pediatr. *144*, 505–511.

Petersen, S., Casellas, R., Reina-San-Martin, B., Chen, H.T., Difilippantonio, M.J., Wilson, P.C., Hanitsch, L., Celeste, A., Muramatsu, M., Pilch, D.R., et al. (2001). AID is required to initiate Nbs1/gamma-H2AX focus formation and mutations at sites of class switching. Nature *414*, 660–665.

Phan, R.T., and Dalla-Favera, R. (2004). The BCL6 proto-oncogene suppresses p53 expression in germinal-centre B cells. Nature *432*, 635–639.

Phan, R.T., Saito, M., Basso, K., Niu, H., and Dalla-Favera, R. (2005). BCL6 interacts with the transcription factor Miz-1 to suppress the cyclin-dependent kinase inhibitor p21 and cell cycle arrest in germinal center B cells. Nat. Immunol. *6*, 1054–1060.

Phan, T.G., Paus, D., Chan, T.D., Turner, M.L., Nutt, S.L., Basten, A., and Brink, R. (2006). High affinity germinal center B cells are actively selected into the plasma cell compartment. J. Exp. Med. *203*, 2419–2424.

Phan, R.T., Saito, M., Kitagawa, Y., Means, A.R., and Dalla-Favera, R. (2007). Genotoxic stress regulates expression of the proto-oncogene Bcl6 in germinal center B cells. Nat. Immunol. *8*, 1132–1139.

Rajewsky, K. (1996). Clonal selection and learning in the antibody system. Nature *381*, 751–758.

Ranuncolo, S.M., Polo, J.M., Dierov, J., Singer, M., Kuo, T., Greally, J., Green, R., Carroll, M., and Melnick, A. (2007). Bcl-6 mediates the germinal center B cell phenotype and lymphomagenesis through transcriptional repression of the DNA-damage sensor ATR. Nat. Immunol. *8*, 705–714.

Reina-San-Martin, B., Chen, H.T., Nussenzweig, A., and Nussenzweig, M.C. (2004). ATM is required for efficient recombination between immunoglobulin switch regions. J. Exp. Med. *200*, 1103–1110.

Reina-San-Martin, B., Nussenzweig, M.C., Nussenzweig, A., and Difilippantonio, S. (2005). Genomic instability, endoreduplication, and diminished Ig class-switch recombination in B cells lacking Nbs1. Proc. Natl. Acad. Sci. USA *102*, 1590–1595.

Revy, P., Muto, T., Levy, Y., Geissmann, F., Plebani, A., Sanal, O., Catalan, N., Forveille, M., Dufourcq-Labelouse, R., Gennery, A., et al. (2000). Activation-induced cytidine deaminase (AID) deficiency causes the autosomal recessive form of the Hyper-IgM syndrome (HIGM2). Cell *102*, 565–575.

Said, J.W., Hoyer, K.K., French, S.W., Rosenfelt, L., Garcia-Lloret, M., Koh, P.J., Cheng, T.C., Sulur, G.G., Pinkus, G.S., Kuehl, W.M., et al. (2001). TCL1 oncogene expression in B cell subsets from lymphoid hyperplasia and distinct classes of B cell lymphoma. Lab. Invest. *81*, 555–564.

Sapkota, G.P., Deak, M., Kieloch, A., Morrice, N., Goodarzi, A.A., Smythe, C., Shiloh, Y., Lees-Miller, S.P., and Alessi, D.R. (2002). Ionizing radiation induces ataxia telangiectasia mutated kinase (ATM)-mediated phosphorylation of LKB1/STK11 at Thr-366. Biochem. J. *368*, 507–516.

Screaton, R.A., Conkright, M.D., Katoh, Y., Best, J.L., Canettieri, G., Jeffries, S., Guzman, E., Niessen, S., Yates, J.R., 3rd, Takemori, H., et al. (2004). The CREB coactivator TORC2 functions as a calcium- and cAMP-sensitive coincidence detector. Cell *119*, 61–74.

Shackelford, D.B., and Shaw, R.J. (2009). The LKB1-AMPK pathway: metabolism and growth control in tumour suppression. Nat. Rev. Cancer *9*, 563–575.

Shaffer, A.L., Yu, X., He, Y., Boldrick, J., Chan, E.P., and Staudt, L.M. (2000). BCL-6 represses genes that function in lymphocyte differentiation, inflammation, and cell cycle control. Immunity *13*, 199–212.

Shaffer, A.L., Lin, K.I., Kuo, T.C., Yu, X., Hurt, E.M., Rosenwald, A., Giltnane, J.M., Yang, L., Zhao, H., Calame, K., and Staudt, L.M. (2002). Blimp-1 orchestrates plasma cell differentiation by extinguishing the mature B cell gene expression program. Immunity *17*, 51–62.

Shaffer, A.L., Emre, N.C., Lamy, L., Ngo, V.N., Wright, G., Xiao, W., Powell, J., Dave, S., Yu, X., Zhao, H., et al. (2008). IRF4 addiction in multiple myeloma. Nature *454*, 226–231.

Shaw, R.J. (2008). LKB1: cancer, polarity, metabolism, and now fertility. Biochem. J. *416*, e1–e3.

Shaw, R.J., Lamia, K.A., Vasquez, D., Koo, S.H., Bardeesy, N., Depinho, R.A., Montminy, M., and Cantley, L.C. (2005). The kinase LKB1 mediates glucose homeostasis in liver and therapeutic effects of metformin. Science *310*, 1642–1646.

Staples, E.R., McDermott, E.M., Reiman, A., Byrd, P.J., Ritchie, S., Taylor, A.M., and Davies, E.G. (2008). Immunodeficiency in ataxia telangiectasia is correlated strongly with the presence of two null mutations in the ataxia telangiectasia mutated gene. Clin. Exp. Immunol. *153*, 214–220.

Taylor, A.M., Metcalfe, J.A., Thick, J., and Mak, Y.F. (1996). Leukemia and lymphoma in ataxia telangiectasia. Blood *87*, 423–438.

Teitell, M.A. (2005). The TCL1 family of oncoproteins: co-activators of transformation. Nat. Rev. Cancer *5*, 640–648.

Teitell, M., Damore, M.A., Sulur, G.G., Turner, D.E., Stern, M.H., Said, J.W., Denny, C.T., and Wall, R. (1999). TCL1 oncogene expression in AIDS-related lymphomas and lymphoid tissues. Proc. Natl. Acad. Sci. USA *96*, 9809–9814.

Tonegawa, S. (1983). Somatic generation of antibody diversity. Nature *302*, 575–581.

Turner, C.A., Jr., Mack, D.H., and Davis, M.M. (1994). Blimp-1, a novel zinc finger-containing protein that can drive the maturation of B lymphocytes into immunoglobulin-secreting cells. Cell *77*, 297–306.

Ward, I.M., Reina-San-Martin, B., Olaru, A., Minn, K., Tamada, K., Lau, J.S., Cascalho, M., Chen, L., Nussenzweig, A., Livak, F., et al. (2004). 53BP1 is required for class switch recombination. J. Cell Biol. *165*, 459–464.

Zhang, X., Odom, D.T., Koo, S.H., Conkright, M.D., Canettieri, G., Best, J., Chen, H., Jenner, R., Herbolsheimer, E., Jacobsen, E., et al. (2005). Genome-wide analysis of cAMP-response element binding protein occupancy, phosphorylation, and target gene activation in human tissues. Proc. Natl. Acad. Sci. USA *102*, 4459–4464.

# APPENDIX II:

## Ampk regulates IgD expression but not energy stress with B cell activation

SCIENTIFIC REPORTS

OPEN

# Ampk regulates IgD expression but not energy stress with B cell activation

Received: 31 October 2018
Accepted: 28 April 2019
Published online: 03 June 2019

Lynnea R. Waters[1,2], Fasih M. Ahsan[2], Johanna ten Hoeve[3,4,5], Jason S. Hong[2], Diane N. H. Kim[6], Aspram Minasyan[3,5], Daniel Braas[3,4,5], Thomas G. Graeber[3,4,5,7,8,9], Thomas A. Zangle[10,11] & Michael A. Teitell[1,2,6,7,8,9,12]

**Ampk is an energy gatekeeper that responds to decreases in ATP by inhibiting energy-consuming anabolic processes and promoting energy-generating catabolic processes. Recently, we showed that Lkb1, an understudied kinase in B lymphocytes and a major upstream kinase for Ampk, had critical and unexpected roles in activating naïve B cells and in germinal center formation. Therefore, we examined whether Lkb1 activities during B cell activation depend on Ampk and report surprising Ampk activation with *in vitro* B cell stimulation in the absence of energy stress, coupled to rapid biomass accumulation. Despite Ampk activation and a controlling role for Lkb1 in B cell activation, Ampk knockout did not significantly affect B cell activation, differentiation, nutrient dynamics, gene expression, or humoral immune responses. Instead, Ampk loss specifically repressed the transcriptional expression of *IgD* and its regulator, *Zfp318*. Results also reveal that early activation of Ampk by phenformin treatment impairs germinal center formation but does not significantly alter antibody responses. Combined, the data show an unexpectedly specific role for Ampk in the regulation of IgD expression during B cell activation.**

B lymphocyte activation is an early step in a humoral immune response, whereby a naïve B cell with a unique antigen receptor recognizes its cognate antigen to trigger growth, division, and differentiation. Following activation, selected B cells can develop into long-lived plasma cells that secrete antigen-specific antibodies to fight infections[1]. During receptor-mediated activation, B cells undergo class switch recombination (CSR), also called immunoglobulin isotype switching, to modify the type of B cell antigen receptor (BCR) expressed by the B cell, such as IgM or IgG1 isotypes[2]. Many of the early signaling events linked to engagement of the BCR are well studied[3]. Recently, we reported a role for the tumor suppressor Lkb1 in B cell activation: *Lkb1* knockout (KO) caused spontaneous B cell activation *in vivo* without specific added antigenic stimulation, resulting in a robust T cell-dependent germinal center (GC) reaction[4,5]. This result was interesting because Lkb1 signaling had not been previously implicated in B cell activation and few models of spontaneous GC formation exist[6]. We therefore sought to determine the mechanism(s) whereby Lkb1 controls B cell activation.

Lkb1 phosphorylates 14 different related kinase family member proteins to control many cellular functions including protein synthesis and cell growth, cell polarity, and metabolism[7]. We elected to examine one of these 14 major downstream Lkb1 targets, 5′ AMP-activated protein kinase (Ampk). Ampk is an energy sensor that couples metabolism with nutrient availability during periods of energetic stress, as might occur during rapid B cell expansion and differentiation[8]. Ampk does this by sensing increasing levels of ADP or AMP with reducing levels of ATP in a cell, which triggers the phosphorylation of well characterized substrate proteins including Tsc2, Acc1/2, and Tbc1d1 to inhibit protein synthesis, promote fatty acid oxidation, upregulate glycolysis, and restore overall cell

[1]Molecular Biology Interdepartmental Program, UCLA, Los Angeles, CA, 90095, USA. [2]Department of Pathology and Laboratory Medicine, UCLA, Los Angeles, CA, 90095, USA. [3]Department of Molecular and Medical Pharmacology, UCLA, Los Angeles, CA, 90095, USA. [4]UCLA Metabolomics Center, UCLA, Los Angeles, CA, 90095, USA. [5]Crump Institute for Molecular Imaging, UCLA, Los Angeles, CA, 90095, USA. [6]Department of Bioengineering, UCLA, Los Angeles, CA, 90095, USA. [7]Jonsson Comprehensive Cancer Center, UCLA, Los Angeles, CA, 90095, USA. [8]California NanoSystems Institute, UCLA, Los Angeles, CA, 90095, USA. [9]Broad Stem Cell Research Center, UCLA, Los Angeles, CA, 90095, USA. [10]Department of Chemical Engineering, University of Utah, Salt Lake City, UT, 84112, USA. [11]Huntsman Cancer Institute, University of Utah, Salt Lake City, UT, 84112, USA. [12]Department of Pediatrics, UCLA, Los Angeles, CA, 90095, USA. Correspondence and requests for materials should be addressed to M.A.T. (email: mteitell@mednet.ucla.edu)

energy balance[9]. While Lkb1 is the major upstream kinase for Ampk, other upstream kinases also phosphorylate Ampk including CamKK2 and Tak1[10–12]. In T cells, CD3 ligation results in rapid Ampk activation in a calcium- and CamKK2-dependent manner[13], and Ampk activation declines in proliferating normal T cells[14]; however, the Ampk activation pattern in B cells is unknown.

Studies of Lkb1 and Ampk have shown overlapping but also unique functions in hematopoiesis. For example, Lkb1 maintains hematopoietic stem cell quiescence by regulating metabolism and the cell cycle using Ampk-dependent and -independent mechanisms[15–17]. In T cells and thymocytes, Lkb1 deletion reduced peripheral T cells and decreased T cell proliferation when stimulated *in vitro*. However, while loss of Ampk in T cells also led to metabolic and activation defects, it did not fully recapitulate the loss of Lkb1[18–20]. There is only one reported study of Ampk in B cells, which showed that a whole mouse knockout of Ampk left isolated B and T cells unable to survive *in vitro* under oxidative stress when exposed to the ATP synthase inhibitor, oligomycin[21]. Given the unexpected role for Lkb1 loss in B cells in triggering a GC reaction, we sought to determine role(s) for Ampk during B cell activation.

## Results

**Ampk activation during B cell stimulation.** Initially, we investigated whether Ampk, a major downstream target of Lkb1, was required for B cell activation[4,5]. Previous studies in T cells showed Ampk activation after T cell receptor stimulation[13]. We examined the phosphorylation of Ampk at T172, a marker residue for Ampk activation[22] and determined that Ampk activation occurs between 18–24 hours post-stimulation of B cells with anti-CD40 antibody plus interleukin (IL)-4 that persists at least through 72 hours (Fig. 1A). Activation of Ampk should initiate cellular processes that halt the accumulation of biomass required for cell division[9]. Instead, anti-CD40 plus IL-4 stimulated B cells to divide rapidly between 48–72 hours (Fig. 1B). Ampk activation with energy stress has been reported many times and occurs by sensing decreasing amounts of ATP linked to increasing ratios of AMP:ATP and ADP:ATP[23]. Therefore, we examined a previously published dataset of nucleotide metabolite levels at 24 hours post-stimulation. UHPLC-MS metabolomics data of $^{13}C_6$-glucose nutrient labeling during initial B cell activation showed unexpected AMP:ATP and ADP:ATP ratios declining at 24 hours with ATP steady-state levels significantly increasing (Fig. 1C)[24]. Additional measurements of extracellular nutrients shows maintenance of high levels of both glucose and glutamine in the culture medium (Fig. 1D), indicating that Ampk activation occurs in stimulated B cells during energy replete conditions.

Since Ampk activation typically inhibits protein, lipid, and additional biosynthetic processes, we turned to live cell interferometry, a form of quantitative phase microscopy, as a high precision and reproducible approach to quantify changes in biomass accumulation during early B cell activation[25] (Fig. 1E). We discovered that isolated naïve mouse B cells steadily increase cell biomass over the first 48 hours of anti-CD40 plus IL-4 stimulated activation (Fig. 1F). Interestingly, the specific growth rate calculated as a percentage of biomass change per hour accelerates for the first 18 hours and then plateaus (Fig. 1G). This growth rate peak coincides with the timing of Ampk activation (Fig. 1A), although despite Ampk activity B cells continue to acquire biomass at the peak (plateau) rate. This growth rate profile suggests that Ampk activation may damp further growth rate acceleration, perhaps as a rate-limiting step, but does not impede the overall growth of B cells.

**Ampk is not required for B cell activation or differentiation.** It was a surprise that Ampk was activated in stimulated naïve mouse B cells because a major role for Ampk in inhibiting lipid and protein synthesis seems incompatible with the high growth rate and cell division of activated B cells. Thus, we sought to determine whether Ampk was required for B cell activation and differentiation by generating a mouse model with B cell specific deletion of Ampk. Because Ampkα1, encoded by *Prkaa1*, is the only α subunit expressed in trimeric Ampk proteins in mature B cells[26], deletion of this catalytic subunit abolishes all Ampk activity. We generated a B cell specific Ampkα1 KO mouse line by crossing *Prkaa1*$^{fl/fl}$ mice with *CD19-Cre* recombinase driver mice to delete Ampk activity in post-pro/pre B cells. To monitor deletion efficiency, we crossed mice with a *Rosa26 lox-STOP-lox YFP* reporter allele (Fig. 2A). Deletion efficiency measured by YFP+ B220+ B cells was >80% in both WT (*Prkaa1*$^{+/+}$ × *CD19-Cre*) and Ampk KO (*Prkaa*$^{fl/fl}$ × *CD19-Cre*) mice (Fig. 2B), suggesting that there is no B cell survival disadvantage with loss of Ampk, in contrast to a major B cell survival disadvantage with Lkb1 loss[4]. Analysis of lysates from naïve and anti-CD40 plus IL-4 stimulated WT and Ampk KO B cells confirmed loss of Ampkα1 protein and abolishment of Ampk activity in Ampk KO B cells (Fig. 2C). Use of a pan-Ampk alpha (α1 and α2) antibody also allows us to conclude that there was no compensatory expression of the Ampkα2 subunit upon deletion of Ampkα1.

To determine whether Ampk deletion affects B cell activation, we stimulated isolated WT and Ampk KO B cells with anti-CD40 plus IL-4 and assessed activation and differentiation of YFP+ B cells. Surprisingly, despite Ampk activation at 24 hours, no changes in the levels of expression of activation markers CD69, CD86 or MHCII occur for the Ampk KO B cells compared to WT B cells. At later time points, no changes in GC-like B cell differentiation at day 3 and a minor reduction in CSR to IgG1 occurred in Ampk KO compared to WT B cells. By day 5, there was a small trending increase in plasmablast differentiation in Ampk KO versus WT B cells (Fig. 2D). These data strongly contrast with deletion of Lkb1 in B cells, which causes opposing results including increased activation marker expression and GC-like B cell differentiation, an increase in CSR, and a decrease in plasmablast differentiation[4]. Together, the results suggest that Ampk is not required for normal B cell function and is not required for Lkb1-dependent B cell phenotypes.

**Ampk does not control a humoral immune response *in vivo*.** We next examined whether Ampk deletion from B cells affects antibody responses *in vivo*. A prior study showed that whole mouse KO of Ampk did not affect IgG responses to Ars-KLH antigen *in vivo*[21]; however, other potential effects on the GC reaction, CSR, or antibody specificity were not examined. We inoculated Ampk KO and WT mice with the T cell-dependent

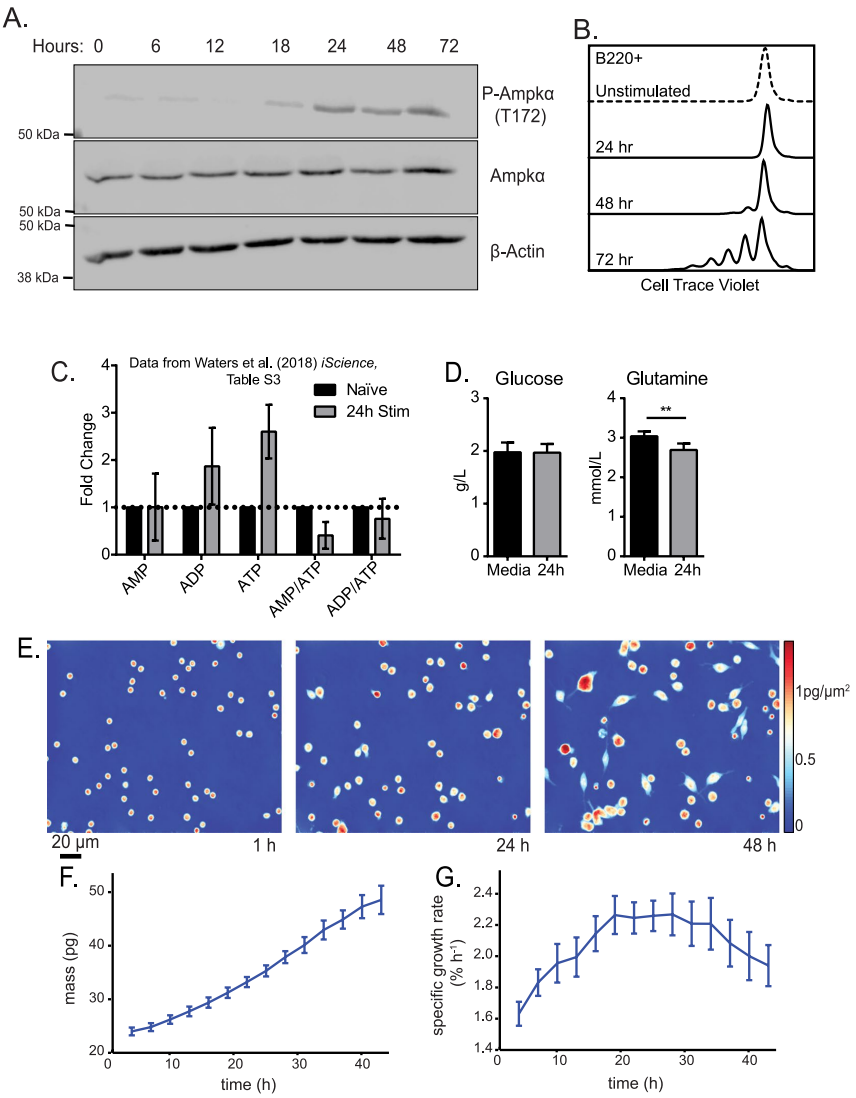


**Figure 1.** Activation of Ampk upon stimulation of B cells is independent of energy stress and does not result in lowered biomass accumulation. (**A**) Representative time course western blot for phosphorylated Ampkα (T172), Ampkα, and β-tubulin during anti-CD40 plus IL-4 stimulation of B cells. Image was cropped for clarity, full-length blots/gels are presented in Supplementary Fig. 1. (**B**) Representative flow cytometry of B220+ B cells at 0, 24, 48 and 72 hours post anti-CD40 plus IL-4 stimulation stained with Cell Trace Violet. (**C**) Relative fold change in previously published UHPLC- MS metabolomics dataset[24] for adenine nucleotides from 24 hours post stimulation with anti-CD40 plus IL-4 relative to naïve B cells ($n = 3$). (**D**) Measurement of extracellular glucose and glutamine at 24 hours post stimulation with anti-CD40 plus IL-4 ($n = 3$). (**E**) Live cell interferometry (LCI) images of anti-CD40 plus IL-4 activated B cells 1, 24, and 48 hours post stimulation showing significant growth, as confirmed by (**F**) a significant increase in average cell mass over time, binned into 3 h increments. (**G**) Average specific growth rate, computed as the instantaneous slope of mass over time for each cell normalized by cell mass, shows a peak at 24 hours, coincident with Ampk inactivation ($n = 5$ independent experiments of at least 200 cells). Data represent mean ± SD (**C**,**D**) or SEM (**F**,**G**). *P* values determined by 2-way ANOVA with Bonferroni correction for multiple comparisons (**C**) or an unpaired two-tailed Student's *t*-test (**D**). $^{**}P \leq 0.01$.

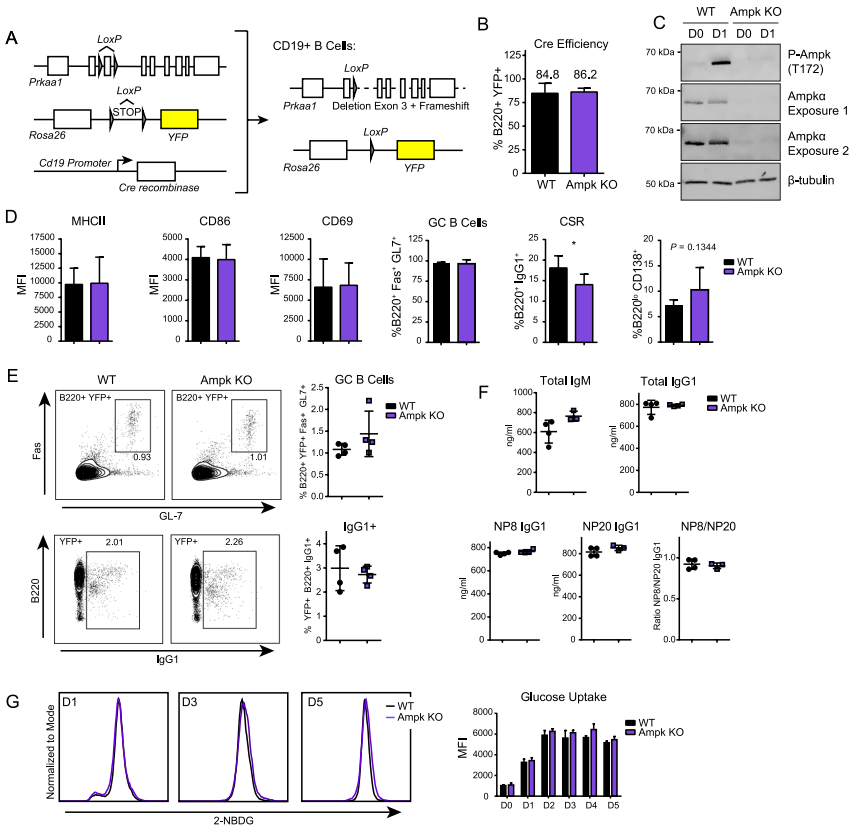


**Figure 2.** Ampk deletion does not significantly impair B cell function. (**A**) Strategy for generating B-cell lineage specific knockout of *Prkaa1* by crossing *CD19-Cre* recombinase (JAX: 006785) mice with *Prkaa1*$^{fl/fl}$ (JAX: 014141) mice and *Rosa26 lox-STOP-lox YFP* (JAX: 006148) mouse lines, yielding mice where CD19+ B cells lack the catalytic Ampkα subunit. (**B**) Quantification of Cre-recombinase efficiency by measurement of percentage of B220+ B cells that have YFP expression by flow cytometry in WT and Ampk KO B cells ($n = 3$). (**C**) Representative Western blot for P-Ampkα (T172), Ampkα and β-tubulin in WT and Ampk KO mice. Two exposures are shown for Ampkα to illustrate some remaining Ampk expression. Image was cropped for clarity, full-length blots/gels are presented in Supplementary Fig. 2. (**D**) Flow cytometry of WT and Ampk KO B cells during activation with anti-CD40L plus IL-4, including activation markers (MHCII, CD86, CD69) at 24 hours, GC differentiation (GC, %B220+ Fas+ GL7+) and CSR (%B220+ IgG1+) at day 3, and plasmablast differentiation (%B220$^{lo}$ CD138+) at day 5 ($n = 5$ for MHCII, CD86, CD69, and PB, $n = 6$ for GC, and $n = 7$ for CSR). (**E**) Flow cytometry of total splenocytes after immunization. Representative plots and quantification of GC differentiation (GC B Cells, B220$^{+}$ Fas$^{+}$ GL7$^{+}$) and CSR (B220$^{+}$ IgG1$^{+}$) 14 days post-immunization with NP-(28)-CGG ($n = 4$). (**F**) Total IgM, total IgG1, NP8 IgG1, NP20 IgG1, and NP8/NP20 IgG1 ratio in serum 14 days after immunization of WT and Ampk KO mice with NP-(28)-CGG ($n = 4$). (**G**) Representative flow cytometry for 2NBDG glucose uptake at day 1, 3, and 5 post stimulation with anti-CD40 plus IL-4, and quantification at day 0 through 5 in WT and Ampk KO B cells ($n = 3$). Data represent mean ± SD (**B**,**D**–**G**). *P* values determined by Student's *t*-test (**B**,**D**–**G**), $^{*}P \leq 0.05$.

antigen, NP-(28)-CGG, and analyzed B cells on day 14 post-immunization. We observed no differences in GC formation or CSR (Fig. 2E), and serum IgG1 levels were similar between WT and Ampk KO mice, with a slight but statistically insignificant difference in total IgM (Fig. 2F). Multivalent NP antigen enables detection of highly specific antibodies by probing for binding to specific NP molar ratios, with fewer NP molecules revealing higher specificity responses. Our data show that both broad spectrum and highly specific IgG1 against NP antigen were similar in WT and Ampk KO mice (Fig. 2F). These results show that Ampk is dispensable for a T cell-dependent humoral immune response, although Ampk may be critical in other contexts, such as T cell-independent, mucosal, or antiviral immune responses.

**Ampk is dispensable for activation-induced glucose uptake.** While we did not detect differences in differentiation patterns of WT and Ampk KO B cells, B cell activation in response to a range of triggering stimuli causes increased glucose import[24,27,28] and the deletion of Ampk in T effector cells reduces glucose uptake *in vivo*[29]. Therefore, we hypothesized that Ampk KO B cells might have defects in glucose uptake. To test this postulate, we utilized a fluorescent glucose analog, 2-NBDG, to measure glucose import in B cells from WT and Ampk KO mice that lack the *Rosa26 lox-STOP-lox* YFP tracer, because YFP and 2-NBDG fluorophore emission spectra overlap (527 nm and 540 nm, respectively). Unexpectedly, there was no difference between Ampk KO and WT B cells in glucose uptake during 5 days of B cell activation (Fig. 2G). Thus, Ampk activation does not regulate glucose import into activated B cells, suggesting an alternative glucose import mechanism.

**Ampk does not affect glucose or glutamine B cell nutrients.** While we did not detect differences in glucose uptake in Ampk KO B cells, Ampk also regulates other metabolic pathways to regulate energy stress, and Ampk activation at 24 hours of stimulation may impact nutrient choice or routing without affecting B cell differentiation or antibody responses. Therefore, we performed metabolomics profiling with $^{13}C_6$-glucose and $^{13}C_5$-glutamine in resting and anti-CD40 plus IL-4 stimulated WT and Ampk KO B cells (Table S1). Principal component analysis (PCA) of total intracellular metabolites revealed that the major segmentation was from differences between stimulation time points, and not from differences between genotypes within each time point (Fig. 3A). We generated correlation circle plots by fitting each of the metabolites to 4 vectors based on the observed clustering (Fig. 3B), which indicated metabolites that are known to be changed upon activation, including increases in ATP with activation and decreases in the AMP/ATP ratio, consistent with prior results (Fig. 1C)[24]. With no significant differences in total metabolites between WT and Ampk KO B cells at rest or for any stimulated time point, we next analyzed specific $^{13}$C-isotopomer labeling. PCA of molecular IDs for isotopomers (Fig. 3C, top) derived from the glucose label (left) or glutamine label (right) showed similar segmentation to the total metabolites, with the largest differences from stimulation time point rather than from genotype. We then assessed whether any biologically relevant metabolites were different between WT and Ampk KO at each time point. As a discovery tool, we plotted the non-corrected *P*-values for naïve, resting (middle row) and anti-CD40 plus IL-4 stimulated (bottom row) B cells labeled with glucose (left) or glutamine (right) (Fig. 3C). The data failed to identify any biologically relevant differentially produced isotopomers (DPIs) linked to known functions of Ampk. These labeling patterns occurred despite >90% uptake of labeled glucose or glutamine in each respective experiment for all conditions examined (Fig. 3D). To further investigate whether there were any DPIs between WT and Ampk KO B cells irrespective of time point, we calculated *P*-values and could not identify metabolites below the corrected false discovery rate of 0.05 (Fig. 3E). We considered that some broad metabolic differences may not be discernible at the individual DPI level, and small changes may accumulate and reveal deficiencies or surpluses in whole pathways. We therefore performed Metabolite Set Variation Analysis (MSVA) utilizing curated KEGG metabolic pathways and again identified significant changes occurred only between naïve and stimulated B cells, with no separation by genotype (Fig. 4F). Together, these results show that Ampk is not modulating metabolism during B cell activation, despite known metabolic roles related to glucose metabolism.

**Ampk regulates IgD levels but not transcripts controlling B cell fate.** Additional canonical Ampk substrates include Hdac4 and Hdac5, proteins that deacetylate histones and thereby regulate gene expression[30]. To assess potential differences in steady-state RNA expression, and to investigate potential alternative processes regulated by Ampk, we performed RNA-Seq in WT and Ampk KO B cells on culture days 0 through 5 using anti-CD40 plus IL-4 stimulation (Table S2). At day 0, there are no PCA plotted statistical differences between WT and Ampk KO naïve B cells. However, as B cells differentiate from day 1 through day 5, Ampk KO B cells cluster separately from their WT counterparts, but follow a similar trajectory towards differentiation (Fig. 4A). We confirmed reduced *Prkaa1* expression in Ampk KO B cells, as expected (Fig. 4B). To determine whether loss of Ampk conveyed a specific gene signature during 5 days of differentiation, we analyzed differentially expressed genes (DEGs) for days 0 through 5 of stimulation and identified 168 genes that were either consistently increased or decreased each day in Ampk KO compared to WT B cells (Fig. 4C). Pathway enrichment analysis of these 168 genes did not reveal any pathways related to B cell activation or differentiation, with the exception of 5 genes linked to apoptotic signaling in response to endoplasmic reticulum stress (*Grina*, *Atf4*, *Trib3*, *Lrrk2*, *Chac1*) (Table S2). Endoplasmic reticulum stress has an important role in plasma cell differentiation and antibody secretion[31]. Therefore, we analyzed activation, GC B cell, and antibody-secreting cell (ASC) gene expression signatures[32,33] as previously reported in our data set (Fig. 2D). Similar to our earlier data, Ampk KO and WT B cells activate similarly and increase GC-signature transcripts equally. Expression of ASC signature genes were similar between WT and Ampk KO samples (Fig. 4D), although Ampk KO B cells showed increases in some ASC transcripts, including *Prdm1* at days 4 and 5 (Fig. 4D). This finding is consistent with a trend towards an increase in plasmablasts at day 5 (Fig. 2D), and a divergence in the PCA plot of days 4 and 5 WT versus Ampk KO B cells (Fig. 4A).

Because of the potential for increased ASCs in Ampk KO mice, despite similar amounts of secreted IgM and IgG1 from *in vivo* immunizations (Fig. 2F), we evaluated the levels of immunoglobulin transcripts in WT and Ampk KO B cells. We determined that heavy chain variable (*Ighv*) region expression levels were similar for WT and Ampk KO B cells, although there was an increase in some transcripts including *Ighv6-3* and *Ighv14-3* in Ampk KO B cells (Fig. 5A). From *in vivo* immunization data, we also detected a slight but insignificant increase in secreted IgM, so we analyzed transcripts for immunoglobulin constant regions to identify potential isotype biases. Whereas *Ighm* transcripts matched our observations *in vivo* with a minor but insignificant increase at day 5 for Ampk KO versus WT B cells, we were surprised to discover that *Ighd* expression was severely repressed in Ampk KO B cells from day 1 stimulation onwards (corrected *P*-value $= 9.5 \times 10^{-30}$ at day 1) (Fig. 5B). IgD is normally co-expressed with IgM on the surface of all mature, naïve B cells, and is a relatively understudied antibody

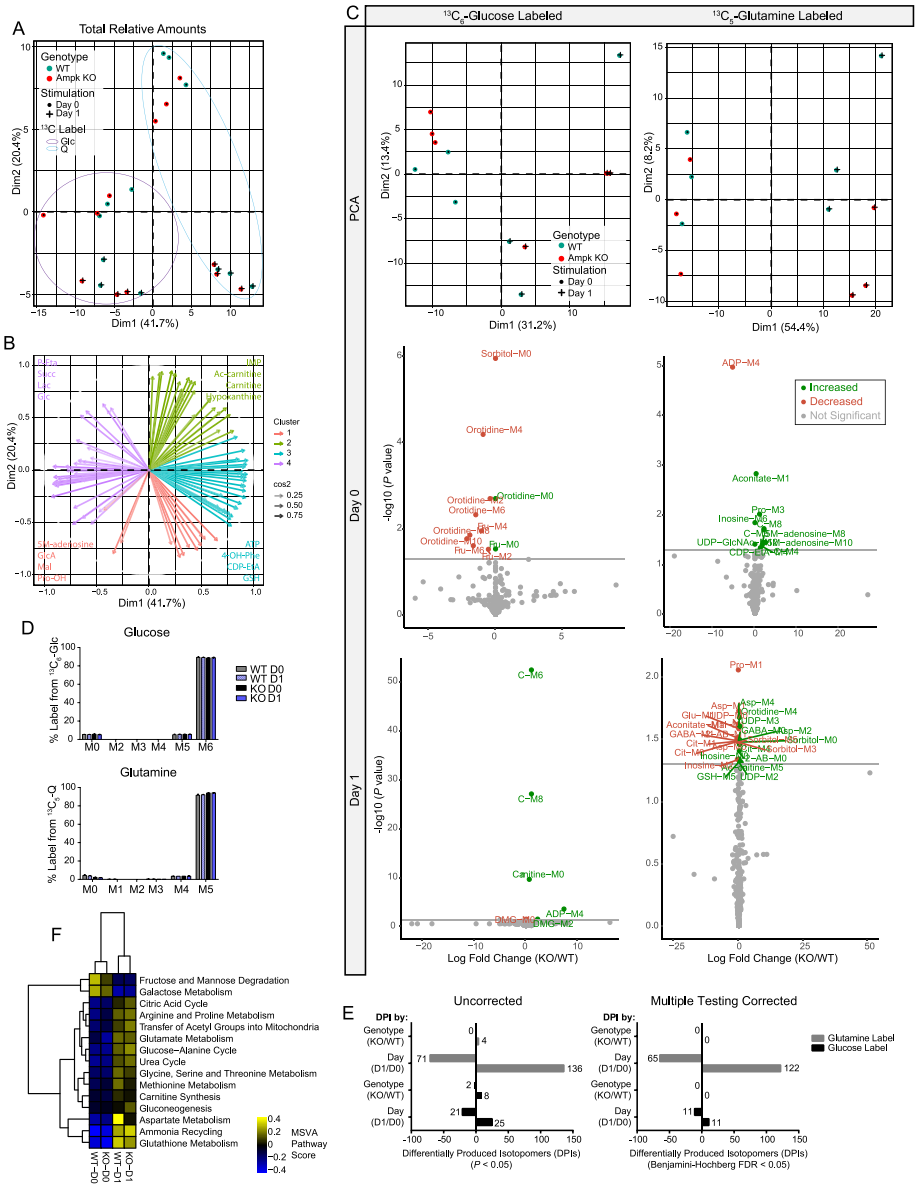


**Figure 3.** Ampk does not control metabolism during B cell stimulation. (**A**) PCA from UHPLC-MS metabolomics analysis of total metabolites isolated from naïve and stimulated B cells from WT and Ampk KO mice. (**B**) K-means clustering analysis of variable loading plots, indicating the contribution of metabolites to variation across principal components in four groups (k = 4). Projection arrow tips indicate Pearson correlation of the listed metabolite. Transparency denotes cosine[2] value or the strength of metabolite representation. Shown are the top 4 metabolites contributing to each cluster. (**C**) Principal component analysis and volcano plots of UHPLC-MS metabolomics of $^{13}C_6$-glucose labeled or $^{13}C_5$-glutamine labeled isotopomers (MID) in naïve and stimulated B cells from WT and Ampk KO mice. Plotted are non-corrected *P* values for KO/WT amounts of specific isotopomers ($n = 3$). (**D**) Isotopomer distribution of labeled glucose or labeled glutamine in naïve or stimulated WT and Ampk KO B cells shows uptake of labeled respective carbon source. (**E**) Quantification of Differentially Produced Isotopomers (DPIs) analyzed both by day and by genotype shows no DPIs between genotypes, only between time points for uncorrected or Benjamini-Hochberg corrected *P* values < 0.05. (**F**) Heatmap of significant (Benjamini-Hochberg

FDR adjusted $P$ value $< 0.05$) metabolite set variation analysis (MSVA) pathway activity scores across WT and Ampk KO naïve and stimulated B cells for curated KEGG metabolic pathways. Data represent the mean ± SD (**D**) of relative metabolite amounts from $n = 3$ independent experiments. Data from separate glucose and glutamine labeling experiments were pooled, and relative amounts analyzed for (**A**,**B**). $P$ values determined by Student's t test (**C**), 2-way ANOVA with Bonferroni correction for multiple comparisons (**D**), or empirical Bayes with Benjamini-Hochberg correction for multiple comparisons (**F**).

class that has potential implications in mucosal immune responses[34]. The expression of IgD is not impacted by activation-induced cytidine deaminase (AID) like most isotype switched immunoglobulins but is instead regulated by Zfp318[35,36]. Interestingly, the most robust DEGs at day 3 are *Ighd* and *Zfp318*, each of which are greater than an order of magnitude more repressed than the next most differentially expressed genes (Fig. 5C). In fact, *Zfp318* expression is repressed throughout the stimulated time course in Ampk KO B cells (Fig. 5D), coinciding with the drop in *Ighd* expression (Fig. 5B). Further supporting the specificity of Ampk loss on Zfp318 regulation of *Ighd* levels, expression of *Aicda*, encoding AID which regulates CSR, is the same in WT and Ampk KO B cells from days 0–4 and increased on day 5 of B cell activation (Fig. 5D). To confirm that the loss of *Ighd* transcripts affects IgD protein levels, we analyzed surface expression over 5 days of differentiation by flow cytometry, which shows that Ampk KO B cells have decreased IgD expression from days 2 through 5, particularly evident for the loss of IgD-high B cells (Fig. 5E). Given the limited number of DEGs, it appears that Ampk exerts highly specific control of IgD during B cell activation, likely through regulation of *Zfp318* expression.

**Pharmacological activation of Ampk.** The limited scope of impact for Ampk loss on B cell physiology seems surprising, so we examined whether the timing of Ampk activation could regulate B cell functions. We utilized two pharmacological activators of Ampk, phenformin and A-769662, to alter the timing of Ampk activation. Phenformin is a mitochondrial electron transport chain complex I inhibitor that activates Ampk by inhibiting ATP production, thereby increasing AMP/ATP and ADP/ATP ratios, and is an analogue of the diabetes drug metformin, whereas A-769662 is a direct and specific activator of Ampk[23]. We examined early activation of Ampk by treating B cells with each activator at the time of anti-CD40 plus IL-4 stimulation in culture and observed that both drugs decreased CD86 activation biomarker expression, but only phenformin reduced CD69 expression (Fig. 6A). Phenformin had a drastic effect on B cell differentiation by day 3 with greatly decreased CSR to IgG1 and inhibited differentiation into GC-like B cells (Fig. 6B). By contrast, A-769662 had little effect on GC-like B cell differentiation and only a slight defect in CSR (Fig. 6B). These results show that electron transport chain activity and ATP production *per se*, and not accelerated Ampk activation, are critical for B cell activation, differentiation, and CSR, in agreement with an effect mainly targeting markedly reduced *Zfp318* and *Ighd* expression levels in stimulated Ampk KO B cells (Fig. 5).

Because of recent interest in using metformin and phenformin clinically to treat B cell malignancies[37], we further evaluated the impact of phenformin on B cell function. To determine whether the effects of phenformin *in vitro* replicate *in vivo*, we immunized mice with NP-(28)-CGG to induce a T cell-dependent humoral immune response while delivering phenformin or sucralose vehicle in the drinking water (Fig. 6C). *In vivo* results show that 14-day treatment with phenformin substantially decreased the percentage of GC B cells in the spleen and reduced the percentage of IgG1+ isotype switched B cells (Fig. 6D). Interestingly, however, mice on phenformin had similar amounts of total IgM and IgG1 in their serum (Fig. 6E). There was a minor but non-significant defect in the generation of NP8-specific high affinity IgG1 antibody in phenformin treated mice, but no effect on broader NP20 IgG1 antibodies (Fig. 6F). Overall, these findings suggest that phenformin reduces GC formation, but still allows for generation of antigen-specific antibody production.

## Discussion

Our recent results showing that loss of Lkb1 kinase signaling triggers the B cell GC reaction[4,5] prompted studies of Ampk as a main Lkb1 target kinase during B cell activation. We found Ampk activation 24 hours after stimulation of naïve B cells with anti-CD40 antibody plus IL-4 (Fig. 1A). A key role for activated Ampk in mammalian cells is to block anabolic processes that consume energy by target protein phosphorylation in response to energy stress. To our surprise, B cell activation with rapid biomass accumulation and cell proliferation coincides with sustained Ampk activation in the absence of energy stress (Fig. 1A,B). We anticipated the opposite result, that Ampk activity would prevent biomass accumulation. While unexpected given the canonical targets and activities of Ampk, including inhibition of major anabolic targets Acc1, Tsc2, and Raptor, these findings also make sense in the biological context of B cell activation. For example, the Ampk target Raptor is essential for *Bcl6* expression and recruitment of activated B cells into GCs[38], and inhibition of Raptor by Ampk at this time would prevent GC formation. Similarly, Ampk-driven inhibition of protein and lipid synthesis through Acc1 and Tsc2 would antagonize the need for biomass accumulation while B cells prepare for rapid division in the GC[24,39,40]. While activation of Ampk during B cell activation was unexpected due to the role of Ampk in biomass accumulation, there are precedents for Ampk activation in other immune contexts. For example, in T cells, Ampk is transiently and immediately activated after CD3 or calcium stimulation[13], and Ampk phosphorylation declines in proliferating T effector cells[14]. This contrasts with B cells, where Ampk activation after 24 hours of stimulation persists during proliferation (Fig. 1A). In T cells, Ampk activation by nutrient limitation, metformin treatment, or AICAR, results in decreased *IFN* gene transcription and reduced T cell effector function[29]. Here, activation of Ampk by phenformin prevents GC differentiation and CSR, but still allows for generation of high-specificity antibodies (Fig. 6A–E).

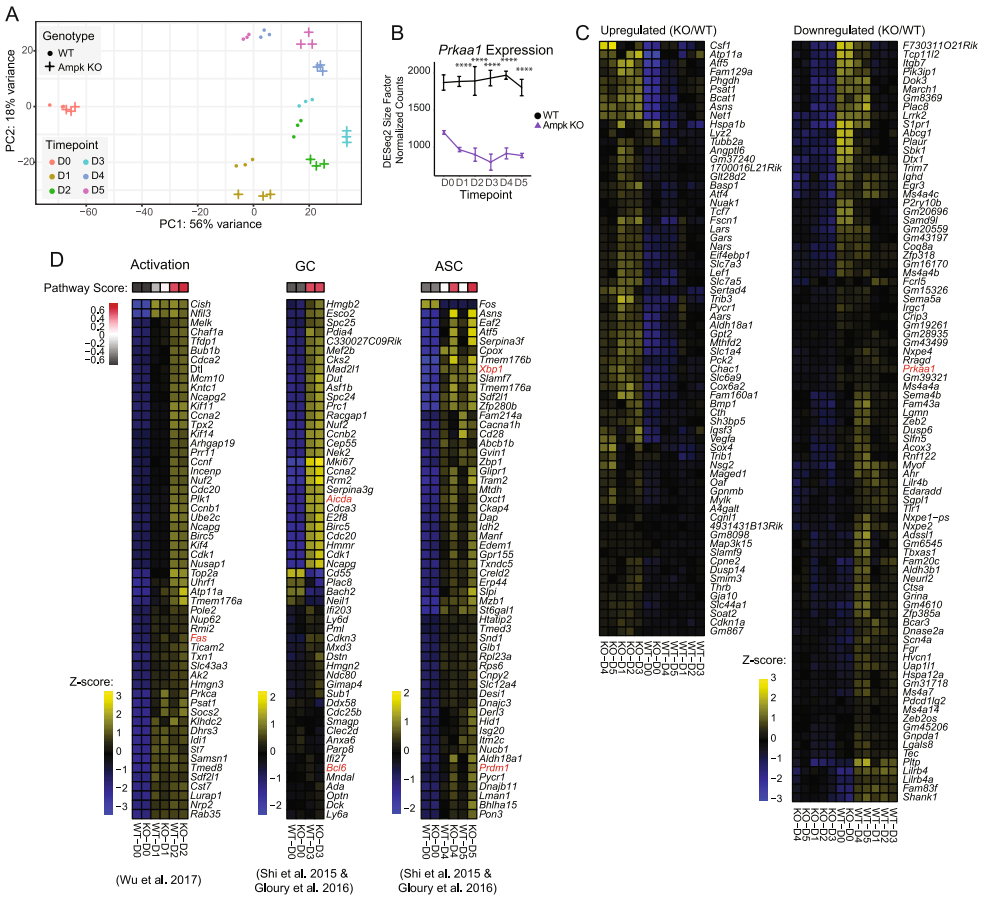


**Figure 4.** B cell activation and differentiation expression signatures are maintained despite loss of Ampk. (**A**) PCA from bulk RNA sequencing analysis of total RNA isolated from day 0 through day 5 stimulated B cells from WT and Ampk KO mice. PC1 and PC2 are shown. (**B**) Kinetic time course expression plot of *Prkaa1* during stimulation. (**C**) Heat map of KO signature gene expression across averaged samples. KO signature was generated as the intersection of all KO/WT DEGs at each time point from day 1 to day 5 of stimulation (adjusted $P$ value $< 0.05$, abs($\log_2$FC) $> 0.5$ at each time point comparison). (**D**) Heat maps for B cell activation, germinal center, and ASC gene signatures from[32,33,55]. Genes shown were selected as the top 55 differentially expressed from the Shi 2015 signatures between WT day 0 and day 2 (activation), WT day 0 and day 3 (GC), and WT day 0 and day 5 (ASC), with *Prdm1* included *post hoc*. Pathway scores represent total GSVA enrichment of the respective Shi 2015 signatures for each comparison (adjusted $P$ value $< 0.05$). Heat map values represent row z-score ($n = 3$ each WT and KO for each time point). Adjusted $P$ values determined by Wald test (**B**). $^{****}P \leq 0.0001$.

To study Ampk during B cell activation *in vivo*, we made a B cell specific KO of the catalytic Ampk alpha subunit, *Prkaa1* that achieved >80% deletion efficiency, but did not detect a phenotype similar to B cell specific *Lkb1* KO mice[4]. In fact, Lkb1 loss increases CSR and decreases plasmablast differentiation, whereas Ampk loss instead decreases CSR and slightly increases plasmablast differentiation (Figs 2D, 4D). These results suggest that Lkb1 acts through substrates other than Ampk to regulate B cell activation and GC formation, or that other related Lkb1 targets may compensate for the loss of Ampk. For example, Lkb1 phosphorylates 13 other Ampk family member proteins including Mark, Brsk, and Nuak proteins[7]. Sik2 and Mark2 are Lkb1 targets that phosphorylate Crtc2[41], a transcriptional co-activator of CREB required for GC exit[42], and their redundant activity might compensate for the loss of Ampk to rescue plasma cell differentiation.

We were further surprised to find no evidence for Ampk in regulating metabolism in B cells. Nutrient uptake and routing was identical in WT and Ampk KO B cells (Figs 2G, 3). One possibility is that Ampk is dispensable for

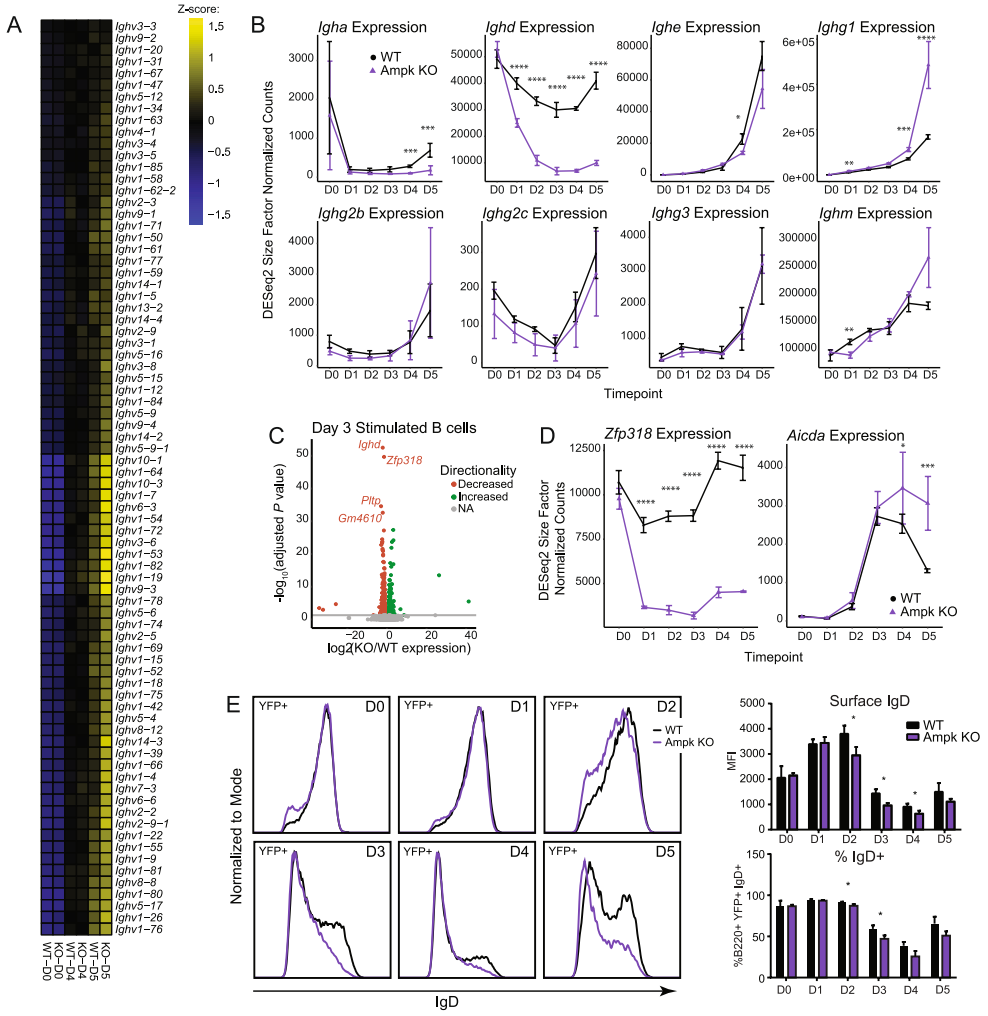


**Figure 5.** Ampk specifically regulates expression of IgD via downregulation of Zfp318 during activation. (**A**) Heat maps for immunoglobulin heavy-chain variable region expression (*Ighv*) across naïve and day 4/day 5 stimulated B cells. Genes were selected based on significant differential expression between WT naïve and day 5 stimulation (adjusted *P* value < 0.05). Values represent row z-score. (**B**) Kinetic time course expression plots for immunoglobulin heavy-chain constant region (*Igh*) expression across genotype and stimulation. (**C**) Volcano plot of differentially expressed genes between Ampk KO and WT at day 3 of stimulation. Adjusted *P* value cutoff represents values < 0.05 calculated using the Wald test following DESeq2 normalization. (**D**) Kinetic time course expression plot of *Zfp318* and *Aicda* across genotype and stimulation. (**E**) Representative flow cytometry plot of IgD at day 0 through day 5 of stimulation in WT and Ampk KO B cells and quantification by MFI (top) and % IgD (bottom) ($n = 3$ each WT and Ampk KO). *P* values were determined by Student's t-test (**E**), adjusted *P* values were determined by Wald test (**B**,**D**) $*P \leq 0.05$, $**P \leq 0.01$, $**P \leq 0.001$, $***P \leq 0.0001$.

homeostatic nutrient handling but required for metabolic adaptations under stressful conditions not examined here. Supporting this idea, studies in T cells show that Ampk can regulate glutamine metabolism during glucose deprivation[29] and total body knockout of Ampk makes B and T cells unable to survive ATP synthase inhibition with oligomycin[21]. Recent studies show that GCs in mice are hypoxic microenvironments[43] and Ampk links to inflammation in hypoxia[44]. Resting and activated Ampk KO B cells express genes and gene profile signatures similar to WT B cells, except for two repressed transcripts, *Zfp318* and *Ighd*. This specificity is remarkable and replicates the specificity of *Zfp318* KO B cells, in which there were only two differentially expressed genes, *Ighd* and

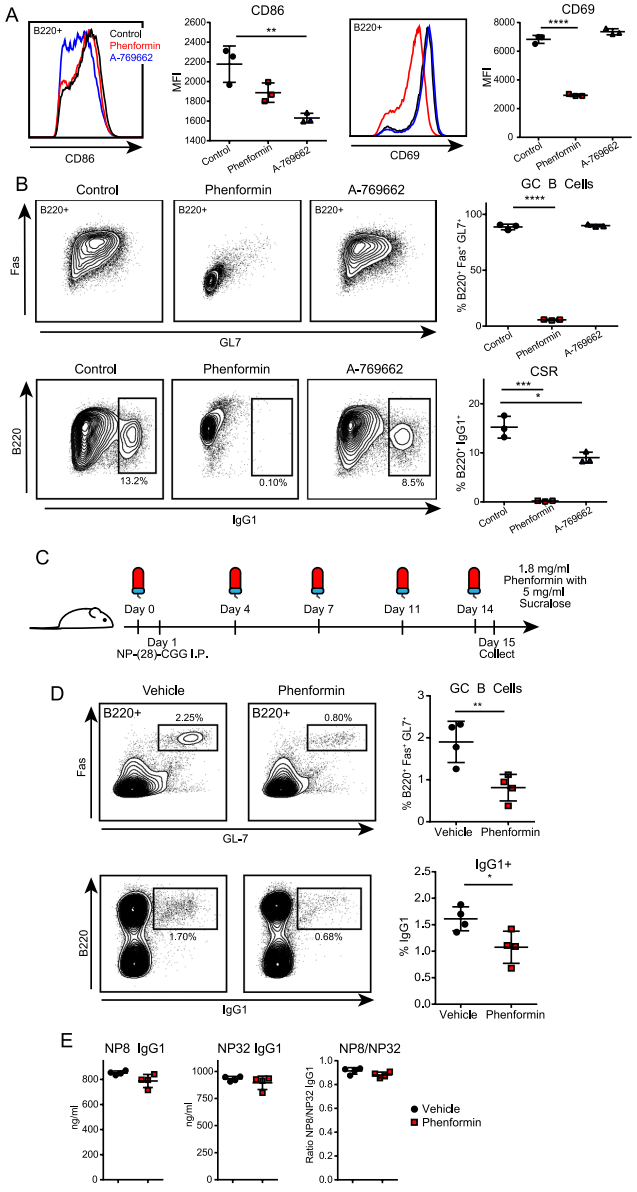


**Figure 6.** Early pharmacological activation of Ampk modifies B cell function both *in vitro* and *in vivo*. (**A**,**B**) Representative flow cytometry plots and quantification of activation markers (CD86, CD69) at 24 hours (**A**), and germinal center differentiation (GC B Cells, %B220$^+$ Fas$^+$ GL7$^+$) and class switch recombination (CSR, %B220$^+$ IgG1$^+$) at day 3 (**B**) of cells during *in vitro* activation with anti-CD40 plus IL-4 and phenformin (100 µM) or A-769662 (50 µM) ($n = 3$). (**C**) Strategy for *in vivo* assessment of B cells responses with Ampk activation. Prior to immunization, mice were given phenformin or vehicle (sucralose) in their water. Water was changed 2×/week, and samples collected 14 days post immunization with NP-(28)-CGG. (**D**) Flow cytometry of total splenocytes after immunization. Representative plots and quantification of GC differentiation (GC B Cells, B220$^+$ Fas$^+$ GL7$^+$) and CSR (B220$^+$ IgG1$^+$) 14 days post-immunization with NP-(28)-CGG ($n = 4$). (**E**) Anti-NP8 and anti-NP32 IgG1 serum response and NP8/NP32 IgG1 ratio by ELISA 14 days after immunization with NP-(28)-CGG ($n = 4$). Data represent mean ± SD. *P* values determined by 2-way ANOVA with Bonferroni correction for multiple comparisons (**A**,**B**), or Student's *t*-test (**D**,**E**), $^*P \leq 0.05$, $^{**}P \leq 0.01$, $^{***}P \leq 0.001$, $^{****}P \leq 0.0001$.

*Sva*, an antigen related to the *Vav-Cre* recombinase deletion construct[35]. Loss of *Ighd* transcripts parallels a loss of surface IgD protein expression in the Ampk KO B cells after stimulation. A possible but less likely contributor to a difference in later time point IgD expression between WT and Ampk KO B cells could be differential increase in cell death in the *in* vitro culture system between days 4 and 5 of stimulation. The role(s) of IgD in B cells remains elusive, as IgD is present at very low levels in human and rodent serum[45], but has recently been suggested to modulate Th2 responses to soluble antigens through interactions with basophils[46]. Because of co-expression of IgM and IgD in immature B cells, IgD may sequester signaling molecules from IgM to inhibit BCR signaling[47], and IgD may play a similar role in mature B cells. Regardless of the role of IgD, the specific regulation of *Zfp318* and *Ighd* by Ampk provides new insight into immunoglobulin gene regulation as a non-canonical role for Ampk.

## Materials and Methods

**Mice.** C57BL/6J, *Prkaa1*$^{fl/fl}$, *CD19-Cre*, and *Rosa26 lox-STOP-lox EYFP* mice (JAX: 000664, 014141, 006785, and 006148) were housed in a specific pathogen-free animal facility at UCLA. All studies were on mixed-sex mice between 6 to 16 weeks of age with approval from the UCLA Institutional Animal Research Committee (#1998-113-63C). All experiments were performed according to the National Institutes of Health and ARRIVE guidelines on the use of laboratory animals. Figures 1, 6 used WT C57BL/6J mice, and Figs 2–5 used B cell specific Ampk KO or Ampk WT littermate mice. Genotypes for WT (*Prkaa1*$^{+/+}$) and Ampk KO (*Prkaa1*$^{-/-}$) mice were as follows: *Prkaa1*$^{wt/wt}$ or *Prkaa1*$^{fl/fl}$, respectively, with *CD19-Cre*$^{+/-}$, and *Rosa26-YFP*$^{+/+}$ or $^{+/-}$ for experiments requiring YFP (Fig. 3B–D,F) or *Rosa26-YFP*$^{-/-}$ for experiments without YFP tracer (Figs 3E,F, 4–6).

**Stimulation of isolated mouse B cells.** Red blood cell-lysed mouse spleen cells were enriched for B cells using CD43 negative magnetic selection (Miltenyi). Cells were grown in RPMI1640 supplemented with 10% FBS and 50 μM β-mercaptoethanol. B cells were stimulated with 1 μg/ml anti-CD40 mAb (BD Pharmingen) and 25 ng/ml IL-4 (R&D Systems). At day 3, anti-CD40 was washed out and cells replated in medium containing only IL-4 until day 5. For early Ampk activation, phenformin (Sigma) was resuspended in 1x PBS, pH 7.4, and used at 100 μM, and A-769662 (Abbott) was resuspended in DMSO and used at 50 μM at the time of stimulation.

**Immunoblotting.** Cells were lysed in Lysis Buffer containing 50 mM Tris HCl pH 7.4, 100 mM NaCl, 1 mM EDTA and 1% Triton X-100 supplemented with Protease Inhibitor and Phosphatase Inhibitor Cocktails 2 and 3 (Sigma). Extracts were quantified and denatured by boiling with DTT and 10–30 μg protein separated by SDS-PAGE and transferred to nitrocellulose before blocking in 5% milk in TBST. Membranes were incubated overnight in the indicated antibodies in 5% BSA in TBST. Membranes were then incubated in fluorescent secondary antibody and imaged using the Odyssey Fc imaging system (LI-COR). Complete antibody information can be found in the Supplemental Methods.

**Flow cytometry.** Single cell suspensions were incubated with Fc Block (BD Pharmingen) at 1:500 for 15 min, then washed and stained for 20 min in 50 μl FACS buffer (2% FBS in PBS) on ice in the dark. Data were obtained on a BD LSRII or BD Fortessa (BD Biosciences) and analyzed with FlowJo software (Treestar). Antibodies were used at a 1:200 dilution. Complete antibody information can be found in the Supplemental Methods. Assessments of glucose import used a 2-NBDG Glucose Uptake Assay Kit (Biovision) according to the manufacturer's instructions.

**Extracellular metabolite analysis.** Glutamine levels in full media and after 24 hours of stimulation were measured by plating $10^6$ cells/ml in 2 ml, centrifuging to remove cells and debris, and analyzing using a BioProfile Basic Analyzer (NOVA Biomedical).

**Live cell interferometry.** Live cell interferometry (LCI) was used to measure biomass accumulation rate[25]. Cells were plated at $7.5 \times 10^5$ cells/ml on Poly-L-Lysine (Sigma) coated μ-Slide 2-Well Ph+ glass bottom slides (Ibidi) and imaged every 15 min for 72 h in a custom-built chamber as previously described[48]. LCI was performed on a Zeiss Axio Observer A1 with stage-top incubation system (Zeiss) using using a $20 \times 0.4$ NA objective. LCI data were captured with a SID4Bio (Phasics) QWLSI camera[49]. MATLAB (Mathworks) was used to analyze LCI data. Quantitative phase microscopy data was processed using SID4Processing (Phasics) to generate phase-shift images compatible with MATLAB. A custom MATLAB script was used to track the mass of individual cells as previously described[50].

**Immunization and ELISA.** Mice were immunized with 50 μg NP-(28)-CGG (Biosearch Technologies) in ImJect Alum (Thermo Scientific) via intra-peritoneal injection. Blood was collected at 14 days and assayed by ELISA. Serum Ig concentrations were determined using anti-mouse Ig as a capture antibody and developed with isotype-specific goat anti-mouse antibodies conjugated to HRP (Southern Biotech). Antigen-specific ELISA was performed by coating a plate with NP-(8)- or NP-(20)-BSA and developed with an isotype specific goat anti-mouse antibody conjugated to HRP. For immunizations with phenformin, mice were given water containing either vehicle (5 mg/ml sucralose, Sigma) or phenformin (1.8 mg/ml, Sigma) with vehicle in amber bottles one day before immunization, and water was changed twice per week.

**Metabolomics.** B cells were grown for 24 hours in media with glucose or glutamine free RPMI (Gibco) supplemented with 2 g/L [U-$^{13}$C] glucose or 3 mM [U-$^{13}$C] glutamine, respectively (Cambridge Isotope Laboratories) and non-dialyzed FBS. Metabolites were extracted with cold 80% methanol and measured using Ultra High Performance Liquid Chromatography Mass Spectrometry (UHPLC-MS), as previously described[24,51,52]. To extract intracellular metabolites, cells were pelleted by centrifugation (1000 RPM, 4 °C) and rinsed with cold 150 mM ammonium acetate (pH 7.3), pelleted again, followed by addition of 1 ml cold 80% MeOH in water. To the cell suspensions, 10 nmol D/L-norvaline were added and rigorously mixed followed by centrifugation ($1.3 \times 10^4$ rpm, 4 °C). The supernatant was transferred into a glass vial and pellet was further extracted with 200 μl

cold 80% MeOH in water. After centrifugation, supernatant was combined, metabolites dried down under vacuum, and resuspended in 70% acetonitrile. For the mass spectrometry-based analysis of the sample, 5 µl were injected onto a Luna NH2 (150 mm × 2 mm, Phenomenex) column. The samples were analyzed with an UltiMate 3000RSLC (Thermo Scientific) coupled to a Q Exactive mass spectrometer (Thermo Scientific). The Q Exactive was run with polarity switching (+3.50 kV/−3.50 kV) in full scan mode with an m/z range of 65–975. Separation was achieved using A) 5 mM NH4AcO (pH 9.9) and B) ACN. The gradient started at 15% A) going to 90% A) over 18 min, followed by an isocratic step for 9 min and reversal to the initial 15% A) for 7 min. Metabolites and isotopomers thereof were quantified with TraceFinder 3.3 using accurate mass measurements (≤3 ppm) and retention times. For isotopologue distribution measurements, data was corrected for naturally occurring $^{13}C$ as described in[53]. Fractional contributions were calculated using the formula $FC = \frac{\sum_0^n i * m_i}{n \sum_0^n m_i}$ as described[54], where $m_i$ denotes the intensity of the isotopologue, and $n$ marks the number of carbons in a given metabolite. Data were normalized to cell counts. Metabolite relative amounts, isotopomer distribution values, MSVA scores, and DPI lists are included in a supplemental excel file (Table S1).

**RNA extraction.** At least $10^7$ WT and Ampk KO B cells were grown in biological triplicates and RNA purified immediately after isolation, or 24 hours after anti-CD40 plus IL-4 stimulation using the RNeasy Mini Kit (Qiagen) and RNase-free DNase (Qiagen) following the manufacturer's protocols. All samples showed an A260/280 ratio >1.99. Prior to library preparation, quality control of the RNA was performed using the Advanced Analytical Technologies Fragment Analyzer (Advanced Analytical, Inc.) and analyzed using PROSize 2.0.0.51 software. RNA Quality Numbers (RQNs) were computed per sample between 8.7 and 10, indicating intact total RNA per sample prior to library preparation.

**RNA-seq library preparation.** Strand-specific ribosomal RNA (rRNA) depleted RNA-Seq libraries were prepared from 1 µg of total RNA using the KAPA Stranded RNA-Seq Kit with Ribo-Erase (Kapa Biosystems, Roche). Briefly, rRNA was depleted from total RNA samples, the remaining RNA was heat fragmented, and strand-specific cDNA was synthesized using a first strand random priming and second strand dUTP incorporation approach. Fragments were then A-tailed, adapters were ligated, and libraries were amplified using high-fidelity PCR. All libraries were prepared in technical duplicates per sample and resulting raw sequencing reads merged for downstream alignment and analysis. Libraries were paired-end sequenced at 2 × 150 bp on an Illumina NovaSeq 6000.

Lists of transcript/gene-level expression values, KO signature ORA results, and differentiation signature GSVA results are included in a supplemental excel file (Table S2).

**Statistical analyses.** All metabolomics and transcriptomics statistical analyses are described in the above methods. Values represent mean ± S.D. or S.E.M. Data were analyzed with Prism 6 (GraphPad) (Figs 1–3, 6), MATLAB (Mathworks) (Fig. 1E–G) or R (Figs 3–5). Parametric data were analyzed using unpaired two-tailed Student's t-tests, or 2-way ANOVA with Bonferroni correction for multiple comparisons. Transcriptomic volcano and kinetic time course expression plots were analyzed using DESeq2 Wald tests with Benjamini-Hochberg FDR correction for multiple comparisons. For all data sets, $P \leq 0.05$ was considered significant. $^*P \leq 0.05$, $^{**}P \leq 0.01$, $^{***}P \leq 0.001$, $^{****}P \leq 0.0001$.

## Data Availability

All raw RNA-Seq reads, transcript abundance values, and processed gene count matrices were submitted to the NCBI Gene Expression Omnibus (GEO) under accession GSE121025. All metabolomics and downstream transcriptomics datasets have been provided as supplemental material in this study (Tables S1 and S2).

## Code Availability

All custom code used for metabolomic/transcriptomic analyses are available on Atlassian BitBucket at http://bitbucket.org/ahsanfasih/AmpkBcell/src/master and detailed descriptions of data analysis can be found in the Supplementary Methods.

## References


1. Hoffman, W., Lakkis, F. G. & Chalasani, G. B Cells, Antibodies, and More. *Clin J Am Soc Nephrol* **11**, 137–154, https://doi.org/10.2215/CJN.09430915 (2016).
2. Xu, Z., Zan, H., Pone, E. J., Mai, T. & Casali, P. Immunoglobulin class-switch DNA recombination: induction, targeting and beyond. *Nat Rev Immunol* **12**, 517–531, https://doi.org/10.1038/nri3216 (2012).
3. Depoil, D. *et al.* Early events of B cell activation by antigen. *Sci Signal* **2**, pt1, https://doi.org/10.1126/scisignal.263pt1 (2009).
4. Walsh, N. C. *et al.* LKB1 inhibition of NF-kappaB in B cells prevents T follicular helper cell differentiation and germinal center formation. *EMBO Rep* **16**, 753–768, https://doi.org/10.15252/embr.201439505 (2015).
5. Waters, L. R., Walsh, N. C. & Teitell, M. A. LKB1 regulates germinal center formation and termination. *Cell Cycle* **14**, 2183–2184, https://doi.org/10.1080/15384101.2015.1056610 (2015).
6. Domeier, P. P., Schell, S. L. & Rahman, Z. S. Spontaneous germinal centers and autoimmunity. *Autoimmunity* **50**, 4–18, https://doi.org/10.1080/08916934.2017.1280671 (2017).
7. Shackelford, D. B. & Shaw, R. J. The LKB1-AMPK pathway: metabolism and growth control in tumour suppression. *Nat Rev Cancer* **9**, 563–575, https://doi.org/10.1038/nrc2676 (2009).
8. Mihaylova, M. M. & Shaw, R. J. The AMPK signalling pathway coordinates cell growth, autophagy and metabolism. *Nat Cell Biol* **13**, 1016–1023, https://doi.org/10.1038/ncb2329 (2011).
9. Herzig, S. & Shaw, R. J. AMPK: guardian of metabolism and mitochondrial homeostasis. *Nat Rev Mol Cell Biol* **19**, 121–135, https://doi.org/10.1038/nrm.2017.95 (2018).
10. Hawley, D. R. & Gonzalez, C. Publication patterns of faculty in commision on accreditation for marriage and family therapy education programs. *J Marital Fam Ther* **31**, 89–98 (2005).

11. Hawley, S. A. *et al*. Complexes between the LKB1 tumor suppressor, STRAD alpha/beta and MO25 alpha/beta are upstream kinases in the AMP-activated protein kinase cascade. *J Biol* **2**, 28, https://doi.org/10.1186/1475-4924-2-28 (2003).
12. Xie, M. *et al*. A pivotal role for endogenous TGF-beta-activated kinase-1 in the LKB1/AMP-activated protein kinase energy-sensor pathway. *Proc Natl Acad Sci USA* **103**, 17378–17383, https://doi.org/10.1073/pnas.0604708103 (2006).
13. Tamas, P. *et al*. Regulation of the energy sensor AMP-activated protein kinase by antigen receptor and Ca2+ in T lymphocytes. *J Exp Med* **203**, 1665–1670, https://doi.org/10.1084/jem.20052469 (2006).
14. Kishton, R. J. *et al*. AMPK Is Essential to Balance Glycolysis and Mitochondrial Metabolism to Control T-ALL Cell Stress and Survival. *Cell Metab* **23**, 649–662, https://doi.org/10.1016/j.cmet.2016.03.008 (2016).
15. Nakada, D., Saunders, T. L. & Morrison, S. J. Lkb1 regulates cell cycle and energy metabolism in haematopoietic stem cells. *Nature* **468**, 653–658, https://doi.org/10.1038/nature09571 (2010).
16. Gurumurthy, S. *et al*. The Lkb1 metabolic sensor maintains haematopoietic stem cell survival. *Nature* **468**, 659–663, https://doi.org/10.1038/nature09572 (2010).
17. Gan, B. *et al*. Lkb1 regulates quiescence and metabolic homeostasis of haematopoietic stem cells. *Nature* **468**, 701–704, https://doi.org/10.1038/nature09595 (2010).
18. Tamas, P. *et al*. LKB1 is essential for the proliferation of T-cell progenitors and mature peripheral T cells. *Eur J Immunol* **40**, 242–253, https://doi.org/10.1002/eji.200939677 (2010).
19. MacIver, N. J. *et al*. The liver kinase B1 is a central regulator of T cell development, activation, and metabolism. *J Immunol* **187**, 4187–4198, https://doi.org/10.4049/jimmunol.1100367 (2011).
20. Cao, Y. *et al*. The serine/threonine kinase LKB1 controls thymocyte survival through regulation of AMPK activation and Bcl-XL expression. *Cell Res* **20**, 99–108, https://doi.org/10.1038/cr.2009.141 (2010).
21. Mayer, A., Denanglaire, S., Viollet, B., Leo, O. & Andris, F. AMP-activated protein kinase regulates lymphocyte responses to metabolic stress but is largely dispensable for immune cell development and function. *Eur J Immunol* **38**, 948–956, https://doi.org/10.1002/eji.200738045 (2008).
22. Hawley, S. A. *et al*. Characterization of the AMP-activated Protein Kinase Kinase from Rat Liver and Identification of Threonine 172 as the Major Site at Which It Phosphorylates AMP-activated Protein Kinase. *The Journal of Biological Chemistry* **271**, 27879–27887 (1996).
23. Hardie, D. G. Regulation of AMP-activated protein kinase by natural and synthetic activators. *Acta Pharm Sin B* **6**, 1–19, https://doi.org/10.1016/j.apsb.2015.06.002 (2016).
24. Waters, L. R., Ahsan, F. M., Wolf, D. M., Shirihai, O. & Teitell, M. A. Initial B Cell Activation Induces Metabolic Reprogramming and Mitochondrial Remodeling. *iScience* **5**, 99–109, https://doi.org/10.1016/j.isci.2018.07.005 (2018).
25. Zangle, T. A. & Teitell, M. A. Live-cell mass profiling: an emerging approach in quantitative biophysics. *Nat Methods* **11**, 1221–1228, https://doi.org/10.1038/nmeth.3175 (2014).
26. Faubert, B. *et al*. AMPK is a negative regulator of the Warburg effect and suppresses tumor growth *in vivo*. *Cell Metab* **17**, 113–124, https://doi.org/10.1016/j.cmet.2012.12.001 (2013).
27. Doughty, C. A. *et al*. Antigen receptor-mediated changes in glucose metabolism in B lymphocytes: role of phosphatidylinositol 3-kinase signaling in the glycolytic control of growth. *Blood* **107**, 4458–4465, https://doi.org/10.1182/blood-2005-12-4788 (2006).
28. Caro-Maldonado, A. *et al*. Metabolic Reprogramming is Required for Antibody Production That Is Supressed in Anergic but Exaggerated in Chronically BAFF-Exposed B Cells. *Journal of Immunology* **192**, 3626–3636, https://doi.org/10.4049/jimmunol.1302062 (2014).
29. Blagih, J. *et al*. The energy sensor AMPK regulates T cell metabolic adaptation and effector responses *in vivo*. *Immunity* **42**, 41–54, https://doi.org/10.1016/j.immuni.2014.12.030 (2015).
30. Chen, H. P., Zhao, Y. T. & Zhao, T. C. Histone deacetylases and mechanisms of regulation of gene expression. *Crit Rev Oncog* **20**, 35–47 (2015).
31. Ma, Y., Shimizu, Y., Mann, M. J., Jin, Y. & Hendershot, L. M. Plasma cell differentiation initiates a limited ER stress response by specifically suppressing the PERK-dependent branch of the unfolded protein response. *Cell Stress Chaperones* **15**, 281–293, https://doi.org/10.1007/s12192-009-0142-9 (2010).
32. Shi, W. *et al*. Transcriptional profiling of mouse B cell terminal differentiation defines a signature for antibody-secreting plasma cells. *Nat Immunol* **16**, 663–673, https://doi.org/10.1038/ni.3154 (2015).
33. Gloury, R. *et al*. Dynamic changes in Id3 and E-protein activity orchestrate germinal center and plasma cell development. *J Exp Med* **213**, 1095–1111, https://doi.org/10.1084/jem.20152003 (2016).
34. Chen, K. *et al*. Immunoglobulin D enhances immune surveillance by activating antimicrobial, proinflammatory and B cell-stimulating programs in basophils. *Nat Immunol* **10**, 889–898, https://doi.org/10.1038/ni.1748 (2009).
35. Pioli, P. D., Debnath, I., Weis, J. J. & Weis, J. H. Zfp318 regulates IgD expression by abrogating transcription termination within the Ighm/Ighd locus. *J Immunol* **193**, 2546–2553, https://doi.org/10.4049/jimmunol.1401275 (2014).
36. Enders, A. *et al*. Zinc-finger protein ZFP318 is essential for expression of IgD, the alternatively spliced Igh product made by mature B lymphocytes. *Proc Natl Acad Sci USA* **111**, 4513–4518, https://doi.org/10.1073/pnas.1402739111 (2014).
37. Biondani, G. & Peyron, J. F. Metformin, an Anti-diabetic Drug to Target Leukemia. *Front Endocrinol (Lausanne)* **9**, 446, https://doi.org/10.3389/fendo.2018.00446 (2018).
38. Raybuck, A. L. *et al*. B Cell-Intrinsic mTORC1 Promotes Germinal Center-Defining Transcription Factor Gene Expression, Somatic Hypermutation, and Memory B Cell Generation in Humoral Immunity. *J Immunol* **200**, 2627–2639, https://doi.org/10.4049/jimmunol.1701321 (2018).
39. Allen, C. D. C., Okada, T., Tang, H. L. & Cyster, J. G. Imaging of Germinal Center Selection Events During Affinity Maturation. *Science* **315**, 528–531, https://doi.org/10.1126/science.1136736 (2007).
40. MacLennan, I. C. M. Germinal Centers. *Annual Review of Immunology* **12**, 117–139, https://doi.org/10.1146/annurev.iy.12.040194.001001 (1994).
41. Altarejos, J. Y. & Montminy, M. CREB and the CRTC co-activators: sensors for hormonal and metabolic signals. *Nat Rev Mol Cell Biol* **12**, 141–151, https://doi.org/10.1038/nrm3072 (2011).
42. Sherman, M. H. *et al*. AID-induced genotoxic stress promotes B cell differentiation in the germinal center via ATM and LKB1 signaling. *Mol Cell* **39**, 873–885, https://doi.org/10.1016/j.molcel.2010.08.019 (2010).
43. Cho, S. H. *et al*. Germinal centre hypoxia and regulation of antibody qualities by a hypoxia response system. *Nature* **537**, 234–238, https://doi.org/10.1038/nature19334 (2016).
44. Chen, X. *et al*. Activation of AMPK inhibits inflammatory response during hypoxia and reoxygenation through modulating JNK-mediated NF-kappaB pathway. *Metabolism* **83**, 256–270, https://doi.org/10.1016/j.metabol.2018.03.004 (2018).
45. Geisberger, R., Lamers, M. & Achatz, G. The riddle of the dual expression of IgM and IgD. *Immunology* **118**, 429–437, https://doi.org/10.1111/j.1365-2567.2006.02386.x (2006).
46. Shan, M. *et al*. Secreted IgD Amplifies Humoral T Helper 2 Cell Responses by Binding Basophils via Galectin-9 and CD44. *Immunity* **49**, 709–724 e708, https://doi.org/10.1016/j.immuni.2018.08.013 (2018).
47. Klasener, K., Maity, P. C., Hobeika, E., Yang, J. & Reth, M. B cell activation involves nanoscale receptor reorganizations and inside-out signaling by Syk. *Elife* **3**, e02069, https://doi.org/10.7554/eLife.02069 (2014).
48. Reed, J. *et al*. Rapid, massively parallel single-cell drug response measurements via live cell interferometry. *Biophys J* **101**, 1025–1031, https://doi.org/10.1016/j.bpj.2011.07.022 (2011).

49. Bon, P., Maucort, G., Wattellier, B. & Monneret, S. Quadriwave lateral shearing interferometry for quantitative phase microscopy of living cells. *Opt Express* **17**, 13080–13094 (2009).
50. Zangle, T. A., Teitell, M. A. & Reed, J. Live cell interferometry quantifies dynamics of biomass partitioning during cytokinesis. *PLoS One* **9**, e115726, https://doi.org/10.1371/journal.pone.0115726 (2014).
51. TeSlaa, T. *et al*. alpha-Ketoglutarate Accelerates the Initial Differentiation of Primed Human Pluripotent Stem Cells. *Cell Metab*, https://doi.org/10.1016/j.cmet.2016.07.002 (2016).
52. Thai, M. *et al*. Adenovirus E4ORF1-induced MYC activation promotes host cell anabolic glucose metabolism and virus replication. *Cell Metab* **19**, 694–701, https://doi.org/10.1016/j.cmet.2014.03.009 (2014).
53. Moseley, H. N. Correcting for the effects of natural abundance in stable isotope resolved metabolomics experiments involving ultra-high resolution mass spectrometry. *BMC Bioinformatics* **11**, 139, https://doi.org/10.1186/1471-2105-11-139 (2010).
54. Fendt, S. M. *et al*. Metformin decreases glucose oxidation and increases the dependency of prostate cancer cells on reductive glutamine metabolism. *Cancer Res* **73**, 4429–4438, https://doi.org/10.1158/0008-5472.CAN-13-0080 (2013).
55. Wu, Y. L. *et al*. Intrinsic transcriptional heterogeneity in B cells controls early class switching to IgE. *J Ex Med* **214**(1),183–196. https://doi.org/10.1084/jem.20161056 (2017).



## Acknowledgements

Flow cytometry was performed at the UCLA Broad Stem Cell Research Center Flow Cytometry Core. We thank Heather Christofk for kind use of the NOVA Bioanalyzer. Metabolomics was performed at the UCLA Metabolomics Center. RNA-Seq was performed at NantWorks, LLC, Culver City, CA, by Justin Golovato and Charlie Vaske. We thank Nicole C. Walsh, Tara TeSlaa, Laura Jimenez, and David Shackelford for technical assistance and helpful discussions. Supported by the University of California Office of the President, UCLA Graduate Division (LRW), NIH grants GM007185 (LRW), CA90571, CA156674, GM073981, CA18589, GM114188 (MAT), CA157940 (TAZ), NIH Instrumentation grant S10OD016387 (TG), NSF GRFP 1144087 (NHDK) and the Air Force Office of Scientific Research FA9550-15-1-0406 (MAT).


## Author Contributions

Conceptualization: L.W., M.A.T. Methodology: L.W., F.A., J.t.H., D.K., A.M., D.B., T.G., T.Z., M.A.T. Software: F.A., J.t.H., D.K., A.M., D.B., T.Z. Formal Analysis: L.W., F.A., J.t.H., J.H., D.K., A.M., D.B., T.Z. Investigation L.W., J.t.H., J.H., D.K. Data Curation F.A., J.t.H., A.M. Writing-Original Draft: L.W. Writing-Review & Editing: L.W., F.A., M.A.T. Visualization: L.W., F.A., J.H., D.K., T.Z. Supervision: T.G., T.Z., M.A.T. Project Administration: L.W. Funding Acquisition L.W., T.Z., M.A.T.

## Additional Information

**Supplementary information** accompanies this paper at https://doi.org/10.1038/s41598-019-43985-y.

**Competing Interests:** The authors declare no competing interests.

**Publisher's note:** Springer Nature remains neutral with regard to jurisdictional claims in published maps and institutional affiliations.